Nano Energy 129 (2024) 110046

Contents lists available at ScienceDirect

Nano Energy

journal homepage: www.elsevier.com/locate/nanoen

Review

Electrocatalytic activity, phase kinetics, spectroscopic advancements, and photocorrosion behaviour in tantalum nitride phases

Raghunath Sharma Mukkavilli [a,b], Niraja Moharana [a,b,f], Bhupendra Singh [c], Thomas Fischer [c], Florian Vollnhals [d], Arun Ichangi [c], K.C. Hari Kumar [b,f], Silke Christiansen [a,d,e], Kwang-Ho Kim [g], Sehun Kwon [g], Ravi Kumar [a,b,*], Sanjay Mathur [a,b,c,**]

[a] Laboratory for High Performance Ceramics, Department of Metallurgical and Materials Engineering, Indian Institute of Technology-Madras (IIT Madras), Chennai 600036, India
[b] Research Centre on Ceramic Technologies for Futuristic Mobility, Indian Institute of Technology-Madras (IIT Madras), Chennai 600036, India
[c] Institute of Inorganic Chemistry, University of Cologne, Greinstr. 6, Cologne 50939, Germany
[d] Institute for Nanotechnology and Correlative Microscopy (INAM), Äußere Nürnberger Str. 62, Forchheim 91301, Germany
[e] Fraunhofer Institute for Ceramic Technologies and Systems, IKTS, Äußere Nürnberger Str. 62, Forchheim 91301, Germany
[f] Calphad Laboratory, Department of Metallurgical and Materials Engineering, Indian Institute of Technology, Madras (IIT Madras), Chennai, 600036, India
[g] Department of Materials Science and Engineering, Pusan National University, Busan, Republic of Korea

ARTICLE INFO

Keywords:
Tantalum Oxynitrides
Electrocatalysis
Hydrogen Evolution Reaction
Oxygen
Evolution Reaction
CALPHAD
Green Hydrogen
Energy Sustainability

ABSTRACT

The search for sustainable energy solutions has led to extensive research on new electrocatalysts that can convert electrical energy into chemical energy and back. Tantalum nitrides stand out as an intriguing class of materials, showcasing exceptional properties such as high melting points, remarkable mechanical strength, and notable resistance to corrosion. These attributes position tantalum nitrides (Ta-N) and allied phases (Ta-N-X) as compelling candidates for diverse applications, notably in electrocatalysis. While traditionally studied for their photocatalytic and photoelectrocatalytic properties, this review ventures into largely uncharted territory, illuminating the untapped potential of tantalum nitrides as electrocatalysts. Electrocatalysis assumes a pivotal role in numerous renewable energy technologies, including fuel cells and water electrolysis, which demand materials adept at catalyzing reactions efficiently. The distinctive characteristics of Ta-N phases, particularly their electrical conductivity, chemical stability, and expansive surface area, mark them as promising contenders in this arena. This comprehensive review article aims to unveil the electrocatalytic prowess of Ta-N phases, examining their catalytic performance concerning the Hydrogen Evolution Reaction (HER), Oxygen Evolution Reaction (OER), and Oxygen Reduction Reaction (ORR). Delving into recent advancements over the past five years, the article scrutinizes strategies employed to counter surface oxidation—a prevailing degradation issue that hampers activity in Ta-N phases. It also describes methodologies to mitigate photocorrosion observed during photocatalytic/photoelectrochemical (PEC) water splitting of Ta-N phases, offering potential blueprints for efficient design of their electrocatalytic counterparts. The exploration encompasses a thorough investigation into the role of various correlative spectroscopy techniques, including X-ray Photoelectron Spectroscopy (XPS), Raman spectroscopy, and Fourier-Transform Infrared Spectroscopy (FTIR), in unraveling the involvement of oxygen-related species within Ta-N systems. Furthermore, the presence of oxygen necessitates an intricate comprehension of the thermodynamic stability of different Ta-N phases, both in the presence and absence of oxygen.

This article underscores the importance of an exhaustive phase diagram analysis for the Ta-N system in the context of water splitting, critically evaluating thermochemical and constitutional data. Despite extensive research efforts, the phase diagram of the Ta-N system remains incomplete, restraining our understanding of phase stability and overall performance. This account aims to enhance understanding of Ta-N phases and provide insights that support cohesive electrocatalyst design, focusing on the key issue of long-term stability in electrocatalysis.

* Corresponding author at: Laboratory for High Performance Ceramics, Department of Metallurgical and Materials Engineering, Indian Institute of Technology-Madras (IIT Madras), Chennai 600036, India.
** Corresponding author at: Institute of Inorganic Chemistry, University of Cologne, Greinstr. 6, Cologne 50939, Germany.
E-mail addresses: nvrk@iitm.ac.in (R. Kumar), sanjay.mathur@uni-koeln.de (S. Mathur).

https://doi.org/10.1016/j.nanoen.2024.110046
Received 12 May 2024; Received in revised form 22 July 2024; Accepted 23 July 2024
Available online 26 July 2024

1. Introduction

The recent advancement of hydrogen-based energy technologies, including the integration of intermittent energy sources like solar and wind power, holds great promise as a solution to meet the growing energy demands and address environmental challenges [1–3]. Of notable significance is the generation of molecular hydrogen through water electrolysis, a technology recognized for its efficiency and compatibility with electricity generated from sustainable sources [4–6]. Consequently, extensive endeavors have been dedicated to optimizing electrocatalytic systems, encompassing the integration of photovoltaic modules with water electrolyzers to establish solar-to-fuel conversion devices [7]. The efficiency and cost-effectiveness of these systems are intrinsically tied to electrocatalytic processes, exerting a profound influence on the economic aspects, purity, and productivity of target chemicals or fuels [8,9]. Critical chemical reactions, including the hydrogen evolution reaction (HER) and the oxygen evolution reaction (OER), within diverse electrolyte settings used in applications such as proton exchange membrane (PEM)-based electrolyzers underscore the pressing need for the development of electrocatalysts characterized by superior activity, selectivity, and stability [10,11]. Catalyst-Coated Membranes (CCMs), for instance, use significant amount of precious metal-based catalysts, Pt and IrO_2, and their high costs (28 USD g^{-1} for Pt and 160 USD g^{-1} for Ir) contribute significantly towards the overall cost of a PEM electrolyzer stack, making the produced H_2 economically less competitive compared to the fossil fuel derived H_2 [12]. Addressing this challenge, researchers have explored the use of earth-abundant metal-based electrocatalysts, particularly carbides, oxides, nitrides and sulfides of transition metals, to reduce the cost of CCMs and improve the affordability and accessibility of PEM electrolyzers [13,14]. Initial studies demonstrated that the presence of nitrogen and carbon in the transition metal lattices modifies the d-band center and thereby improves the functionality towards water splitting [15–17]. This led to an explosion of reports on transition metal based electrocatalysts, particularly nitrides and oxynitrides of transition metals, owing to their remarkable electronic conductivity and excellent stability in harsh operating conditions [14,18]. By virtue of their stability in highly acidic conditions, tantalum nitrides and oxynitrides stand out as promising electrocatalysts [19]. The PEC/photocatalytic behavior of tantalum nitrides and oxynitrides is extensively reviewed [20–23], primarily due to their low band gaps (1.9–2.1 eV) and bandgap positions that are ideally located for water splitting [21,22]. Nurlaela et al. [20], for example, focused on key parameters associated with photo-absorption, catalytic efficiency and mass transport to present an overview of various experimental and theoretical approaches to improve photocatalytic water splitting. Similarly, Zhen et al. [21] and Xiao et al. [22] summarized various synthesis strategies to improve efficiency and stability of Ta-O-N phases for PEC water splitting. Nevertheless, there has been no exclusive focus on electrocatalytic activity of Ta-N phases and therefore to address this the present review attempts to summarize the electrocatalytic behavior of Ta-N phases, bringing out the state-of-the-art. A major concern emanating from the electrocatalytic and photoelectrocatalytic studies of Ta-N phases thus far is the presence of oxygen-either as a surface oxidation layer or as a contaminant-that impedes the long-term electrocatalytic activity and causes photocorrosion of the material [23]. We update various strategies incorporated in the last 5 years to mitigate surface oxidation, which in principle can also be extended to improve the stability of Ta-N electrocatalysts. Understanding the inevitable presence of oxygen also necessitates a thorough understanding of various spectrochemical techniques, which will be summarized here. Ongoing advancements in correlative spectroscopy, such as in-situ or operando spectroscopy, that hold promise for real-time monitoring and further unravelling the complex oxygen interactions in Ta-N compositional space is recommended. The lack of commercial realization, when it comes to these nitrides, also stems from our limited understanding of the phase stabilities and their associated electrocatalytic performances. The binary (Ta-N and Ta-O) and ternary (Ta-O-N) phase diagrams exhibit a multitude of compositions such as Ta_3N_5, Ta_2N, TaN, TaO_xN_y, Ta_4N_5, Ta_5N_6 that manifest diverse electronic, structural and oxidation properties. A thorough understanding of stability of these phases through thermochemical and constitutional data is summarized. Finally, a holistic design strategy seeking combinatorial inputs from the phase stability diagrams and correlative spectroscopy analysis coupled with various mitigation strategies to address surface oxidation is proposed to develop next-generation tantalum nitride based electrocatalysts with long-term stability and improved activity.

2. Ta-N phases as electrocatalysts

Historical interest in tantalum nitrides can be traced back to 1876 when Jolly discussed the preparation and existence of Ta_3N_5 and TaN_2 [24,25]. In 1924 Van Arkel suggested the existence of a 1:1 stoichiometric TaN with wurzite-type hexagonal structure [25,26]. In 1950s, Brauer and Zapp [27,28] and Schönberg [25], however, were the first to perform systematic X-rax investigation of Ta-N system. Subsequently, numerous Ta-N phases has been identified, which include stoichiometric ε-TaN [29], δ-TaN [30], η-TaN [31], θ-TaN [32] and ν-TaN [33], metal-rich Ta_2N [34], and N-rich Ta_2N_3 [35], Ta_2N_3 [31], Ta_3N_5 [36,37], Ta_4N_5 and Ta_5N_6 [38]. The presence of defects such as vacancies, oxygen impurities, antisite atoms, etc. play crucial role in affecting the stability and stoichiometry of tantalum nitrides [31], with the inevitable presence of oxygen (up to 3 at. percent, at%) in Ta-N system imparting a stabilization effect in some nitrides [39–45].

For the synthesis of tantalum nitrides, numerous methods such as high-temperature ammonolysis of Ta or Ta_xO_y [39,46–48], radio-frequency/DC magnetron sputtering [49–53], self-propagating high--temperature synthesis [54–56], chemical vapor deposition (CVD) [35,57,58], atomic layer deposition (ALD) [59–62], ion beam-assisted deposition [63], electron beam evaporation [64], high-pressure high--temperature (HP-HT) synthesis [31,65,66], hydrothermal/solvothermal [48,67,68] and flux-assisted nitridation [69–71] have been employed. Using these methods, powders, monoliths and films having morphology of nanopowders [72–74], nanotubes [75–77], nanorods [46,50,67,78,79], nanograins [80,81], etc. are obtained. Table 1 presents a brief summary of various methods used for the synthesis of Ta(O)N. To fabricate thin films of Ta(O)N materials for PEC applications, however, high-temperature nitridation of Ta(oxide)-based precursors has been widely used. For nitridation, mostly ammonia is used as the nitrogen source and conditions such as gas flow rate, temperature, pressure and time, play important role in determining the final product, with higher temperature, longer duration and high NH_3 flow rate favoring oxygen-free Ta_3N_5 phase [82–84]. Numerous methods, such as sol-gel synthesis [84–86], hydrothermal [48,67], CVD [87], anodization [75,88,89] and flame heating [90], have been employed to fabricate the Ta-precursor (film, power, or monolith) to be employed in subsequent nitridation step.

Obviously, TN_x system is extremely diverse and may have numerous stable phases (solid–solution α-Ta(N), hexagonal γ-Ta_2N, and hexagonal ε-TaN) and metastable phases (bcc β-TaN, hexagonal δ-phase TaN, hexagonal WC-structure θ-TaN, cubic B1 rock salt-structure δ-TaN_x, hexagonal Ta_5N_6, tetragonal Ta_4N_5, and orthorhombic Ta_3N_5) [38,40,105,106]. Moreover, the mechanical, electrical, optical and catalytic properties of these nitride phases vary extensively depending upon their composition, phase and processing [23,51,106,107]. For example, depending upon the nitrogen content their electrical conductivity can vary from being strongly metallic (TaN, Ta_2N) to more resistive (Ta_5N_6) and to dielectric (Ta_3N_5), which may be due to Ta vacancies and anti-site defects or the formation of thermodynamically stable N-rich phase [51,106]. Accordingly, the attributes like high hardness, good chemical and thermal stability, and tunable electrical resistivity and band gap make them attractive candidates for a range of applications, such as diffusion barrier [108], wear and corrosion-resistant materials [109,110], thin

Table 1
A brief summary of various methods used for the synthesis of tantalum nitrides.

Method	Ta source, key process parameters	Phase, morphology	Ref.
High-temperature ammonolysis	Ta_2O_5 on HF-etched Ta; NH_3, 1000 °C for 6 h	Ta_3N_5 nanorod	[46]
High-temperature ammonolysis	Anodized TaO_x on Ta; N_2 + NH_3 (90: 10, v/v), 950 °C for 2 h	Ta_3N_5 nanotube	[75]
High-temperature ammonolysis	Anodized Ta_2O_5 nanorods grown on Ti foil, NH_3, 1000 °C for 2 h	Ta_3N_5, Ta_2N	[89]
RF magnetron sputtering + nitridation	Ta target, N_2 and NH_3, 825 °C for 1 h	Ta_3N_5 nanograins	[80]
DC magnetron sputtering + nitridation	Ta target, 15 mA and 700 V, N_2+Ar, 2.6 Pa for 2 h	TaN and Ta_2N	[51]
DC magnetron sputtering + nitridation	Ta target, pulsed DC mode, 50 W; NH_3 annealing	Metastable Ta_2N_3 *via* O incorporation	[91]
DC magnetron sputtering + nitridation	Ta target, 100 W, N2+Ar, 2.6×10^{-4} Pa, 500–600 °C for 2 h	Ta_4N_5 nanocolumn arrays	[92]
CVD	Ni foam, [Ta(NEt)$(NEt_2)_3$] precursor, 500 °C	Amorphous TaNx(Oy)	[93]
ALD + nitridation	Ta_2O_5 /Si nanowires etched on Si wafer	Ta_3N_5, morphology varies with Ta:N ratio	[94]
ALD	Glass/FTO; $TaCl_5$ and NH_3, 550 °C	Ta_3N_5	[59]
Reactive templating	Ta precursor + graphitic-C_3N_4, (Ar + N_2 + NH_3) carrier gas, 750–1300 °C	TaN, Ta_2CN, and TaC	[95]
Ammonolysis of nanofibers	Tantalum ethoxide/PVP fibers, NH_3, 800–1000 °C for 8 h	1D Ta_3N_5-(O) nanofibers	[96]
Sol-gel	Alkoxide precursor + urea, (N_2 + 3 % H_2) 500–900 °C	Ta-O-N	[85]
Plasma-assisted DC sputtering	$N_2/(Ar+N_2)$= 0.05–0.15; Plasma power (W)= 100–400 W	TaN_x; N_2 fraction and W-dependent microstructure	[97]
Ammonolysis of sol-gel grown Ta-oxide	Carbon sphere, NH_3, 700–1150 °C for 2 h	TaON, Ta_3N_5, Ta_4N_5 and TaN	[84]
Hydrothermal + ammonolysis	(Ta foils + HF + H_2O_2 solution); ammonolysis at 1000 °C for 2 h	Ta_2O_5 nanorod	[67]
HP-HT synthesis	Compacted Ta_3N_5 powder, 1500–1700 °C, 11 GPa for 15–30 min	η-Ta_2N_3	[31]
HP-HT synthesis	Ta nitride and ammonium halide precursors, 1–5 GPa,1000–1400 °C	TN nanowire crystals	[98]
HT synthesis	Thermolysis of electrospun Ta_3N_5 fibers at ~1000 °C in N_2	θ-TaN	[32]
Confined ammonia looping	Ta–$(NCNH_2)_x$ precursor, 900–1000 °C; inert/Ar	Ta_4N_5 and Ta_3N_5	[99]
Decomposition + ammonolysis	Ta substrate, $Ta(EtO)_5$ + $TaCl_5$ precursor, NH_3 700–900 °C	Ta_3N_5	[100]
Self-sacrificial Ta_2O_5 template conversion	Na_2CO_3 + NH_3 flow at 600–950 °C (10 °C min^{-1}) for 0–5 h	Ta_3N_5 crystals	[101]
Mechanosynthesis	High-energy ball-milling of Ta and hexagonal boron nitride	Metastable cubic δ-$Ta_{1-x}N$	[102]
Ca reduction of oxides + nitridation	(750–900°C for 1–6 h)	Ta, θ-TaN and Ta_2N	[103]
Flux-assisted direct nitridation	Nitridation of Ta foil (NH_3, 900 °C, 2 h) in presence of flux ($CaCO_3$, $(NH_4)_2CO_3$)	Ta_3N_5	[69]
One-step low-temperature synthesis	Heating (Ta_2O_5 + NH_4C + Mg) in autoclave, 650°C for 10 h	Ta_2N nanocrystals	[104]

film resistors [52], and (photo)electrocatalysts [20,23,111,112].

Due to their high power density and low operating temperature, polymer electrolyte fuel cells and water electrolyzers —which use a thin polymer membrane with protonic conduction—are envisaged to be used for portable applications, particularly automotive use [113,114]. Currently, a highly dispersed cathode catalyst made of carbon powder and platinum is employed commercially to enable practical realization of a promising theoretical efficiency [115,116]. However, given the scarce deposits and exorbitant price of platinum, catalysts based on with nitrogen, phosphorus, and sulphur compounds of cheaper/earth-abundant transition metals are being pursued currently [117]. In this regard, given the highly acidic conditions in a PEM electrolyzers/fuel cells, transition metal nitrides offer superior properties in terms of long-term stability, electrical conductivity and low overpotential for water splitting/fuel cell reactions [118,119]. Among various transition metals, due to its high melting point, good biocompatibility and high corrosion resistance in concentrated and hot (up to 200 °C) acidic electrolytes, metallic Ta attracts a lot of interest and is regarded as a promising material [120–122]. Thus, tantalum-nitrides and oxynitrides for water splitting applications will be summarized in this section.

Initial studies by Ishihara et al. [123] found that Ta_3N_5 showed no visible catalytic activity with an onset potential of around 0.4 V vs. reversible hydrogen electrode (RHE) due to its poor conductivity, whereas $TaO_{0.92}N_{1.05}$ delivered appreciable current with an onset potential of 0.8 V vs. RHE (Fig. 1(a)). Similar studies on TaO_xN_y, electrophoretically deposited on titanium foil to improve the electrical contact between the current collector and the catalyst, exhibited an onset potential of 0.75 V vs. RHE. However, it displayed improved stability (Fig. 1(b)) in prevailing acidic medium (0.1 mol dm^{-3} H_2SO_4 at 50 °C) with a much lower solubility (3.3×10^{-3} mol dm^{-3}) compared to Pt (9.7×10^{-3} mol dm^{-3}) [124]. The authors were the first to report [123,125] that tantalum (oxy)nitride could provide sites for ORR, which also agreed with the theoretical studies by Watanabe et al. [126]. Moreover, Ishihara et al. [111] reported that tantalum oxynitride films prepared via radio frequency magnetron sputtering on glassy carbon substrate displayed different surface ionization potentials as a function of heat treatment temperature, as the ionization potential decreased with increasing temperature, which could be attributed to increased formation of surface oxygen defects (Fig. 1(c)).

In the study by Pasqualeti et al. [127], tantalum oxynitrides doped with titanium (Ti) and niobium (Nb) were synthesized to elucidate the impact of doping on ORR activity. The introduction of aliovalent titanium with a +4 charge led to a remarkable threefold enhancement in ORR activity, quantified by a substantial increase in current density. Specifically, at a potential of 0.3 V, the undoped catalyst exhibited a current density of 0.25 A g^{-1}, whereas the Ti-doped counterpart demonstrated a significantly elevated current density of 0.75 A g^{-1} at the same potential. Conversely, doping with niobium at a +5 charge showed negligible effects on ORR activity. This enhancement in ORR activity was attributed to the concurrent increase in electrical conductivity and the presence of surface defects, which facilitated more efficient reaction kinetics. However, despite the initial improvement, catalyst performance exhibited pronounced degradation after six hours. This degradation was ascribed to the formation and subsequent growth of tantalum oxide (TaO_x) species on the catalyst surface, impeding effective electron transfer to the active tantalum oxynitride (TaO_xN_y) species and resulting in a gradual decline in performance over time.

The role of various phases towards ORR activity of Ta-O-N system is investigated in a few reports [84,85,128]. Ohgi et al. [128] synthesized mixed compositions of $TaN/TaO_xN_y/Ta_2O_5$ by different degree of oxidation (DOO; ratio of oxygen-containing phases to overall phases) of TaN. The composition with DOO=0.27, having TaON as the only oxygen-containing phase (Fig. 2(a)), displayed maximum ORR activity in acidic medium with onset potential of 0.8 V (Fig. 2(b)). Moreover, the compositions exclusively containing TaN or Ta_2O_5 phase displayed low onset potential and negligible current density, indicating TaO_xN_y being the ORR-active phase in the composites. Similarly, Seifitokaldani et al. [85] investigated the effect of composition and processing temperature on ORR activity of mixed Ti and Ta oxynitride electrocatalysts prepared by urea-based sol-gel synthesis. During ORR activity test, the onset potential increased with increasing heat-treatment temperature or Ta content, which was attributed to the increase in surface area/-electrochemically active surface area with temperature, although no

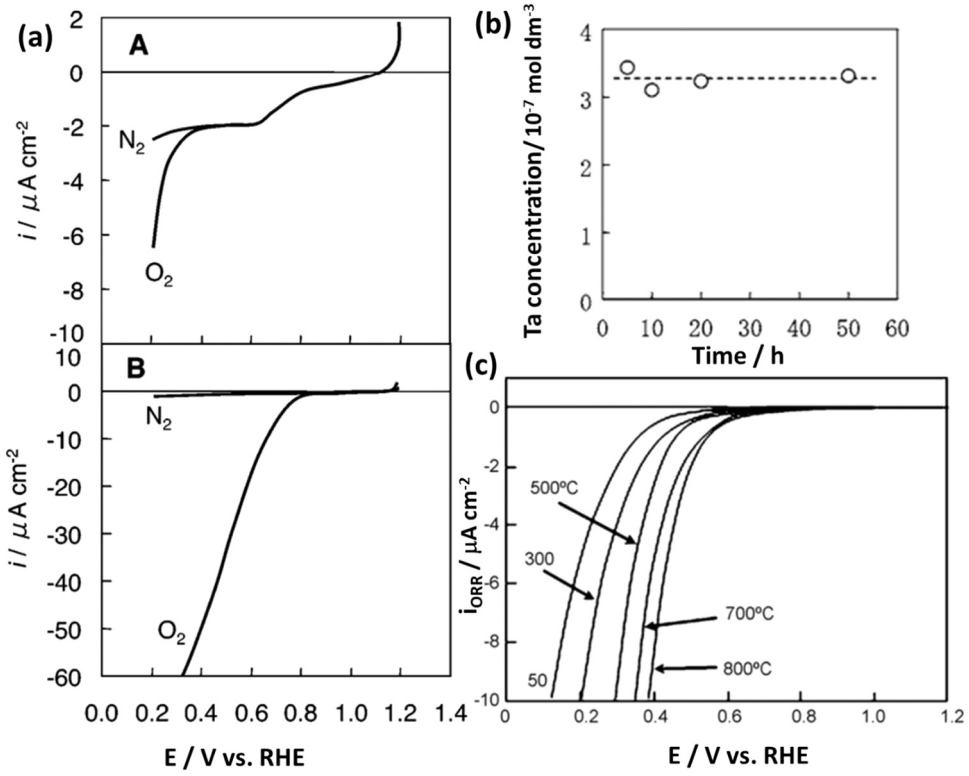

Fig. 1. Ta-O-N system as ORR electrocatalysts; (a) First reports of TaO_xN_y as ORR electrocatalyst, *Reused with permission from IOP publishing* [123]; (b) Excellent stability of TaO_xN_y in acidic solution for 60 h, *Reused with permission from IOP publishing* [124]; (c) Dependence of iORR/iN2 at 0.4 V of the TaO_xN_y on the substrate temperature [111].

surface area measurements were performed. The compositions were electrochemically stable (100 cycles). Electrochemical measurements concluded that the ORR activity of mixed compositions was in order of TaO_xN_y < $Ti_{0.25}Ta_{0.75}O_xN_y$ < $Ti_{0.75}Ta_{0.25}O_xN_y$ < TiO_xN_y, with TaO_xN_y displaying 100 times smaller current density than TiO_xN_y.

Till date, the most promising study designed to generate higher current densities with enhanced stability in Ta-O-N systems was reported by Wassner et al. [84]. In this study, by depositing tantalum oxide shell over a porous carbon core, which upon nitridation led to core shell structure. During nitridation, the Ta-O-N phases evolved with temperature, changing from amorphous TaO_xN_y (700 °C) to crystalline TaO_xN_y/Ta_3N_5 (850 °C), Ta_3N_5/Ta_4N_5 (1000 °C), and Ta_4N_5/TaN (1150 °C). The highest ORR activity was displayed by the composition nitrided at 1000 °C (TaON@CN-1000), with the onset potentials of 0.7 vs. RHE in acidic medium (0.5 M H_2SO_4; Fig. 2(b)) and 0.9 vs. RHE in alkaline medium (0.1 M KOH; Fig. 2(c)). Accelerated degradation test (ADT) for 1000 cycles displayed significant decrease in onset potential and current density (Fig. 2(d)). Correlating the electrochemical analysis with the post-mortem XPS and Transmission Electron Microscopy (TEM) analyses, authors concluded that surface oxidized Ta_4N_5 was the ORR active phase.

The earliest reports relating tantalum nitrides to HER involved Ta_3N_5 microparticles, synthesized via high temperature nitridation in NH_3 atmosphere at 800 °C, which showed an overpotential of 530 mV in 0.1 M H_2SO_4 solution [129]. In another study, tantalum nitride (Ta_3N_5/Ta) thin films obtained by ammonolysis of oxidized tantalum foil exhibited an overpotential of 540 mV vs RHE in 0.1 M H_3PO_4 solution at pH=4 [130]. Density Functional Theory (DFT) calculations by Abghoui et al. [19] indicated that for HER tantalum nitrides have a low overpotential (0.09 eV) compared to other transition metal nitrides and an activation energy on par with platinum (Fig. 3).

Alhajri et al. [95] prepared Ta-N-C nanocatalysts by reacting tantalum precursor with mesoporous graphitic carbon nitride at different temperatures in nitrogen atmosphere. The samples prepared at 750 and 850 °C exclusively contained tantalum nitride phases and displayed significant HER activity in acidic condition (Fig. 3(c)). The sample prepared at 750 °C, having TaN as the major phase, observed the lowest overpotential of 160 mV. Increased electrocatalysis by TaN, which otherwise have low HER activity, was attributed to electron tunneling from the conductive substrate to the TaN catalyst surface. Zhang et al. [112] reported fabrication of porous Ta_5N_6 centimeter-scale single crystals, grown on the $LiTaO_3$ crystal through high-temperature nitridation in NH_3 atmosphere. The resulting single crystals possessed high density of active metal–nitrogen moieties on an interconnected open framework, which could provide long-range electronic connectivity and electroactivity. When applied for HER activity, Ta_5N_6 crystals delivered stable current density of 10 mA cm^{-2} at an overpotential of 84 mV for >120 h, displaying a performance at par with the current state-of-the-art non-noble earth-abundant catalysts (Fig. 3(d)). Recently, carbon-coated cobalt nanoparticles spatially distributed on a porous Ta_3N_5 film demonstrated bifunctional (OER and HER) electrocatalytic behavior (Fig. 4(e)) [131]. The ensemble of highly active cobalt nanoparticles grown inside the Ta_3N_5 substrate having an ideal Gibbs adsorption free energy of zero led to such an outstanding behavior. Also, the presence of nitrogen doped carbon core shell structure with a high surface area allowed enhanced electron transfer, resulting in a hydrogen evolution overpotential of 59.1 mV and 93 mV in acidic and alkaline medium. Further, low overpotentials of 358 mV were required for oxygen evolution to occur in 1 M KOH. Moreover, the exciting potential of Ta-N systems towards HER was recently demonstrated by Yan et al. [132] where platinum deposited on tantalum nitride nanorods exhibited an over potential of 27 mV at a current density of 10 mA cm^{-2} with stability of over 2000 cycles.

We have performed a few studies to improve the electrocatalytic behavior of T-O-N system towards HER [93,96,133]. Mukkavilli et al. [96] obtained nanostructured 1D Ta_3N_5-(O) fibers through a

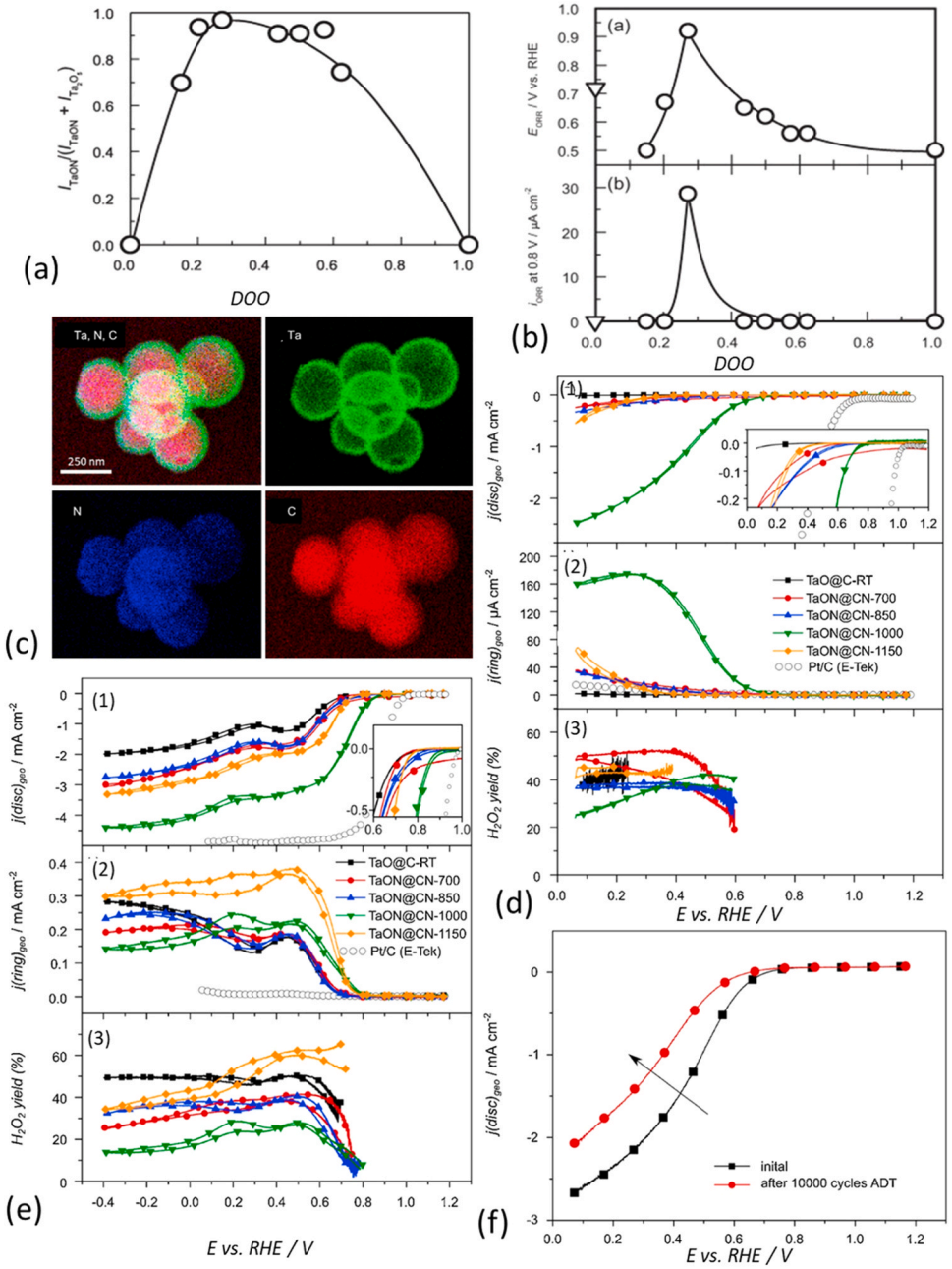

Fig. 2.
(a) Variation of TaON/TaON+Ta_2O_5 ratio (a) and ORR activity (b) with DOO in T-O-N system, *Reused with permission from Elsevier* [128]; Elemental mapping of TaON@CN-700 showing overlay of Ta (green), N (blue) and C (red) elemental maps (c); ORR current densities (1), ring current densities (2) and H_2O_2-yield (3) with TaON@CN samples and commercial Pt/C catalyst (catalyst loading=0.28 mg cm^{-2}) in O_2-saturated 0.5 M H_2SO_4 (d) and O_2-saturated 0.1 M KOH (e); ADT showing ORR activity of TaON@CN-1000 before (initial) and after (10000 cycles) (O_2-saturated 0.5 M H_2SO_4, 1600 rpm, 10 mV s^{-1}), catalyst loading of 0.28 mg cm^{-2} (f), *Reused with permission from Elsevier* [84].

combination of electrospinning and thermal ammonolysis (Fig. 4(c)). The electrocatalyst demonstrated enhanced HER activity in acid medium, displaying an overpotential of 320 mV to deliver 10 mA cm^{-2} at a low mass loading of 0.15 mg cm^{-2}. When applied to a PEM water electrolyzer, the electrocatalyst delivered a performance (0.1 A cm^{-2} for 6 h) on par with earth-abundant electrocatalysts such as MoS_2 (Fig. 4 (d)). Similarly, Thiyagarajan et al. [93] reported chemical vapor deposited amorphous $Ta(O)_xN_y$ coating on nickel foam (NF) as a potential HER electrocatalyst (Fig. 4(a)). The self-supported $Ta(O)_xN_y$/NF electrocatalyst displayed improved HER activity compared to the NF (Fig. 4(b)), with a lower onset overpotential (50 mV vs. 166 mV) and Tafel slope (151 mV dec^{-1} vs. 179 mV dec^{-1}) in 0.5 M H_2SO_4. The authors proposed a synergistic effect between nickel foam (having strong H_2O adsorption but weak H desorption) and tantalum (having weak H_2O adsorption but strong H desorption) as the major contributing factor for enhanced hydrogen evolution kinetics. Moreover, Mukkavilli et al. [133] investigated electrocatalytic HER activity of tantalum oxynitride (TaO_xN_{1-x}) fibers with a diameter of 800 nm, synthesized using a centrifugal spinning method that focused on large-scale, safe and rapid synthesis of fibers. The oxynitride fibers exhibited excellent electrocatalytic performance, requiring lower overpotential (250 mV) to achieve a current density of 10 mA cm^{-2} in acidic medium. However, the activity of oxynitride fibers diminished in basic environment, due to the high oxyphilicity of tantalum ions and negative Gibbs adsorption free

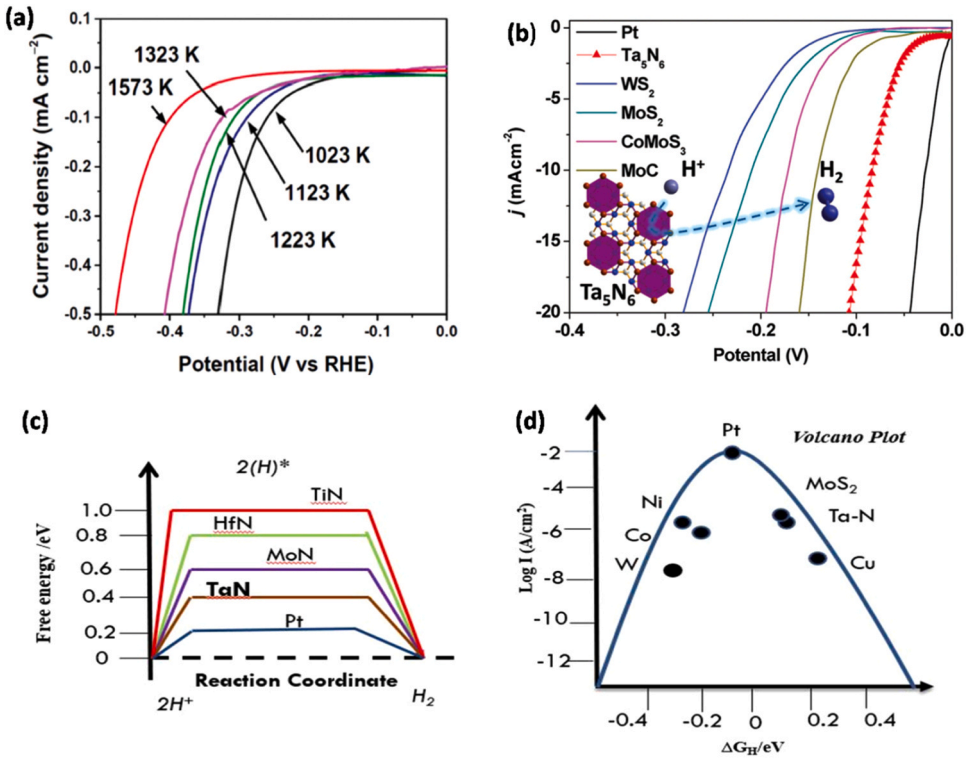

Fig. 3. Ta-N system as electrocatalysts for HER: (a) HER voltammograms of tantalum-based samples synthesized at different temperatures under N_2 flow, *Reused with permission from RSC* [95]; (b) Comparison of the best performing Ta-N phase (Ta_5N_6) with the state-of-the-art non-noble metal based electrocatalysts for HER in 0.5 M H_2SO_4, *Reused with permission from Wiley* [112]; (c) the free energy/ eV in Ta-N system nearest to platinum compared to other transition metal nitrides, and (d) Volcano plot indicating the unraveled potential of Ta-N with an optimum Gibbs adsorption free energy, *Adapted with permission from American Chemical Society Copyright {2024}* [19].

energy (−0.62 vs. 0.15 eV in acid medium, obtained from computational methods) that led to the poisoning of active sites.

The important results pertaining to the HER and ORR activity of Ta-(O)-N systems is presented in Table 2. Nevertheless, the electrocatalytic behavior of Ta-(O)-N system is recently investigated for some other electrochemical processes, such as formic acid oxidation [134], methanol oxidation [134,135], ethanol oxidation [136], triiodide reduction [137,138], polysulfide interconversion [139], and ethylene glycol oxidation [140,141]. Dang et al. [137] investigated triiodide reduction activity of Ta-O-N counter electrodes in dye-sensitized solar cells. From electrochemical impedance spectroscopy (EIS) measurements, TaO_x, TaON, and Ta_3N_5 displayed charge transfer resistance (R_{ct}) of 22.66, 11.38, and 25.21 Ω cm^2, respectively, and from polarization measurements the limiting current density was in order of TaON > TaO_x > Ta_3N_5, indicating higher electron transfer ability and electrocatalytic activity of TaON. Ye et al. [134,142] investigated the role of TaN phase in alkaline methanol oxidation reaction and acidic formic acid oxidation reaction, using Pd/TaN, PdCu/TaN-C and Pd/TaN-C composite electrocatalysts. The catalysts displayed enhanced reaction kinetics, anti-CO poisoning and stability compared to the commercial Pd/C catalyst, which, based on experiments and theoretical calculations, was attributed to strong interfacial interaction between metal and TaN phases that led to unique electronic structure and proper d-band center. Moreover, encouraged by the ability of TaN to favorably influence the electronic structure of metals, Ye et al. [136,143,144] reported PdSn/TaN/C electrocatalyst for C-C bond splitting in alkaline ethanol oxidation and $PdNi_x(OH)_y$-TaN/C and non-noble metal-based NiCu(Sn)-TaN/C electrocatalysts for alkaline methanol oxidation.

The catalytic performance of transition metal nitrides (TMNs) arises from the d-band contraction in metal centers due to nitrogen incorporation [145]. Transition metal doping can further redistribute the d-band electronic configuration in TMNs, forming new spin-polarized valence bands [146]. This enhances electron donor capacity for adjacent metal centers and boosts electrical conductivity. The electronic interaction between the adsorbate valence states and transition-metal d states induces the formation of separate bonding and antibonding states. The bonding states, fully filled with electrons, are far below the Fermi level (E_f), while the antibonding states, near the E_f, contribute to bond strength. Therefore, the d-band center (E_d) model effectively describes the adsorbate-metal interaction. For instance, simultaneous doping of cobalt and aluminum in TMNs led to the formation of d-band centers with energies significantly lower than the E_f energy [147]. This configuration allowed more electrons to transfer to antibonding states, thereby lowering the hydrogen adsorption energy and improving the HER behavior. Compared to pristine Fe_2N, which required an overpotential of 461 mV to achieve a current density of 10 mA cm^{-2}, only 146 mV was needed upon cobalt and aluminum co-doping to achieve the same current densities. Similarly, Cr-doped Co_4N nanorod arrays on carbon cloth (Cr–Co_4N/CC) exhibited remarkable HER performance with an extremely low overpotential of 21 mV to achieve a current density of 10 mA cm^{-2}, along with long-term stability in 1.0 M KOH solution [148]. Cr doping modifies the electronic structure of Co_4N, shifting the d-band center of Co atoms further from the Fermi level. This adjustment enhances the HER activity of Cr–Co_4N. Chen et al. [149] reported that V-doped Co_4N (V-Co_4N) nanosheets exhibit an overpotential of 37 mV at 10 mA cm^{-2} in alkaline media, outperforming Co_4N and nearing the efficiency of benchmark Pt/C catalysts. The E_d of Co_4N and V-Co_4N, calculated to be −1.79 eV and −1.85 eV relative to the E_f respectively, demonstrate that V doping shifts the d-band center further from the Fermi level. Also, Yao et al. [150] reported Co-doped WN nanowire arrays grown on carbon cloth reveal that Co dopants not only serve as active sites but also enhance the activity of W sites by shifting the d-band center of W sites downward due to electron transfer from W to Co. The HER catalytic activity of WN can be effectively

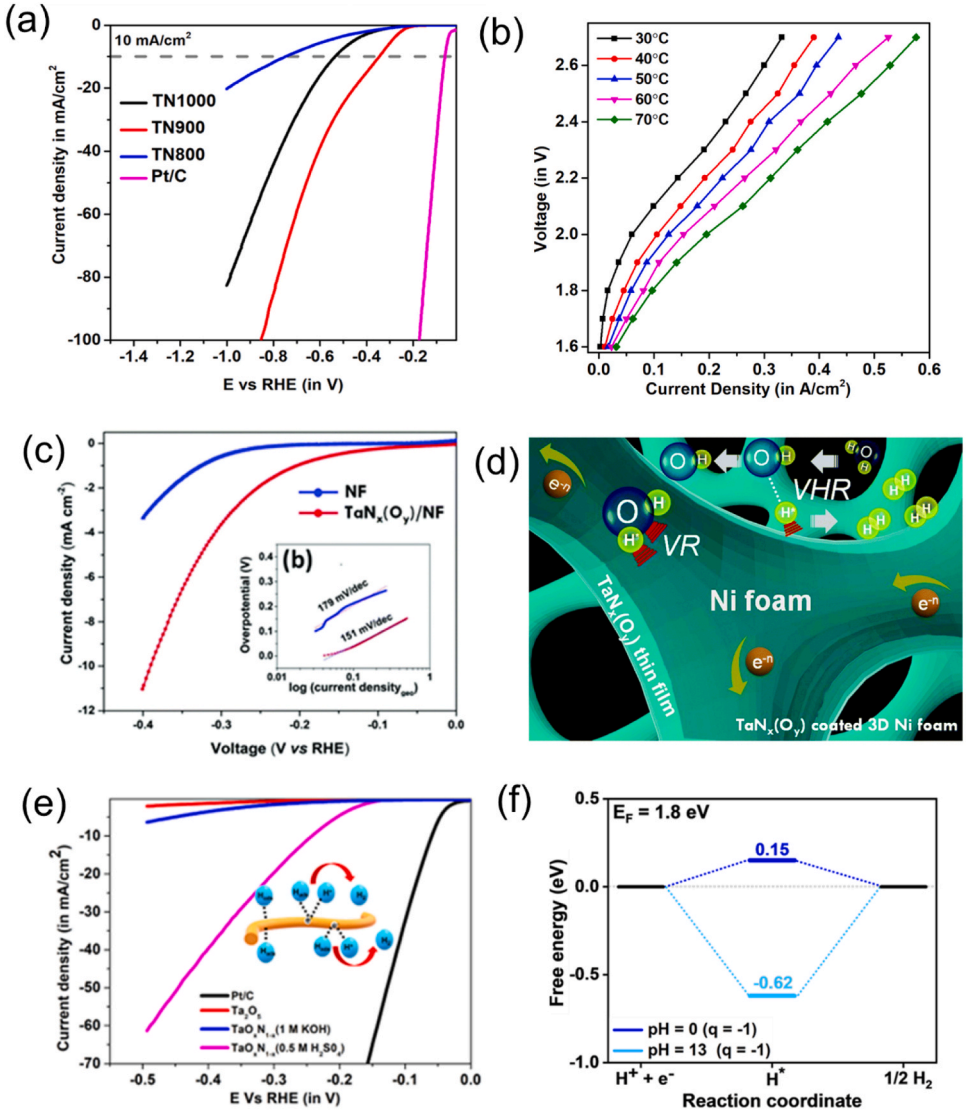

Fig. 4. Attempts to improve the electrocatalytic HER through various strategies, (a) & (b) Electrospun 1D fibers leading to hydrogen evolution kinetics on par with other earth-abundant electrocatalysts such as MoS_2 [96]; (c) & (d) Self-supported amorphous Ta_3N_5-(O) thin film resulting in lower charge transfer resistance than Nickel foam [93]; (e) & (f) large scale synthesis of centrifugally spun TaO_xN_{1-x} demonstrating an over potential of 250 mV vs RHE, poor HER kinetics in basic media attributed to negative Gibbs adsorption free energy resulting in poisoning of active sites [133].

controlled by adjusting its d-band electronic structure. Co dopants not only alter the electronic properties of WN but also serve as highly active sites. The optimal HER performance is achieved with the composition Co/WN-20 having atomic ratio of Co/W about 12.2 %, which exhibits a low overpotential (η_{10}) of 151 mV and a Tafel slope of 82 mV dec^{-1} in alkaline solution, 209 mV and 92 mV dec^{-1} in acidic solution, and 165 mV and 92 mV dec^{-1} in neutral solution. Additionally, the catalyst demonstrated excellent durability, maintaining 99 % voltage retention after 20 hours. Recent study has demonstrated that co-doping vanadium nitride (VN) nanowires with cobalt (Co) and phosphorus (P) leverages the synergistic effects of Co, P and VN, resulting in superior properties for both HER and OER [151]. Specifically, this catalyst exhibited notably lower onset overpotentials (137 mV for HER and 335 mV for OER) and reduced Tafel slopes, alongside improved stability compared to VN and VN-Co counterparts. Electronic structure modification based on d-band modulation is an unexplored strategy in the realm of tantalum nitrides. Also, Reports indicate that transition metal-based carbonitrides provide significant advantages over pristine carbides and nitrides, such as the formation of heterostructures that enhance catalytic activity [152–155]. However, there are limited studies on the catalytic behavior of tantalum carbonitrides, where both nitrogen and carbon are incorporated simultaneously into the tantalum lattice. In this context, we developed a straightforward method for synthesizing TaCN/TaN nanocomposites on Ta foil using melamine and thiourea, without NH_3 and at lower temperatures [156]. XRD and Raman studies confirmed the formation of TaCxNy, with thiourea also revealing Ta_2CS_2 and g-C_3N_4. SEM and XPS analyses indicated Ta-C-S bonds. The catalyst from thiourea showed superior electrocatalytic performance compared to melamine, delivering 8 mA cm^{-2} at 350 mV vs RHE, versus 0.8 mA cm^{-2} for melamine. EIS showed lower resistance for Ta/thiourea (2.5 Ω) compared to Ta/melamine (40 Ω), attributed to the improved charge transfer and reduced interfacial resistance of the Ta-C-S structure.

In summary, the electrocatalytic behavior of Ta-O-N phases demonstrates the importance of nanostructuring. Especially in the case of HER, the earliest reports on Ta_3N_5 micro particles or even when grown as a thin film exhibited poor HER kinetics with overpotentials >500 mV vs. RHE. In contrast, the nanostructured fibers or porous self-supported architectures improved the performance. Also, in terms of phases, the best performing HER electrocatalyst was found to be Ta_5N_6 wherein its metallic nature was enough to generate 10 mA cm^{-2} at a low

Table 2
A summary of various Ta-O-N electrocatalysts for HER and ORR.

S.No	Electrocatalyst (reaction type)	Electrolyte	Parameters (Vs RHE)	Reference
1.	TaO_xN_y (ORR)	0.1 M H_2SO_4	0.8 V	[123]
2.	TaO_xN_y/CNT (ORR)	0.1 M H_2SO_4	0.9 V	[161]
3.	TaO_xN_y/Ti	0.1 M H_2SO_4	0.75 V	[124]
4.	TaO_xN_y film/glassy carbon (ORR)	0.1 M H_2SO_4	0.75 V	[111]
5.	TaO_xN_y/Ta_2O_5 (ORR)	0.1 M H_2SO_4	0.8 V	[128]
6.	Ti/TaO_xN_y	0.1 M H_2SO_4	0.7 A g^{-1} at 0.3 V RHE	[127]
7	Nb/TaO_xN_y	0.1 M H_2SO_4	0.1 A g^{-1} at 0.3 V NHE	
8.	TaO_xN_y/CN spheres (ORR)	M $H_2SO_4$0.5 M KOH	0.7 V 0.9 V	[84]
6.	Ta_3N_5 particles (HER)	0.1 M H_2SO_4	η_{onset} ~ 530 mV	[129]
7.	Ta_3N_5/Ta thin film (HER)	0.1 M H_3PO_4	η_{onset} ~ 540 mV	[130]
8.	TaN ((HER)	0.05 M H_2SO_4	η_{onset} ~ 160 mV	[95]
9.	Ta_5N_6 ((HER)	0.5 M H_2SO_4	η_{10}= 84 mV	[112]
10.	TaO_xN_y/Ni ((HER)	0.5 M H_2SO_4	η_{onset} ~ 50 mV	[93]
11.	Ta_3N_5/ 1D fibres (HER)	0.5 M H_2SO_4	η_{10} = 320 mV	[96]
12.	Co/Ta_3N_5 (HER)	0.5 M H_2SO_4 1 M KOH	η_{onset} ~ 59.1 mV η_{onset} ~ 93 mV	[131]
13.	TaO_xN_y (HER)	0.5 M H_2SO_4 1 M KOH	η10 =320 mV η1 = 320 mV	[133]

η: overpotential (Vs RHE); η_1: Overpotential required to deliver 1 mA cm^{-2}; η_{10}: Overpotential required to deliver 10 mA cm^{-2}; NHE: Normal Hydrogen Electrode; RHE: Reversible Hydrogen Electrode.

overpotential of 85 mV. Another common thread in almost all of the reports is the inevitable presence of oxygen impurities and surface oxidation of the Ta-N phases. Though the presence of surface-oxidation activation layer boosts the performance of the catalyst in some cases, it limits the stability, due to continuous oxidation rendering inactivity as the testing progresses. Interestingly, this concern is not limited to only electrocatalysts [157,158]. In fact, in photo-electrocatalysis, during illumination, the generated carriers (e^-/h pairs) cause self-oxidation/reduction of the catalysts, deteriorating the catalytic activity. Incidentally, Ta_3N_5 boasts of a high theoretical solar-to-hydrogen conversion efficiency of 15.2 %, but in practice the maximum possible conversion rate was only 3 % [159,160]. This disparity is due to the phenomenon of photocorrosion that impedes lab-to-fab transfer and, therefore, in the next section various mitigation strategies to address photodegradation is summarized.

3. Influence of oxygen impurities and photocorrosion

3.1. Addressing photocorrosion in Ta-N phases

One of the glaring drawbacks with industrial application of Ta_3N_5 despite its high theoretical efficiency is self-induced oxidation or photocorrosion. Ta_3N_5 undergoes surface oxidation upon reaction with accumulated holes on the surface as shown in the reaction below:

$$Ta_3N_5 + 15h^+ + 15OH^- \rightarrow \frac{3}{2}\ Ta_2O_5 + \frac{5}{2}N_2 + \frac{15}{2}H_2 \quad (1)$$

The formed oxide layer can induce positive band gap shift and thereby increased charge transfer resistance at the electrode/electrolyte interface. Further, this may also lead to the formation of amorphous Ta_xON_y layer. Such surface oxidation can result in retarded carrier transfer kinetics, lowered photon transmission due to the scattering and absorption by the oxide layer, and consequently increased charge transfer resistance [162,163]. Interestingly, the majority of the non-oxide semiconductors are unstable in the aqueous media, as there is a propensity for anions such as N^{3-}, P^{3-}, and S^{2-} to undergo transformation to their stable counterparts. This also extends to tantalum oxynitride, which in principle should imbibe the stability of the parent oxide and at the same time demonstrate an improved photocatalytic behavior, due to a reduction in band gap. However, with its band edge position similar to Ta_3N_5, TaO_xN_y also undergoes oxidation by the photo-illuminated holes (Fig. 5) [164].

Thin amorphous oxide layer on the surface resulted in a drop of efficiency by 50 % in a span of minutes, especially when there was no deposition of any passive layer. In this regard, various strategies were tried out to enhance the stability and improve the performance [72]. Among these, nanostructuring for enhanced surface reaction sites and facilitated charge carriers separation and transport [88,165–171], use of co-catalyst and hole storage layer for timely extraction of photogenerated holes [89,172–174], metal doping or surface modification by metal salts for enhanced charge carriers separation and carrier transport [167,169,175–179], and passivation by grafting and surface protection layer [180–186] (Table 3). Initial studies involved deposition of oxygen evolution catalysts, such as NiOOH and FeOOH, which act as hole extraction sites, thus increasing the stability (Fig. 6) [89,174,187,188]. For instance, in a study by Xu et al. [188] $Co(OH)_x$ decorated Ta_3N_5 nanotubes displayed an impressive current density of 2.3 mA cm^{-2}, albeit low stability. This was then overcome by deposition of a double co-catalyst layer of cobalt phosphate (Co-Pi) which acted as hole storage layer (HSL), slowing down the photocorrosion caused by the holes on the surface. However, given the ion-permeable nature of such catalysts to hydroxide ions, an overall degradation could not be averted. Wang et al. [89] fabricated arrays of Ta_3N_5 nanorods by template-anodization of Ta foil to Ta_2O_5 nanorods and subsequent nitridation at 1000 °C for 2 h (Fig. 6(a)). The nanorods were decorated with NiFe layered double hydroxide (LDH) co-catalyst to inhibit the photocorrosion. The resulting NiFe-LDH/Ta_3N_5 photoanode retained ~90 % photocurrent density even after 2 hours of irradiation. Further, loading the NiFe-LDH/Ta_3N_5 with Co-Pi and $Co(OH)_x$ to obtain Co-Pi+$Co(OH)_x$/NiFe-LDH/Ta_3N_5 configuration resulted in a photocurrent density of 6.3 mA cm^{-2} at 1.23 V.

The inability of co-catalyst layers in completely preventing the photocorrosion has prompted search for coatings that can lead to well-passivated surfaces. One such study involved deposition of 50 nm thick GaN on Ta_3N_5 in conjunction with Co-Pi co-catalyst, resulting in an onset potential by 150 mV and a stable photocurrent density of 8 mA cm^{-2} at 1.2 V vs. RHE for >10 h (Fig. 7) [181]. GaN by virtue of its corrosion resistance and suitable band gap positions to reduce charge recombination, coupled with its superior hole-lifetime, enabled enhanced stability for over 12 h. Nurlaela et al. [189] worked on enhancing the hole transfer efficiency from Ta_3N_5 layer to Mg-doped gallium nitride (Mg:GaN) layer deposited on the surface. The Ta_3N_5 film was grown by RF magnetron sputtering and subsequent nitridation, whereas Mg:GaN was deposited on its surface by plasma-enhance chemical vapor deposition and subsequent annealing under N_2/NH_3 atmosphere. For Mg:GaN films post annealed in N_2, the band positions altered favorably, leading to a more efficient charge transfer from Ta_3N_5 to Mg:GaN that resulted in the photoanode exhibiting onset potential of 0 V. However, the photocurrent density was lower than the bare Ta_3N_5 film, whereas the Mg:GaN films post-annealed in NH_3 displayed a photocurrent density on par with the bare Ta_3N_5, with an onset potential of 0.35 V. This work brought forth the possibility of unassisted PEC performance, although further work to enhance the photocurrent density is still required.

Zhao et al. [190] demonstrated that photocorrosion can be substantially reduced by using an intermediate AlO_x dielectric layer between the Ta_3N_5 photoanode layer and ferrihydrite (Fh) hole storage layer. The dielectric AlO_x layer not only suppressed the formation of trap sites but also promoted the formation of a negatively charged interface that led to enhanced charge separation and higher photocurrents. The best performing Ta_3N_5 based photoanode, so far, displayed an

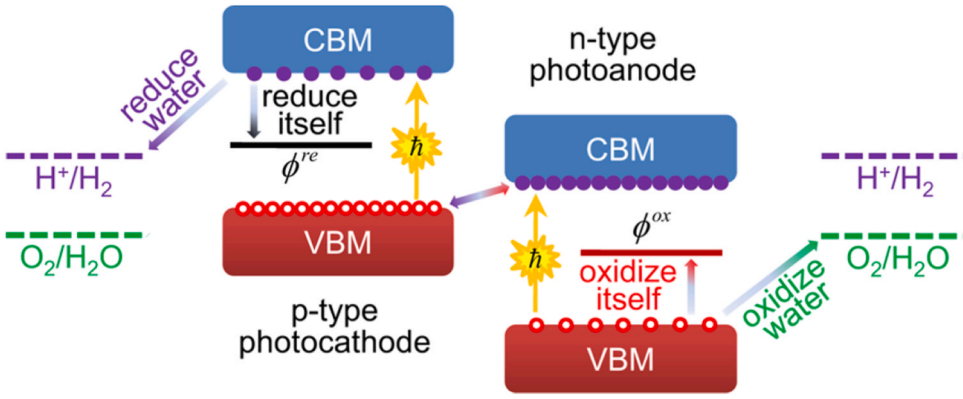

Fig. 5. Interplay of band-edge positions with respect to water oxidation potential as a major criterion for stability prediction.
(a) Interestingly, Ta_3N_5 and TaO_xN_y have their valence band minimum positioned at potentials higher than water oxidation potentials at all pH conditions leading to poor stability via self-oxidation, *Reprinted (adapted) with permission from American Chemical Society Copyright {2024}*[164].

Table 3
A summary of some important results addressing the photocorrosion of Ta_3N_5 photoanode.

Photoanode	OP/ PC	Stability	Ref.
NiCoFe-Bi/Gradient Mg:Ta_3N_5/Nb	0.4/ 8.00	Mg doping suppressed deep-level defects (5 h)	[204]
B doped–Ta_3N_5/Ta	0.25/ 0.95	B doping suppresses surface defects (5 h)	[72]
FeNiOx/Ta_3N_5-NRs/ Ta	~0.57/ 9.95	NRs do not undergo photocorrosion (70 min)	[50]
CoPi/Ba-Ta_3N_5/Ta	0.65/ 6.7	CoPi as an oxygen evolution cocatalyst (100 min)	[79]
$Co(OH)_x$/Ta_3N_5/Ta	0.82/ 5.5	Improved stability by surface exfoliation (2 h)	[210]
Co_3O_4/Fh/Ta_3N_5/Ta	~0.55/ 5.2	Fh as a HSL (6 h)	[174]
$Ni(OH)_x$/MoO_3/ Ta_3N_5/Ta	0.25/ ~2.25	$Ni(OH)_x$/MoO_3 bilayer as a HSL (24 h)	[198]
Co_3O_4/Fh/AlOx/ Ta_3N_5/Ta	~0.55/ 12.5	AlO_x layer enhance propensity of photogenerated holes migration from Ta_3N_5 to Fh (24 h)	[185]
CoPi/GaN/ Ta_3N_5/Ta	~0.65/ 8.0	conformal coating of p-type GaN on n-type Ta_3N_5 films form buried p/n junctions (12 h)	[181]
Co/Ir complex /Ni $(OH)_x$/Fh/TiO_x/ Ta_3N_5/Ta	~0.55/ 12.1	Co/Ir complex as a MO; $Ni(OH)_x$/Fh for extracting/collecting holes and passing the stored holes to MO; TiO_x as a blocking layer for spatial separation between electrons and oxidizing equivalents (Rapid decay of photocurrent after 30 min)	[187]

OP- Onset potential (V_{RHE}); PC-Photocurrent at ~1.23 V_{RHE} (mA cm^{-2}); MO- Molecular catalyst

ultra-stable photocurrent of 11.8 mA cm^{-2} at 1.23 V *vs.* RHE over 120 h (Fig. 8(a)) [190]. Das et al. [191] proposed the use of two-dimensional graphitic carbon nitride (g-C_3N_4) nanosheets to address photocorrosion of Ta_3N_5, primarily due to its narrow band gap energy (2.7 eV) visible light absorption-ability, and photostability in acidic and basic medium. Here, a thin *g*-C_3N_4 nanosheet layer was deposited over the Ta_3N_5 nanotubes (NT) grown onto Si substrate. Compared to Ta_3N_5 NT/Si photoanode, the *g*-C_3N_4/Ta_3N_5 NT/Si photoanode demonstrated 2-fold higher photocurrent density (0.59 mA cm^{-2} at 1.23 V_{RHE}) for 2 h in highly basic medium (Fig. 8(b)). Such an improved performance was attributed to a lower recombination rate leading to an improved charge carrier density (3.142×10^9 cm^3) and a lower R_{ct} (~ 940 Ω vs. ~15,000 Ω for Ta_3N_5/Si) leading to an effective charge transfer. In another study, electrodeposition was used to deposit CoOOH on Ta_3N_5 with a complex morphology. Further, in combination with Mg-doped Ta_3N_5, such a protective coating resulted in retention of 70 % of initial current density beyond 70 minutes. The presence of Mg further led to increased electronic conductivity, improved charge separation efficiency exhibiting a photocurrent of 6.6 mA cm^{-2} at 1.23 V vs RHE [170]. Tailoring the pH of the electrolyte and addition of hole scavengers ($Fe(CN)_6^{3-}$/$Fe(CN)_6^{4-}$, VO^{2+}, H_2O_2, Na_2SO_3, and KI) are also effective strategies for resisting photocorrosion of Ta_3N_5 [130,192–194]. For instance, the degradation mechanisms of Ta_3N_5 in different media were elucidated [192]. Irrespective of the pH of the electrolyte, the formation of TaO_x layer and its growth by transpassivation was observed. However, in the basic medium, by virtue of a narrow transpassive region, the Ta_3N_5 continued to oxidize and was not entirely protected leading to performance degradation. In contrast, in the acidic medium, only when the applied potential exceeded 2 V vs. RHE (a potential beyond the range of interest for water electrolysis (Fig. 8(c)), Ta_3N_5 being oxidized by transpassivation was observed. The authors attributed molecular (H_2O or H_3O^+) adsorption onto the passive TaO_x layer occurring only in acidic media as the additional cause for the enhanced corrosion protection. However, using a Co_3O_4/Ta_3N_5 photoanode, Liao et al. [195] demonstrated that changing the electrolyte from acidic Na_2SO_4 (pH ~ 6.5) to basic NaOH (pH ~ 13.5) led to improved performance and stability of photoanode. The numerous compact nano-junctions formed between uniformly distributed Co_3O_4 nanoparticles, which are highly stable water oxidation catalyst in alkaline medium, resulted in 75 % retention of the initial photocurrent post 2 h of illumination and an impressive current density of 3.1 mA cm^{-2} at 1.2 V vs. RHE. It is argued that the poor photostability and performance of Co_3O_4/Ta_3N_5 photoanode in Na_2SO_4 electrolyte may arise due to two factors- insufficient chemical stability of Co_3O_4 in acidic neighboring environment after oxygen production and/or the kinetic constraints on water oxidation due to the poor proton removal rate in neutral electrolyte. The alkaline pH of NaOH electrolyte improved the chemical stability of Co_3O_4/Ta_3N_5 photoanode. Moreover, as proton removal step is key step in water oxidation reaction, poor proton-accepting ability of the supporting electrolytes like Na_2SO_4, due to its neutral pH, makes the proton-diffusion process sluggish and leads to the accumulation of holes, resulting in a slow water oxidation kinetics. The high alkaline environment of NaOH electrolyte prevents the unfavorable accumulation of holes and also ensures faster removal of protons, thus contributing towards photostability and performance enhancement of Co_3O_4/Ta_3N_5 photoanode [195].

Wang et al. [197] used an ultrathin CoO_x interlayer between the Ta_3N_5 photoanode layer and $Ni(OH)_x$ HSL to improve performance and stability. During PEC water oxidation, reversible formation of Co(IV) species inside the CoO_x layer regulated the hole-storage process, facilitating the photogenerated hole extraction capacity and suppressing the charge recombination. As a result, compared to bare Ta_3N_5 and CoO_x/Ta_3N_5, the bilayer deposited Ta_3N_5 showed lower R_{ct} along with stable oxygen evolution for 30 h (Fig. 9(a)). Kim et al. [72] reported the

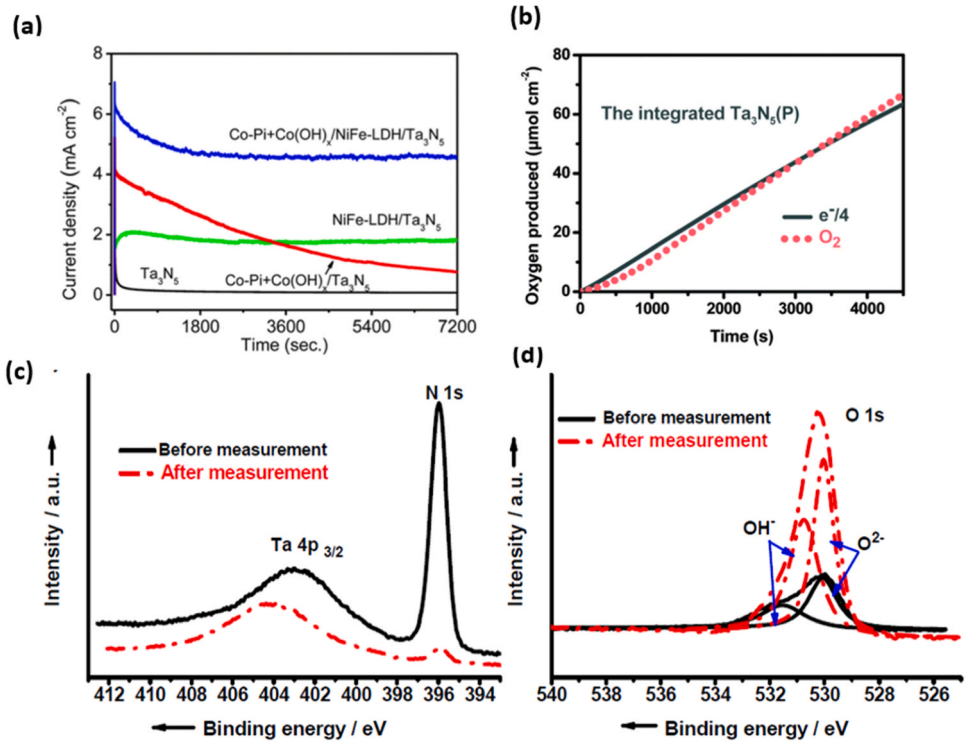

Fig. 6. (a) Rapid deterioration in current density values for bare Ta_3N_5, *Reprinted (adapted) with permission from American Chemical Society, Copyright {2024}* [89]; (b) increase in stability upon deposition of layered hydroxides based on nickel and iron *Reused with permission from RSC* [187]; (c) and (d) XPS analysis of bare Ta_3N_5 photoanode before and after measurement indicating increase in oxygen peak and negligible presence of nitrogen, if any, on the surface, *Reused with permission from Wiley* [174].

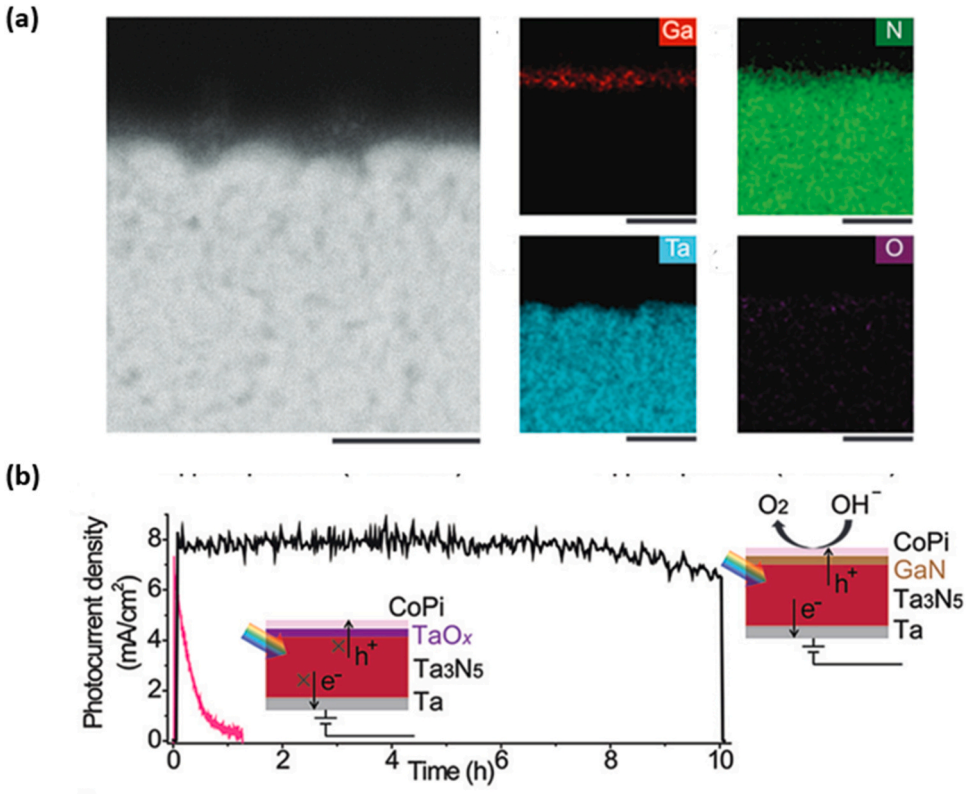

Fig. 7. (a) Cross-sectional Energy Dispersive Spectroscopy (EDS) mapping images of Scanning Transmission Electron Microscopy (STEM) image of GaN/Ta_3N_5 at a scale bar of 100 nm depicting a crystalline nitride on nitride structure, (b) Time-course photocurrent density curves for the CoPi/GaN/Ta_3N_5 (black) and CoPi/Ta_3N_5 (pink) photoanodes in 0.5 m KPi solutions at pH13 under simulated solar light (AM 1.5 G) illumination at 1.2V_{RHE} demonstrating stability for 10 h, *Reused with permission from Wiley* [181].

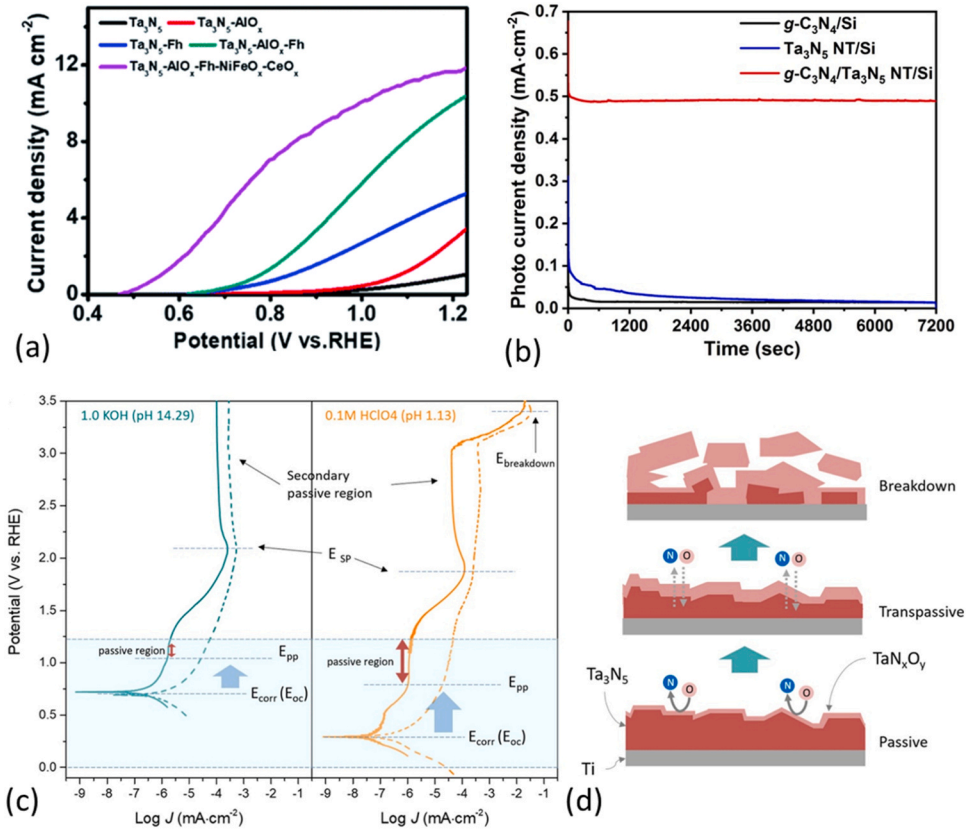

Fig. 8.
(a) (a) Current–potential curves of Ta_3N_5, Ta_3N_5–AlO_x, Ta_3N_5–Fh, Ta_3N_5–AlO_x–Fh, and Ta_3N_5–AlO_x–Fh–$NiFeO_x$–CeO_x photoanodes under AM 1.5 G simulated sunlight at 100 mW cm^{-2} in 1 M NaOH aqueous solution (pH = 13.6), *Reused with permission from RSC* [190]; (b) Chronoamperometry curve of *g*-C_3N_4/Si, Ta_3N_5NT/Si and *g*-C_3N_4/Ta_3N_5NT/Si films under AM 1.5 G simulated sunlight at 1.23 V in 0.5 M NaOH aqueous solution (pH = 12.5), *Reused with permission from Elsevier* [196]; (c) Potentiodynamic polarization curve of Ta_3N_5 in different electrolytes. (b) Dashed lined and the solid line was obtained by light illumination and dark condition, respectively and (d) schematic diagram of corrosion process of Ta_3N_5, *Reused with permission from Elsevier* [192].

effect of boron incorporation (0–30 at%) into Ta_3N_5 on improving the stability in acidic media. For 10 % B-Ta_3N_5 with Co-Pi as co-catalyst, a solar efficiency of 0.54 % was achieved at 0.9 V vs RHE (Fig. 9(b)). The improved performance was attributed to the presence of amorphous B-O bonds on the surface that played the crucial role of protecting the surface of Ta_3N_5 and changing the band gap edge positions, resulting in cathodic shift of the onset potential. Liu et al. [198] explored the efficacy of Ni$(OH)_x$/MoO_3 bilayer as a HSL to stabilize the Ta_3N_5 photoanode, composed of highly porous Ta_3N_5 cubes grown on Ta foil via nitridation of $NaTaO_3$ (Fig. 9(c)). The Ni$(OH)_x$/MoO_3/Ta_3N_5 photoanode observed 0.6 V reduction in cathodic onset potential, compared to the Ta_3N_5 photoanode, and delivered a stable photocurrent density for 24 h (Fig. 9 (d)).

Truc et al. [183,184] proposed the use of conducting polymers, such as polyaniline (PANI), polythiophene (PTh), and polypyrrole (PPy) for simultaneous charge carrier separation and photocorrosion protection in Ta_3N_5 photoanodes. It is proposed that in conducting polymer-covered Ta_3N_5 composites, the conducting polymer could act as charge acceptors for quick migration of the produced h^+ to their surface and thus minimize contact between the nitride and h^+, thus protecting the Ta_3N_5 particles from self-photocorrosion [183,184, 199–201]. These polymers due to their high charge transport properties and better absorption coefficients were also reported to enhance the photo catalytic activity when in conjunction with other materials such as MoS_2 and TiO_2 [202,203]. When applied for PEC water splitting in visible light, Ta_3N_5/PANI and Ta_3N_5/PTh delivered, respectively, 60.5 and 45.1 μmol g^{-1} h^{-1} of H_2, with PTh displaying slightly lower productivity owing to its inferior electrical conductivity compared to PANI [183]. Similarly, with Nb-Ta_3N_5/PPy photoanode, where Nb doping also led to a decrease in band gap, a stable production rate of 65.1 μmol g^{-1} h^{-1} of H_2 for 5 cycles was obtained [184]. Surface modification by metal doping [75,79,204–206] has been proposed for improving the photo-stability of Ta_3N_5 photoanodes. To achieve an optimum trade-off between light absorption and carrier transport while addressing the issue for photocorrosion, the strategy of dual atom doping is proposed [178,207–209]. Xiao et al. [207] employed a heterogeneous doping strategy for La and Mg doped Ta_3N_5 photoanode where surface La doping enhanced light absorption and gradient Mg doping resulted in efficient carrier transport in the bulk. Recently, Wang et al. [178] used dual atom (Cu and Zr) doping for morphology modification and band structure modulation of Ta_3N_5. In a two-step method, Cu doping and a pressure-assisted gradient doping of Zr (Zr_g) was performed which resulted in bending of band structure of Ta_3N_5 to form a built-in electric field. The Cu,Zr_g suppresses grain boundary recombination by allowing rapid transfer of electrons to the surface of Cu,Zr_g–Ta_3N_5. When used as photoanode along with a borate-intercalated NiCoFe-LDH (denoted as NiCoFe-B_i) co-catalyst in 1 M KOH under AM 1.5 G simulated sunlight, the NiCoFe–B_i/Cu,Zr_g–Ta_3N_5/FTO resulted in the best performance for FTO-based Ta_3N_5 photoanodes, displaying an onset potential of 0.38 V_{RHE} and a photocurrent density of 8.9 mA cm^{-2} at 1.23 V_{RHE} (Fig. 10).

3.2. *Role of oxygen impurities in Ta-N system on the photoelectrocatalytic behaviour*

The results of PEC measurements have indicated a synthesis method-

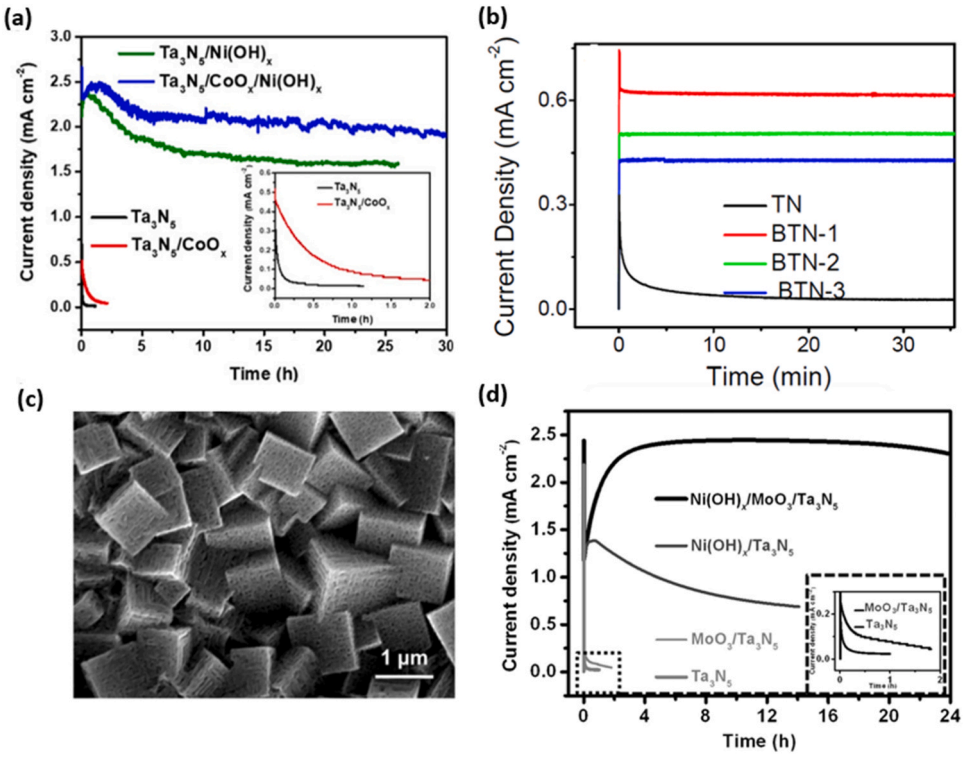

Fig. 9. (a) Stable oxygen evolution over a period of 30 h upon growth of CoOx and $Ni(OH)_x$ on Ta_3N_5 as hole-storage layers, *Reprinted (adapted) with permission from American Chemical Society Copyright {2024}* [197]; (b) boron doped Ta_3N_5 also displaying stable photocurrents, *Reprinted (adapted) with permission from American Chemical Society Copyright {2024}* [72]; (c) Highly porous Ta_3N_5 cubes grown on Ta foil obtained via nitridation of $NaTaO_3$, and (d) $Ni(OH)_x/MoO_3$ as hole storage layers on porous Ta_3N_5 exhibiting stability till 24 h, *Reused with permission from Wiley* [198].

dependent water splitting performance behaviour by Ta_3N_5, which is closely related with the oxygen impurities that are either present as a residue from the ammonolysis/nitridation of oxide precursor or incorporated during synthesis [39,211]. Additionally, as Ta_3N_5 can be easily oxidized during PEC applications, certain crystallographic facets may experience different rate of oxidation [212]. Theoretical calculations have indicated that the incorporation of oxygen impurities alter the PEC properties of Ta_3N_5 [83,212–214], and therefore for designing a durable Ta_3N_5 photoanode, role of oxygen impurities and exposed facets need to be examined. Khan et al. [215] reported the influence of oxygen concentration on PEC water splitting behaviour of anodized porous Ta_3N_5 nanotubes (Fig. 11). It was observed that Ta_3N_5 NTs with preferential orientation along the (110) direction, obtained by a careful optimization of ammonolysis temperature (800–1000 °C), displayed better performance than previously reported doped Ta_3N_5 phases. With increasing ammonolysis temperature, the crystallinity and grain size of Ta_3N_5 NTs increased whereas the oxygen content decreased. The Ta_3N_5 NTs obtained at 900 °C exhibited maximum photogenerated current density of 7.4 mA cm^{-2}. The NTs obtained at 800 and 1000 °C displayed lower performance, the former one due to its lower crystallinity and the later one due to the compromise on nanotube morphology. Moreover, R_{ct} (from EIS, Fig. 11(b)) and carrier recombination rate (from photoluminescence spectra) decreased with increasing for ammonolysis temperature (800–900 °C), further emphasizing the role of crystallinity and crystallographic orientation, grain size and oxygen content on PEC behaviour of Ta_3N_5.

To quantify variations in photoelectrochemically-relevant properties as a function of oxygen content, Rudolph et al. [216,217] prepared magnetron sputtered Ta_3N_5 thin films with different concentrations of oxygen (C_{O2}). The investigation of stability by XPS, before and after the photoelectrolysis, indicated that although certain amount of oxygen was invariably necessary for the formation and stabilization of Ta_3N_5 phase, the material properties deteriorated with increased oxygen incorporation during the film growth [217]. Specimen deposited at C_{O2}<1 % displayed lower bandgap (<2.0 eV), higher charge diffusion path length, and good surface stability (Fig. 11(c)). Whereas the deposition at higher C_{O2} resulted in the amorphization and surface–oxidation, with subsequent loss in stability due to the reaction with electrolyte during photoelectrolysis.

Similarly, Narkeviciute and Jaramillo [94] investigated the role of oxygen on the performance of Si-Ta_3N_5 photoanodes having different composition and morphology, and fabricated by nitridation of thin (10 nm) Ta_2O_5 films deposited on planar or nanostructured Si substrate. With increasing ammonolysis temperature (700–1000 °C), the oxygen content increased (10–20 at%), thereby decreasing N/Ta ratio and forming the domains of N-deficient and correspondingly O-rich areas. A direct correlation between the oxygen content and the overall catalytic activity was observed (Fig. 11(d)), as O defects could act as recombination centers or, when present at the surface, as a hole-blocking layer to the electrolyte.

Moreover, given the multitude of phases in Ta-N system, few studies also reported on the role of oxygen incorporation in synthesis and photoresponse of metastable tantalum sesquinitride (Ta_2N_3) sputtered films. Ta_2N_3 being electronically conductive transformed into a semiconductor, by virtue of oxygen incorporation during the synthesis. With a band gap of 1.6 eV and in the presence of a sacrificial hole acceptor, Ta_2N_3–(O) films with a n-type character exhibited an onset potential of 0.8 V vs RHE [91].

In summary, the susceptibility of Ta-N phases to photocorrosion underscores the need to assess their stability and understand the contributing factors. Consequently, it becomes crucial for a fundamental understanding of intrinsic properties of Ta-N system in the presence of oxygen. Standard methods commonly employed to explore electrode corrosion and photostability encompass electrochemical techniques like cyclic voltammetry and chronoamperometry/chronopotentiometry. These methods allow the observation of changes in PEC behavior.

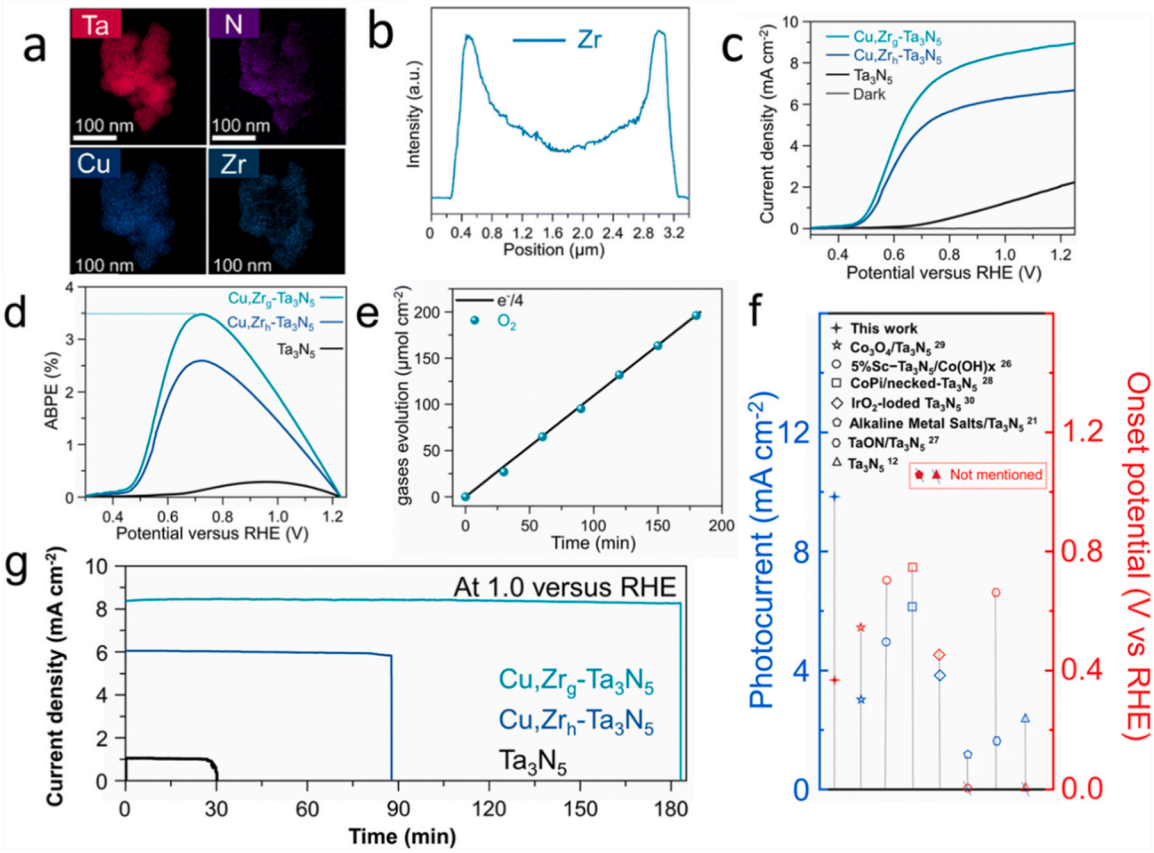

Fig. 10. (a) EDS elemental mappings images of Cu,Zr$_g$–Ta$_3$N$_5$, (b) the corresponding line-scan EDS profile obtained along the cyan dotted-line from (a) photoanodes with a NiCoFe–B$_i$ co-catalyst in 1 M KOH under AM 1.5 G simulated sunlight; (c) *J–V* curves of Ta$_3$N$_5$, Cu,Zr$_h$–Ta$_3$N$_5$ and Cu,Zr$_g$–Ta$_3$N$_5$ photoanodes with a NiCoFe–B$_i$ co-catalyst in 1 M KOH under AM 1.5 G simulated sunlight; (d) ABPE of the photoanodes calculated from the *J–V* curves in (c); (e) amount of oxygen evolved from the NiCoFe–B$_i$/Cu,Zr$_g$–Ta$_3$N$_5$/FTO photoanode under an applied potential of 1.0 V *vs.* RHE; (f) comparison of the photocurrent and onset potential between our NiCoFe–B$_i$/Cu,Zr$_g$–Ta$_3$N$_5$/FTO and other Ta$_3$N$_5$-based photoanodes deposited on FTO [178] (open access).

Additionally, ex situ analyses involving scanning electron microscopy (SEM), TEM, X-ray diffraction (XRD), XPS, and inductively coupled plasma mass spectrometry (ICP-MS) provide valuable insights into the variations in morphology, crystal structure, surface chemical states, and dissolved elements. In the upcoming section, we present perspectives from various correlative spectroscopy techniques that are vital in understanding the extent of photocorrosion and the effectiveness of various mitigation strategies.

4. Perspectives from correlative spectroscopy and electron microscopy analysis

The literature on the characterization of TaN$_x$ and TaO$_x$N$_y$ materials mainly focusses on XRD or grazing incidence (GI)-XRD to determine the crystal phases and qualitative bulk composition of the synthesized material [217–224]. Čapek et al. [220,224], e.g., deposited TaO$_x$N$_y$ films on bare/SiO$_2$-covered Si wafers by high-power impulse magnetron sputtering of tantalum metal in a tunable Ar-O$_2$-N$_2$ mixture and subsequent vacuum annealing. Depending on the nitrogen fraction in the reactive gas mixture (f_{N2}), TaO$_x$N$_y$ film displayed different stoichiometry in Wavelength Dispersive X-ray Spectroscopy (WDX; Fig. 12 (a)-(b)) and corresponding crystal phases in XRD (Fig. 12 (c)-(d)). The film fabricated in $f_{N2}\leq 75$ % displayed only orthorhombic Ta$_2$O$_5$ phase, but oxynitride phases started to appear in $f_{N2}>75$ % [224] and for $f_{N2}=90$ % a complex mixture of phases ranging from monoclinic β-TaON, cubic bixbyite-Ta–O–N (b-Ta–O–N), cubic bixbyite-Ta$_2$N$_2$O (b-Ta$_2$N$_2$O) to cubic TaN (c-TaN) was observed [220]. These data clearly showed that even the presence of very small amounts of oxygen in the gas mixtures resulted in a complex mixture of crystal phases. Nevertheless, in most cases, a more detailed view of the chemical composition as well as structural information is compiled by Energy or Wavelength Dispersive X-ray Spectroscopy (EDS/EDX, WDX) in SEM/STEM for the determination of concentrations and, if required, lateral variations of the composition of the material.

In SEM/EDX, the information depth (and lateral resolution) varies with the energy of the applied electron beam and ranges from few tens of nm to μm. As a consequence, chemical compositions found by SEM/EDX are measures of the surface-near region of a material rather than the composition of the bulk or the immediate surface. Surface and interfaces are therefore studied by XPS or Auger Electron Spectroscopy (AES) in ultrahigh vacuum. Typically, the N1s, O1s and Ta4f regions are reported in the XPS analysis. The Ta4f$_{5/2}$/4 f$_{7/2}$ doublet appearing at around 28.4–28.7 and 26.5–26.8 eV is attributed to Ta^{5+} in Ta$_2$O$_5$, while in Ta$_3$N$_5$ a shift to lower binding energy is reported (Ta4f$_{5/2}$ is located at 26.7 eV and Ta4f$_{7/2}$ at 24.8 eV) [211,215,225]. The correct assignment of XPS peaks for various other species is subject to discussion in literature, c.f. Simpson et al. [225] for TaO$_x$ species and Cristea et al. [226] for TaO$_x$N$_y$. An especial factor in the XPS analysis of oxygen-rich TaO$_x$N$_y$ is the presence of the O2s band at around 23 eV, which may need to be considered in the fitting procedure [226]. Fig. 13 shows an example of the Ta4f region of TaO$_x$N$_y$ materials, prepared by reactive magnetron sputtering of Ta metal in Ar atmosphere with additional reactive gas (15 % O$_2$ / 85 % N$_2$) at various partial pressures, and the respective peak assignment and fitting for various chemical bond types. The presence of the O2s peak, which is often overlooked or not included in the analysis of Ta4f spectra, is especially noticeable [226].

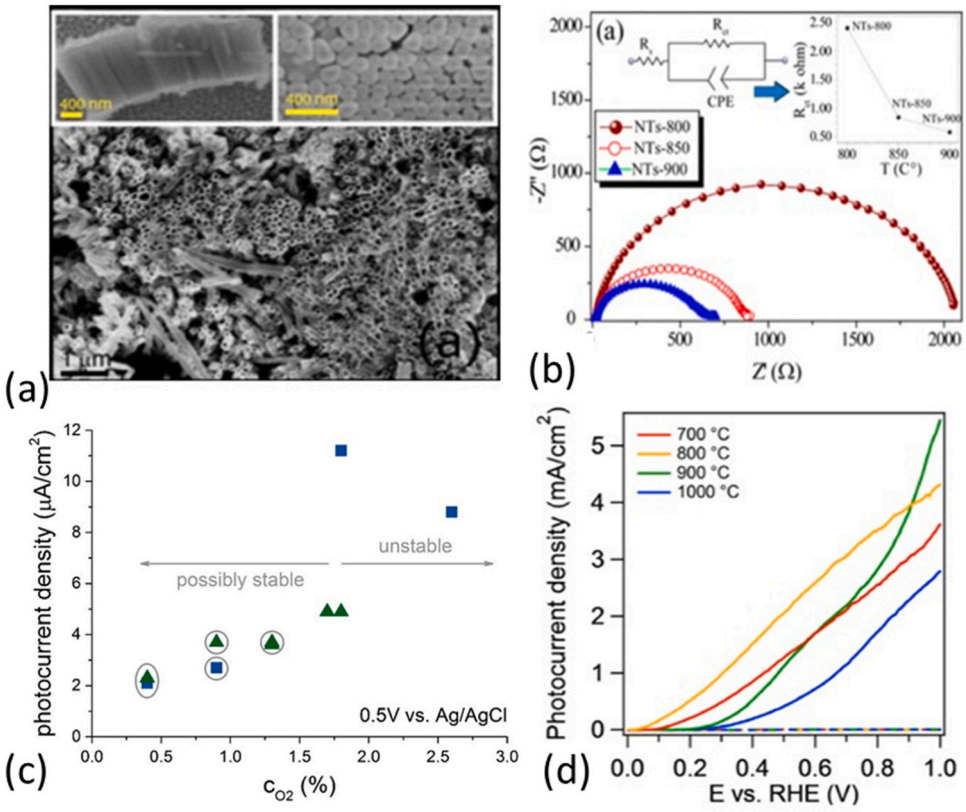

Fig. 11.
(a) (a) Ta_3N_5 nanotubes for PEC water splitting, (b) nanotubes ammonolysed at 900 °C demonstrated lowest charge transfer resistance and thus improved hydrogen evolution kinetics, *Reprinted (adapted) with permission from American Chemical Society, Copyright {2024}* [215]; (c) influence of oxygen concentration in magnetron sputtered Ta_3N_5 thin films, Gray circles indicate samples with the Ta_3N_5 phase, *Reused with permission from Elsevier* [217]; (d) Linear scan voltammograms of photoelectrochemical ferrocyanide oxidation illuminated and in the dark (dashed lines) Si-Ta_3N_5 photoanodes, *Reused with permission from Wiley* [94].

AES provides a spectroscopic mean to characterize the surface composition with an information depth of 2–10 nm of the surface, like XPS [227]. Scanning Auger Microscopy (SAM) can be used as an imaging tool with resolution down to the tens of nanometers using a focused electron probe rather than a broad beam electron/X-ray source. Narkeviciute and Jaramillo [94] used a combination of SEM and AES to analyze the distribution of Ta, N and O in the coexisting Ta/O/N phases on the surface of TaO_xN_y thin films, fabricated by nitridation of Ta_2O_5 deposited on silicon by atomic layer deposition (Fig. 14).

An overview of the spectral assignment for amorphous and crystalline Ta_2O_5 was published by Joseph et al. [228], whereas Nurlaela et al. [229] added the assignment for TaO_xN_y and Ta_3N_5. Chang et al. [230] investigated the growth of TaO_xN_y thin films prepared by magnetron sputtering, by using a correlative approach by combining XRD for the determination of the crystal phases, XPS for the analysis of the chemical bonding, and elastic recoil detection analysis (ERDA) for the determination of the atomic composition vs. thickness. The data showed that in the absence of oxygen in the reactive gas mixture (Ar + N_2), only metallic δ-TaN phase was formed. Only when some oxygen (2 %) was added to the gas mixture, Ta_3N_5 could be observed in the XRD and XPS analysis, indicating the presence of oxygen being a prerequisite for the formation of Ta_3N_5 phase. The ERDA analysis also indicated an increase in the oxygen uptake of the deposited film depending on the total pressure in the sputter reactor under the applied conditions. Up to about 10 at% the characteristic XRD and XPS signals for a Ta_3N_5 phase were observed, although a decrease in lattice constant from 10.30 Å to 10.17 Å and an increase in bandgap from 2.22 to 2.66 eV was found. The authors attributed this to the substitution of O for N and the formation of Ta vacancies in the Ta_3N_5 crystal. The authors also claimed that even higher total pressures of O_2 (at constant ratio of 2 % O_2 in the gas mixture), the Ta sputter target begins to oxidize, leading to the deposition of O-rich, partially amorphous mixtures including TaO_xN_y and Ta_2O_5.

The second route to prepare Ta_3N_5, based on the nitridation of Ta_2O_5, was investigated by Narkeviciute and Jaramillo [94]. The authors prepared thin (~10 nm) films of Ta_2O_5 on planar Si wafers and Si nanowires, followed by nitridation using ammonia gas at different temperatures (700–1000 °C). XPS analysis displayed a decrease in the N-content and an increase in the O-content of the material for T>800°C. The XPS data also indicated the formation of TaON and TaN species at these temperatures. The SEM images displayed the formation of regions of different morphology coexisting after exposure to T>900°C, which when analyzed by AES indicated that they differ in the N/Ta and N/O ratios. The difference in stoichiometry indicated that the morphology difference in SEM corresponded to a phase separation and coexistence of different TaO_xN_y materials, which most likely also influenced the local catalytic activity and chemical reactivity. For lower temperatures, lower crystallinity is observed in XRD. As the sample nitride at 800 °C displayed the best PEC performance, the authors suggested that this temperature provided the best compromise between high crystallinity and low oxygen defect density.

Photocorrosion is a well-recognized aspect in semiconductor-based PEC chemistry, e.g., water splitting [231,232]. Guo et al. [231] determined that the thermodynamic stability is strongly coupled to the energy positions of the valence band, with a highest possible potential at 2.48 V *vs.* NHE. However, for TaN_x and TaO_xN_y materials with a low O/N ratio, less positive valence band edges were predicted by DFT, suggesting that such materials suffer from thermodynamic instability in solution and are prone to oxidation. To overcome this, the use of a stable oxide or hydroxide passivation layer was suggested, which was also

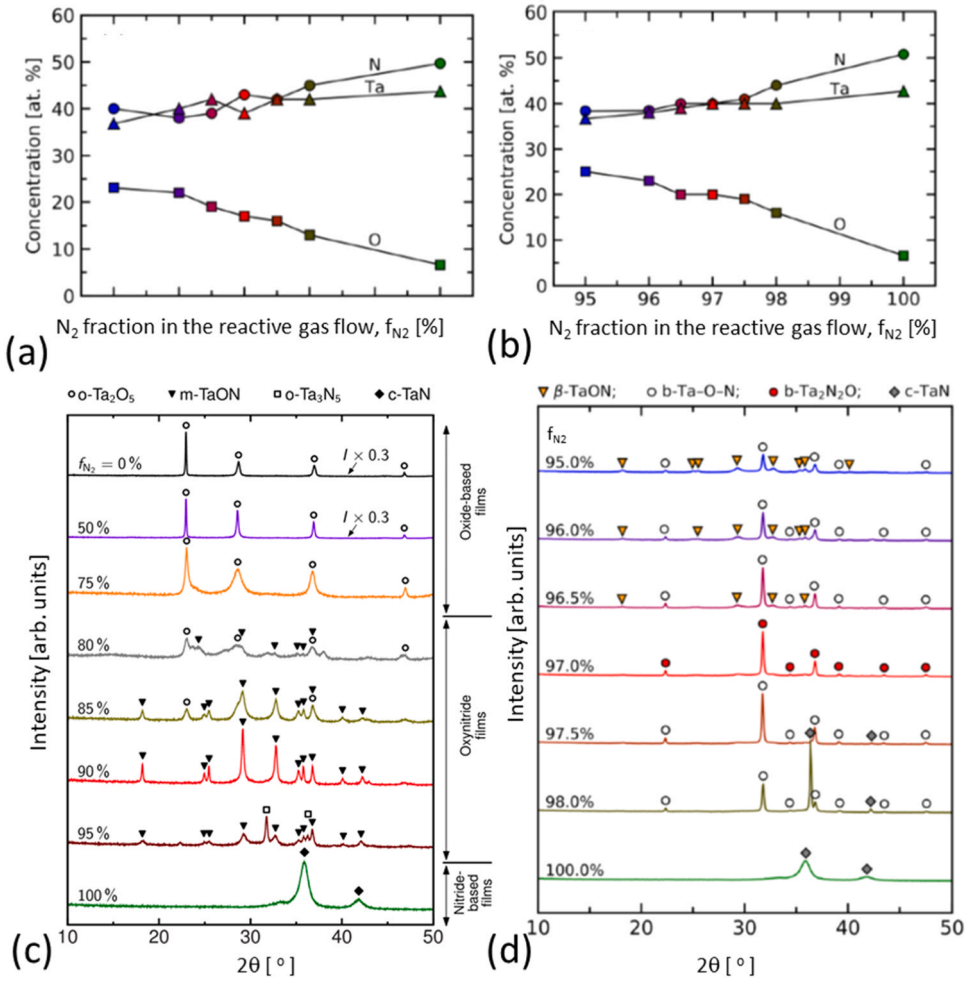

Fig. 12. Elemental composition of TaO_xN_y films, as-prepared (a) and vacuum-annealed (b). XRD data after vacuum annealing at different f_{N2} (c) and (d), *Reused with permission from AIP publishing* [220], *Reused with permission from Elsevier* [224].

experimentally demonstrated using transition metal oxide/hydroxide compounds like NiOOH or FeOOH [231]. Experimental evidence for the performance deterioration of the cell during PEC application is common and is discussed in Section 3. Postmortem analysis of such systems by XPS and other techniques indeed reveals an increase in the oxygen content on the surface. He et al. [194], e.g., attributed the loss of PEC performance in Ta_3N_5 to the self-limiting surface oxidation, leading to the formation of a thin (~3 nm) amorphous layer. This layer could not be detected by Raman and UV-Vis spectroscopy or XRD, but was observable in TEM (Fig. 15 (a)) and spectroscopically detectable by XAS and XPS (Fig. 15(b)). This finding shows that photocorrosion in Ta_3N_5 (and likely other TaO_xN_y species) is mainly a surface phenomenon, highlighting the insights gained by the correlation of high-resolution TEM and electron spectroscopies.

Postmortem analytics are usually performed ex situ and allow for the use of (relatively) common experimental techniques, predominantly XPS and XRD, to determine the physical and/or chemical changes, but they suffer from the disassociation of PEC experiment from analysis. Especially the need for vacuum compatibility in conventional high-resolution imaging (TEM, SEM, Photoemission Electron Microscopy (PEEM), etc.) and spectroscopy (XPS, Secondary-ion mass spectrometry (SIMS), EDS/WDS, etc.) necessitates drying of samples before analysis, which can change the morphology as well as the chemical structure of a material. In the absence of other components of the PEC environment (solvent, salts, gasses), ex situ analysis does not necessarily show the actual active state of the material. To address this issue, characterization of the materials in PEC benefits from being carried out under in situ or operando conditions, i.e., within the typical PEC environment or during operation.

Pishgar et al. [233] have recently summarized the available techniques for in situ analysis especially of EC and PEC systems, including the optical techniques (UV-Vis, Raman), electron spectroscopies (XAS), and in situ TEM and scanning probe techniques (Electrochemical Atomic Force Microscopy, EC-AFM, etc.). These approaches make use of sophisticated, miniaturized (photo-)electrochemical cells to perform spectroscopic analysis while the (P)EC experiments are conducted. In contrast to TEM, X-ray photoelectron spectroscopy is not easily adapted to operando analysis, albeit ongoing efforts to study liquid surfaces and near ambient pressure setups [234]. As an alternative approach, XAS is a synchrotron-based technique that can be used to investigate the electronic structure of materials using transmitted X-rays. XAS can be adapted to study materials using electrochemical cells similar to those used in TEM and thus allows for the characterization of various properties (chemical composition, charge transfer, oxidation states, chemical environment, etc.) under in situ/ operando conditions [235]. While there have been studies of the photocorrosion semiconductor/electrolyte interface of related semiconductor PEC materials like perovskites, operando studies of photocorrosion seem to be limited [236]. The nature and distribution of energy states in electrode/electrolyte interface is a key parameter that plays a role in predicting the photostability of Ta_3N_5. In general, the surface of Ta_3N_5 has numerous defects, which lead to the presence of new energy states wherein the Fermi level can be pinned. When such a pinning happens the generated holes and electrons cannot cross the interface, leading to

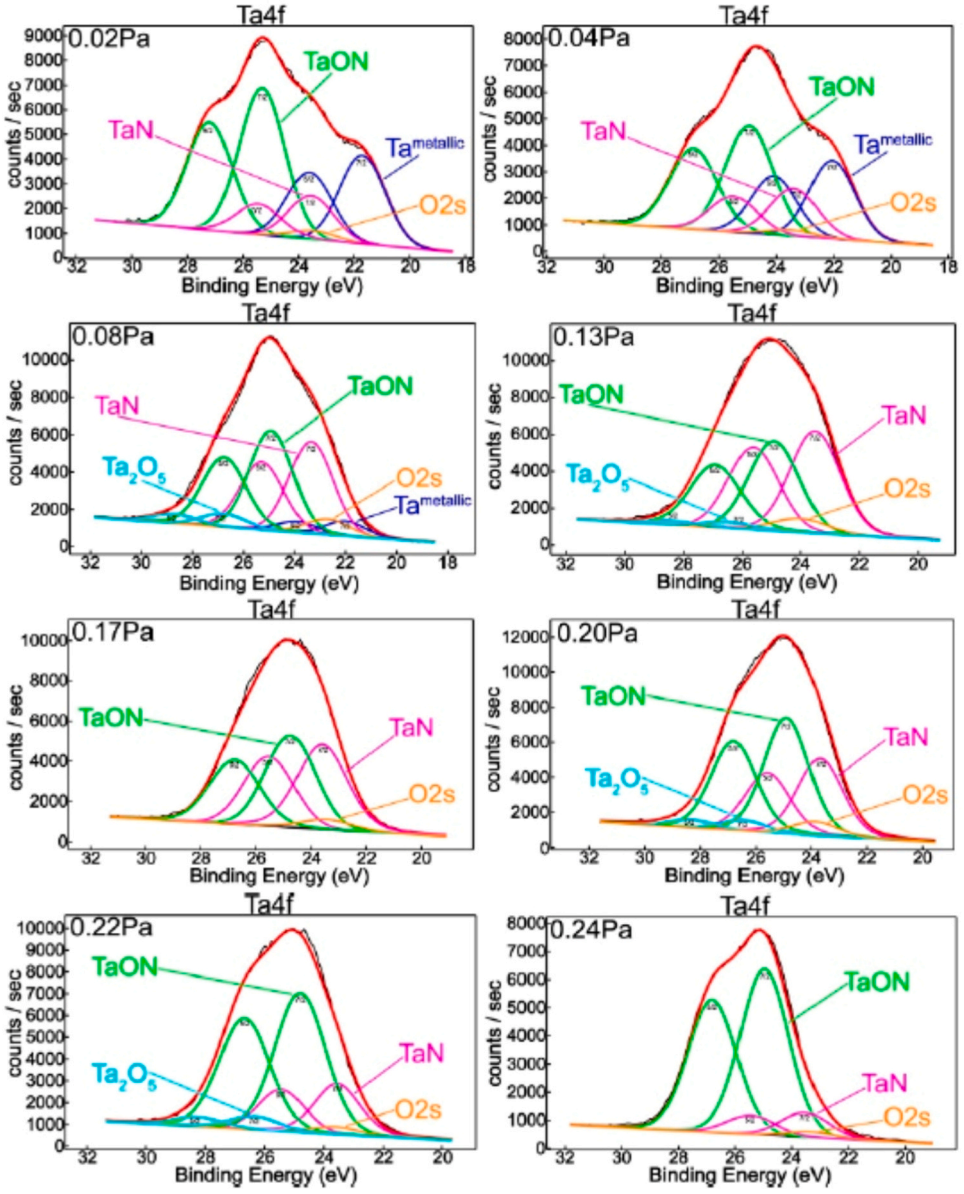

Fig. 13. XPS analysis of TaO_xN_y species prepared by magnetron sputtering of Ta in Argon atmosphere with a 85 % N_2 / 15 % O_2 reactive gas mixture at varying partial pressures [226] (open access).

self-oxidation or photocorrosion of the electrode. In contrast, the presence of sub-nanometer thick NiO_x can combat photocorrosion. Such a layer can passivate the already existing defect states that can result in unpinning of the quasi Fermi levels of the photogenerated holes. These holes can then quickly transport from Ta_3N_5 layer, resulting in suppressed photo corrosion. Recently, Dahl et al. [237] brought such an unpinning phenomenon to light by operando XPS studies on Ta_3N_5/Ta and Ta_3N_5/NiO_x/Ta photoelectrodes in dark and illuminated conditions. For Ta_3N_5 photoanode, Ta 4 $f_{7/2}$ peak position was independent of the applied potential in both dark and illuminated conditions, indicating the Fermi level pinning. Whereas Ta_3N_5/NiO_x photoanode having NiO_x as a protection layer, exhibited a negative shift (-0.57 eV) in Ta 4 $f_{7/2}$ binding energy under bias in illuminated condition (Fig. 16(d)), indicating increased surface band bending and improved charge separation, resulting in improved PEC performance and durability. Post-operation XPS analysis also allowed further discerning the role of surface passivation, where new peaks corresponding to binding energies indicative of Ta-O linkages were dominant in samples without NiO_x. The results were in close agreement with the bright field STEM images, where an amorphous oxide layer (7 nm) was found only in Ta_3N_5 photoanode.

In another study, Venugopal et al. [238] used operando PEC attenuated total reflection Fourier transform infrared (PEC-ATR-FTIR) spectroscopy to study the metal oxide/electrolyte interface with $BiVO_4$ as a model anode material. The authors demonstrated that upon illumination under open circuit condition, vanadium dissolved preferentially from the material, while both bismuth and vanadium dissolved under an anodic potential during illumination. This resulted in dynamic change in surface Bi:V ratio, subsequently altering the band bending and further impacting the overall PEC performance. In summary, the study of photocorrosion in PEC materials and TaO_xN_y in particular requires a correlative approach using high-resolution imaging and electron spectroscopy for surface/interface analysis in addition to bulk analysis by spectroscopy, electron microscopy and electrochemical characterization. While ex situ analysis using XPS and TEM allows to draw some conclusions, there is a need for additional verification of these results by in situ/operando characterization to exclude artifacts caused by a change of the environment between PEC performance characterization and material analysis. In order to further the understanding of TaO_xN_y

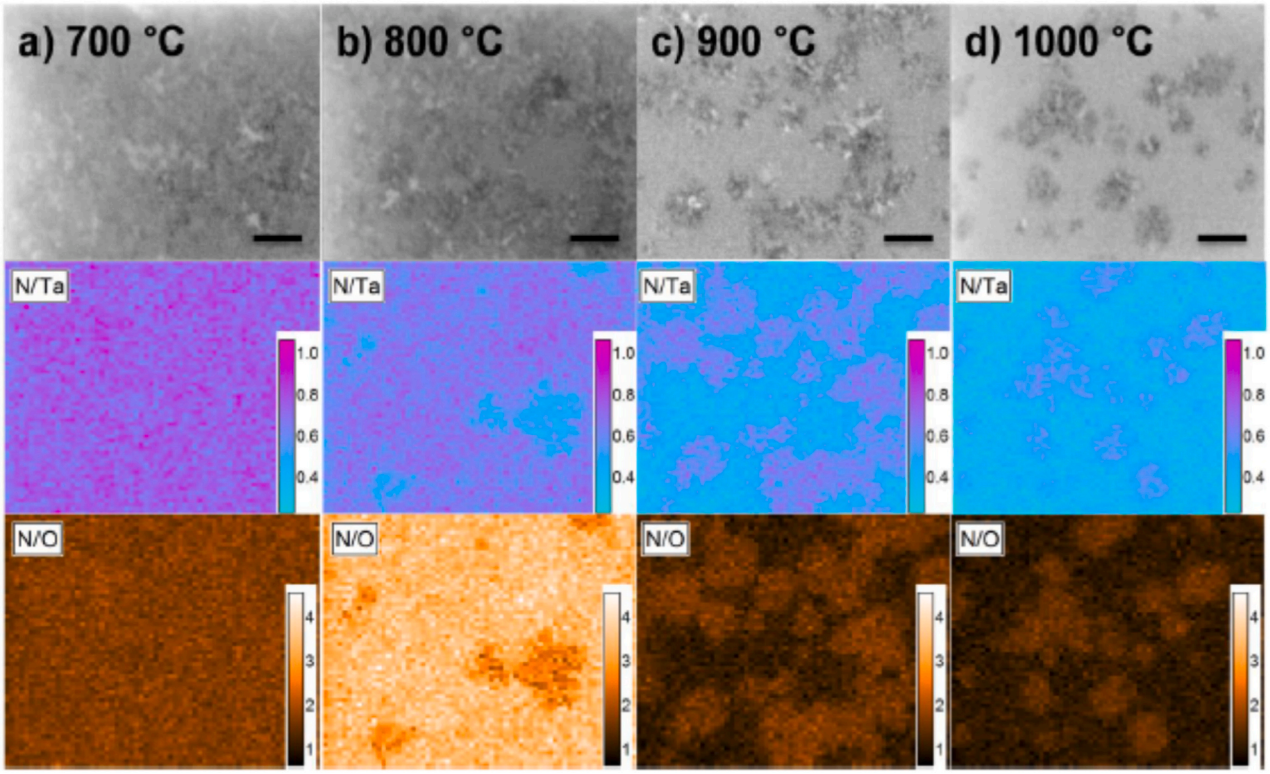

Fig. 14. SEM (top row) and Scanning Auger Microscopy (middle and bottom row) of Ta_2O_5 thin films after nitridation by NH_3 at different temperatures (as indicated). The scale bar is 500 nm. The SE images show the presence of coexisting domains of clearly distinguishable morphology and the correlated N/Ta- and N/O-ratios determined by SAM allow for the identification of O-rich and N-depleted domains for nitridation temperature >800°C [94], *Reused with permission from Wiley*.

materials for PEC applications, the potential use of advanced in situ analytical techniques, especially operando TEM and synchrotron based XAS, should be evaluated. The inevitable presence of oxygen, both as impurities and in the form of surface oxide layer, as evident from various correlative spectroscopy techniques indicates a greater affinity of Ta-N phases to oxygen. This also means that there is a higher thermodynamic stability of oxynitrides compared to pristine nitrides. Thus, a fundamental understanding of the phase stabilities of various Ta-N phases in the presence of oxygen and various other defects will serve important guidelines for further development of electrocatalysts. In the upcoming section, we summarize, for the first time, the crystallographic, thermochemical and constitutional data of these phases and compile various computational studies that comment on catalytic activity in the presence of oxygen.

5. Review of crystallographic, thermochemical, and constitutional data- *Understanding the phase stabilities*

The previous sections have ample evidence for the presence of oxygen in several of the tantalum nitrides reported in the literature, which indicates the higher thermodynamic stability of oxygen-containing nitrides compared to pure nitrides. Before reviewing the oxygen- containing nitrides, it would be ideal to discuss the stability of pure nitrides.

The phase diagram studies have considered ε-TaN ($P\bar{6}2m$) [29] and Ta_2N ($P\bar{3}1m$) [34] stable at room temperature and the high temperature δ-TaN ($Fm\bar{3}m$) [30] as equilibrium phases. Other than these, TaN ($P6/mmm$), Ta_3N_5 ($Cmcm$) [36,37], Ta_4N_5 ($I4/m$), Ta_5N_6 ($P6_3/mcm$) (Terao-1971), Ta_2N_3 ($Ia\bar{3}$) (Ganin-2004) and Ta_2N_3 ($Pbnm$) (Zerr-2009) are also reported [31,35,38]. However, only ε-TaN ($P\bar{6}2m$), Ta_2N ($P\bar{3}1m$), and δ-TaN ($Fm\bar{3}m$) are used as the basis for thermodynamic modelling by Frisk [239]. Thus, there is no clarity about the thermodynamic stability of the remaining phases. In this regard, the computational approach can come to aid and suggest about their stability. The crystal structure of various tantalum nitrides are shown in Fig. 17.

5.1. Stability of pure tantalum nitrides

Among the computational methods, DFT is the most widely used technique to calculate the total energy of a molecular or periodic structure at 0 K [240,241]. The formation enthalpy ($\Delta_f H^\circ$) of a compound Ta_nN_m at 0 K can be enumerated from total energies using Eq. (2)

$$\Delta_f H^\circ = \frac{E^{total}_{Ta_nN_m} - nE^{total}_{Ta,bcc} - m\frac{E^{total}_{N_2,gas}}{2}}{m+n} \quad (2)$$

where $E^{total}_{Ta_nN_m}$, $E^{total}_{Ta,bcc}$, and $E^{total}_{N_2,gas}$ are the total energies of the compound, bcc-Ta, and N_2 (gas), respectively, and n and m are the stoichiometric numbers of Ta and N in the nitride considered [40]. The calculated $\Delta_f H^\circ$ should be negative for a structure to be stable at 0 K. Further, the convex hull approach where the formation enthalpies of the interested compound needs to be compared against all other phases or combination of phases at that composition, can be used to identify the stable phases at 0 K. Phases that lie on the convex hull (created by connecting the lowest energy structures) are thermodynamically stable and the ones above it are metastable or unstable (Fig. 18) [33].

Stampfl and Freeman [105] investigated the relative stability of several tantalum nitrides – namely, ε`-TaN, δ-TaN, β-Ta_2N, α-Ta_3N_5, Ta_4N_5, and Ta_5N_6 using DFT. The $\Delta_f H^\circ$ of various tantalum nitrides was plotted as a function of the chemical potential of nitrogen, from which they suggested Ta_5N_6 as the most stable phase over a wide range of nitrogen content. The formation of β-Ta_2N and α-Ta_3N_5 was favored at nitrogen-poor and rich regions, respectively, while the remaining nitrides were metastable. Identical conclusions were drawn from the study

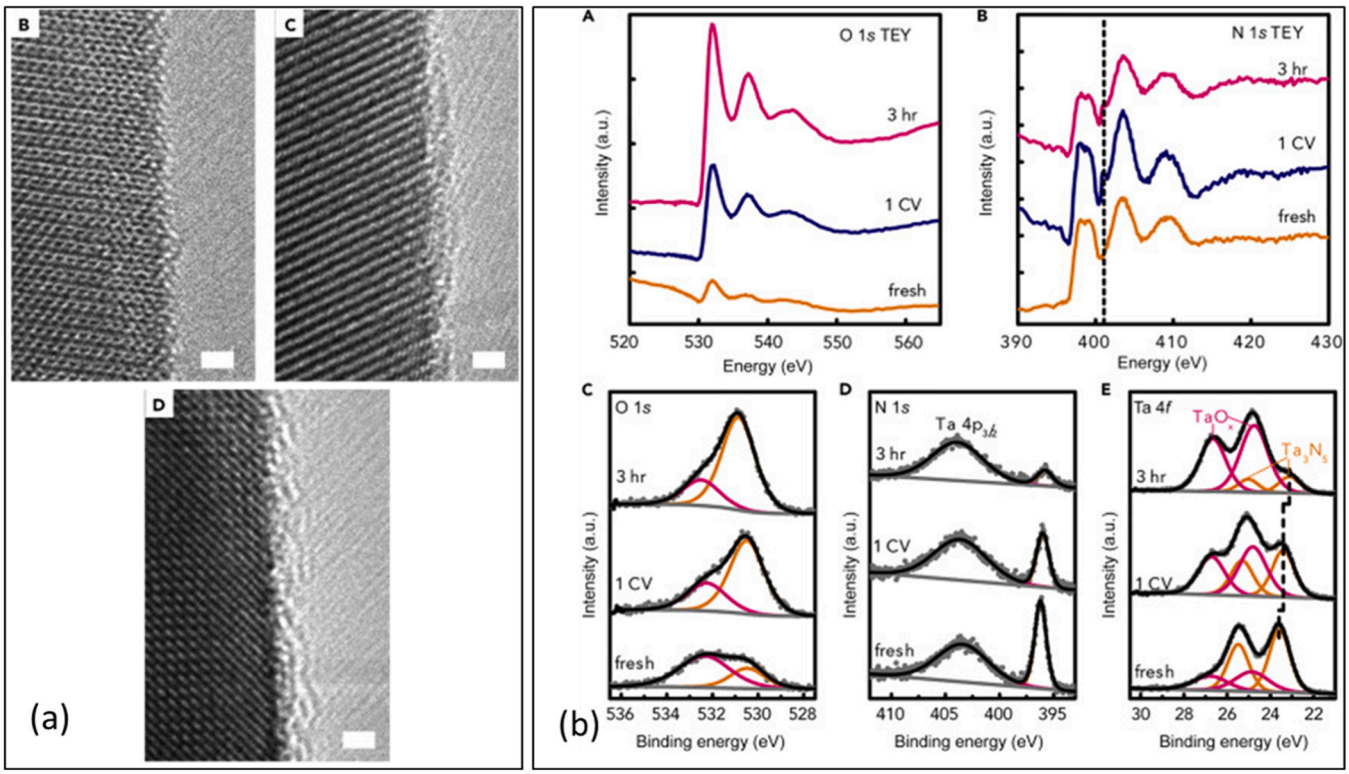

Fig. 15. (a) TEM image of the Ta_3N_5 surface, as prepared (B), after one cycle of CV scan (C), and after 3 h of photoelectrolysis at 1.23 V (D), Scale bars represent 1 nm. The scale bar is 1 nm; (b) X-Ray Spectra of Ta_3N_5. (A and B) Total electron yield of O 1 s and N 1 s X-ray absorption spectra. The dotted vertical line in (B) serves as a visual guide. (C–E) Binding energies of O 1 s (C), N 1 s (D), and Ta 4 f (E) electrons as measured by XPS. Samples compared in this figure include as-prepared (fresh), after one cycle of CV (1 CV), and after 3 h of photoelectrolysis (3 hr). The dotted vertical line in (E) serves as a visual guide [194], *Reused with permission from Elsevier*.

by Violet et al. [41]. Zhao et al. [242] compared $\Delta_f H^{\circ}$ of 8 structural variants of tantalum mononitride (ε-TaN, *ν*-TaN, $P6_3/mmc$-TaN, δ-TaN, $F\bar{4}3m$-TaN, $P6_3mc$-TaN, $Pm3m$-TaN and ε`-TaN) using the convex hull approach. They concluded that ε-TaN was the most stable amongst these, followed by *ν*-TaN. Li et al. [243] utilized the USPEX (Universal Structure Predictor: Evolutionary Xtallography) code [244,245] together with DFT to predict the thermodynamically stable phases. According to them, *ν*-TaN was the most stable mononitride, whereas β-Ta_2N, Ta_5N_6, Ta_4N_5, β-Ta_2N_3 and α-Ta_3N_5 were the other nitrides present on the convex hull. Weinberger et al. [33] followed the same technique and concluded that ε-TaN was one of the thermodynamically stable phases along with α-Ta_3N_5, Ta_5N_6 and β-Ta_2N.

It was first believed that the space group of ε-TaN was $P6/mmm$ (through X-Ray diffraction) [28], but later, based on the neutron diffraction investigation, a modified symmetry of $P\bar{6}2m$ was assigned [29]. Due to this contradictory finding on the low temperature TaN space group, ε-TaN is absent in many reports [41–43]. The first-principle calculations by Grumski et al. [40] indicated that the enthalpy of formation of ε-TaN with $P\bar{6}2m$ symmetry is more negative than ε-TaN with $P6/mmm$ symmetry. Therefore, the former is thermodynamically more stable at ambient conditions i.e., ε-TaN with $P\bar{6}2m$ symmetry is the most stable form among all tantalum nitrides [33,242]. Therefore, it can be concluded that the convex hull constructions developed by Weisenberger et al. [33] is precise. In addition, a very close difference between the formation enthalpies of the Ta-N phases suggests that the lack of the temperature effect sometimes may hinder the appearance of an energetically or experimentally more favorable phase.

5.2. Stability of tantalum nitrides with defects

The stability and stoichiometry of tantalum nitrides are affected by the presence of defects such as vacancies, oxygen impurities, antisite atoms, etc. It is reported that large amount of oxygen ions are present in the 3-coordinate anion sites of α-Ta_3N_5 when it was produced by ammonolysis of Ta_2O_5, even after a longer duration of heat treatment at higher temperatures, such as at 900°C for 120 h [39]. Zerr et al. [31] utilized the high temperature – high pressure route to synthesize η-Ta_2N_3, which contained approximately 3 at% oxygen. Hence, it can be concluded that the presence of oxygen plays a crucial role in stabilizing some nitrides. In this part of the report, the stability of the structures concerning the defects is assessed.

The energy required for forming a vacancy or defects in a perfect lattice can be predicted using the following Eq. (3).

$$\Delta_f H^X = E^X_{Vac,\ n-1} - E_n + E^X \tag{3}$$

where $\Delta_f H^X$ is the defect formation enthalpy, $E^X_{Vac,n-1}$, E_n, n and E^X are the energy of the supercell with defects, the energy of the perfect supercell, total number of atoms in the prefect supercell, and energy of species (X) removed from the supercell, respectively [40]. A negative value of $\Delta_f H^X$ suggests that the off-stoichiometric phase would be thermodynamically more stable than the stoichiometric one.

Stampfl and Freeman [42] modelled δ-TaN with defects such as N and Ta vacancies (V_N, V_{Ta}), N interstitials (N_{int}), and N antisite (N_{Ta}). It was found that δ-TaN with 1 V_N and 1 V_{Ta} per unit cell were more stable in nitrogen-poor and rich regions, respectively, compared to the perfect δ-TaN. Moreover, the structure with higher amount of V_N was even more stable, whereas the structures with N_{int} and N_{Ta} were energetically unfavorable. This aspect was further confirmed by Violet et al. [41] and Grumski et al. [40]. The positive enthalpy of vacancy formation in ε-TaN and ε′-TaN indicated their instability when vacancy was introduced [40].

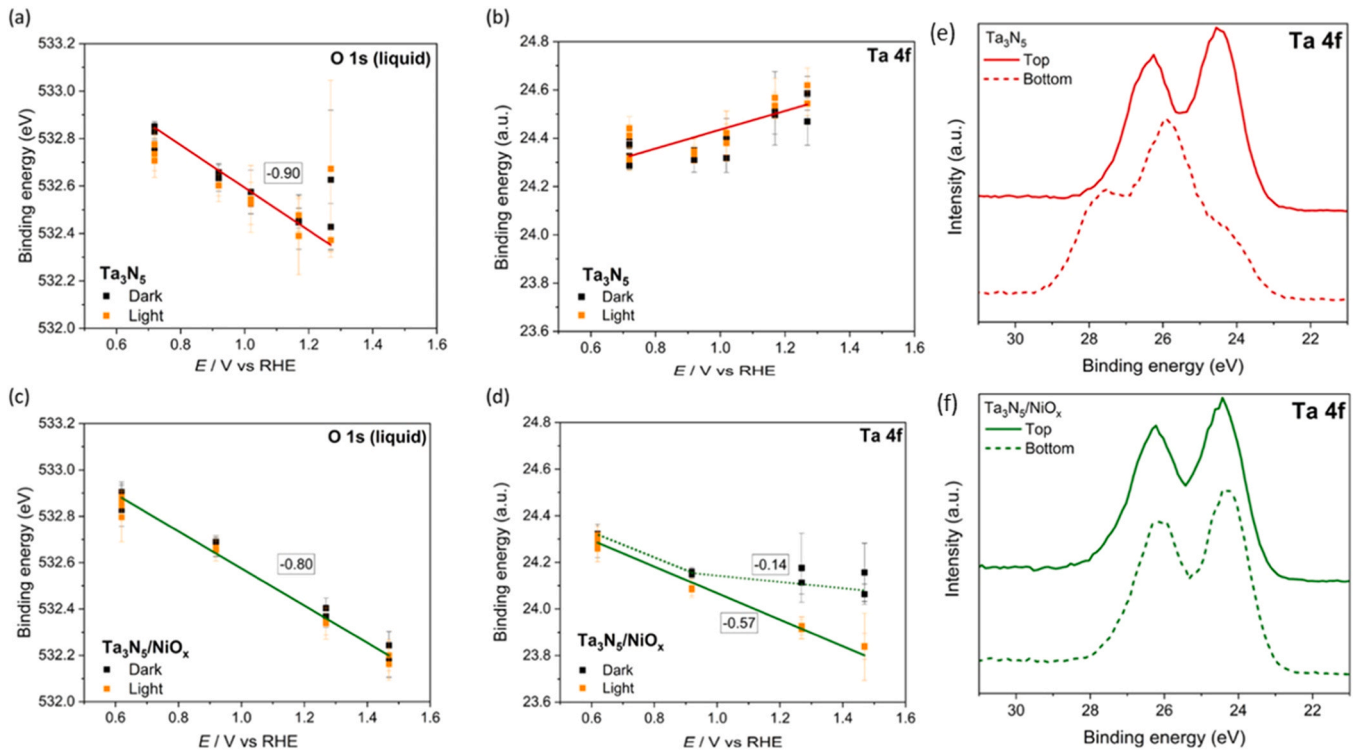

Fig. 16. Binding energy of the Ta 4 $f_{7/2}$ component and liquid contribution in the O 1 s spectra during operando AP-XPS measurements for (a) and (b) Ta_3N_5 and (c) and (d) Ta_3N_5/NiO_x. Black and yellow markers represent measurements under dark and illuminated conditions, respectively; Post-operation XPS measurements under vacuum conditions of used (e) Ta_3N_5 and (f) Ta_3N_5/NiO_x. Dashed lines (labeled: bottom) are measured on areas that were immersed in the electrolyte during the operando AP-XPS measurements, and solid lines (labeled: top) are from areas that were not in contact with the electrolyte [237], (*open access*).

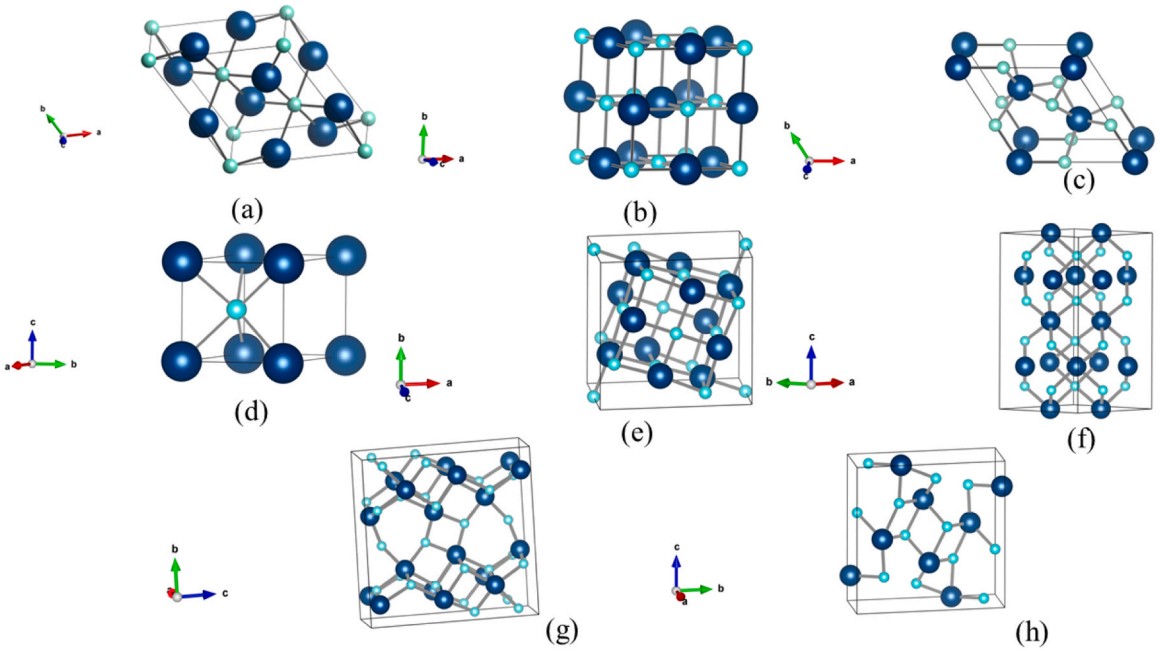

Fig. 17. The crystal structures (a) Ta_2N ($P\bar{3}1m$) (b) δ-TaN ($Fm\bar{3}m$) (c) ε-TaN ($P\bar{6}2m$) (d) ν-TaN ($P\bar{6}m2$) (e) Ta_4N_5 ($I4/m$) (f) Ta_5N_6 ($P6_3/mcm$) (g) Ta_3N_5 (*Cmcm*) (h) Ta_2N_3 (*Pbnm*) (Blue, and cyan colors indicate Ta, and N atoms, respectively).

An extensive study was conducted by Wang et al. [44] in an attempt to understand the stability of α-Ta_3N_5 with O_N, V_N, V_{Ta}, N_{int}, Ta_{int}, N_{Ta}, and Ta_N. In α-Ta_3N_5, the Ta atom is in coordination with six neighboring N atoms and the N atom is coordinated with either three (denoted as N3) or four (denoted as N4) Ta atoms. The system with O_{N3} defect has the lowest energy (Fig. 19 (a)), which also has been experimentally verified [39]. Zerr et al. [31] synthesized η-Ta_2N_3 via a high temperature - high pressure route; however, ~3 at% oxygen was present as an impurity. It was suspected that the presence of oxygen might have influenced the thermodynamic stability of η-Ta_2N_3. In another study, Jiang et al. [246]

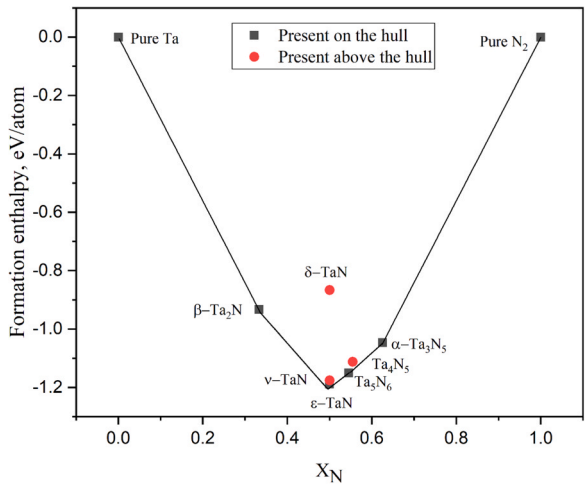

Fig. 18. Convex hull for the Ta-N system at 0 K. The smooth line represents the hull. The nitrides represented by squares (β-Ta_2N, ε-TaN, Ta_5N_6 and α-Ta_3N_5) are present on the hull, hence, are thermodynamically stable. The nitrides represented by circles (ν-TaN, δ-TaN, Ta_4N_5) are unstable [33], *Reused with permission from Elsevier*.

calculated the formation enthalpy and elastic constant of η-Ta_2N_3 using the DFT technique, in order to interpret its thermodynamic stability. Even though the formation enthalpy was negative, it was not mechanically stable because of its negative elastic constants. However, a minor substitution of oxygen at the nitrogen site led to atomic rearrangement, causing the redistribution of charges and a stronger Ta-N covalent bond that would resist the shear strain, significantly improving its elastic constant and stabilizing η-Ta_2N_3 [45]. In a recent study, Moharana et al. [32] established the thermodynamic stability of the high-pressure ν-TaN at atmospheric pressure with oxygen substitution. The formation of O_N defect in ν-TaN exhibited the smallest formation of energy (-1.307 eV/atom) compared to pure ν-TaN (-1.292 eV/atom) and ν-TaN with nitrogen vacancy (-1.181 eV/atom). The oxygen-doped ν-TaN was also verified to be both mechanically and dynamically stable. The presence of a certain amount of oxygen (~0.2 at%) in Ta_5N_6 was confirmed in the experiment by Houmes and Loye [247]. This amount was meagre compared to the oxygen in η-Ta_2N_3 (~ 3 at%) and α-Ta_3N_5 (~ 1.5 at%) [31]. The formation energy-based calculation revealed the instability of Ta_5N_6 with an increase in the O_N amount (Fig. 19(b)). It was clarified that the excess electron resulting from the O_N defect was localized near the impurity. This localization did not enhance its structural stability with the introduction of additional O_N defects [248].

For the mononitrides, the stability of the defect structures with V_N is more, whereas α-Ta_3N_5, η-Ta_2N_3 and Ta_5N_6 are more stable with oxygen anti-site (O_N). The formation of a sufficient amount of nitrogen vacancy can allow the formation of the Ta-Ta bond, which is stronger and helps in their thermodynamic stabilization. The presence of O_N is causing the atomic rearrangement, hence strengthening the atomic cohesion and enhancing the structural stability of α-Ta_3N_5 and η-Ta_2N_3. Therefore, it can be concluded that the presence of oxygen in some of the tantalum nitrides is inevitable, which can further play an essential role during their real-world applications such as photocatalysis, electrocatalysis, sensing, solar cells etc.

Having understood the inevitable presence of oxygen in Ta-N system, wherein the structural stability and cohesion is enhanced [43], we now summarize various reports from literature that comment on its effect on the water splitting behaviour using theoretical DFT studies (Fig. 20). To begin with, the clear role of oxygen defects in Ta_3N_5 still remains unaddressed. For instance, in few studies, it was observed that O_N defects result in shallow donor defect states that eventually improve the photogenerated current due to improved n-type conductivity [204,207,249]. Conversely, few reports also comment on the detrimental role of oxygen wherein such defects can retard water adsorption kinetics, resulting in poor onset potential of Ta_3N_5 photoanodes [194,249]. In another theoretical study based on partially oxidized Ta_3N_5 and partially nitrided TaON surfaces, the relative change in band gap edge positions and its effect on photocatalytic water splitting was clearly elucidated. It was observed that pure Ta_3N_5 was ideal only for hydrogen evolution, as the valence band edge was further negative from the oxidation potential. The authors also predicted that at certain compositions ($Ta_{2.75}N_{3.75}O_{1.25}$), the presence of oxygen impurities could ideally catalyze both water oxidation and hydrogen evolution reactions. On the contrary, the partial nitridation of TaON had no effect on improving H^+ reduction [83].

As an extension, in another study, O_N was found to be beneficial, as it resulted in surface saturation and simultaneous reduction of conduction band gap maximum. Further, it was concluded that among the different surfaces, Ta_3N_5 (100) surface showed the strongest reduction capability, in agreement with few experimental studies [250]. Later, another study signifying the surface orientation of Ta_3N_5 on water splitting was reported. In accordance with promising PEC water splitting reports, Ta_3N_5 (110) surface with oxygen impurities was theoretically probed. Based on the surface energy calculations, it was observed that Ta_3N_5 (110) facet has fewer oxygen impurities than Ta_3N_5 (100) surface. The water

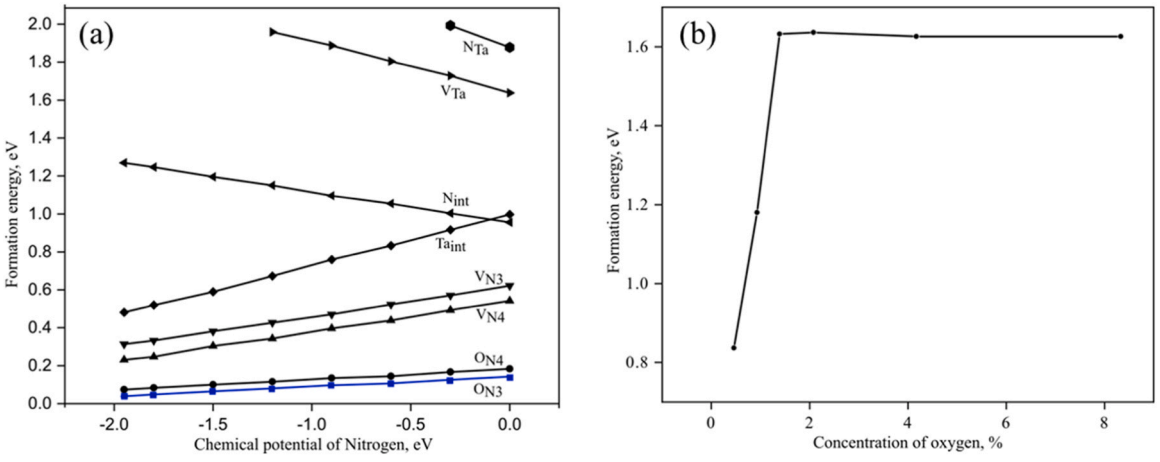

Fig. 19.
(a) (a) The formation energy of different defects in α-Ta_3N_5 as a function of the chemical potential of nitrogen where, oxygen antisite (O_N) has the lowest formation energy (blue line) [44], *Reused with permission from Elsevier* (b) The formation energy of Ta_5N_6 as a function of the concentration of oxygen impurities, and it is indicating higher formation enthalpy with more O_N defects [248], *Reused with permission from Elsevier*.

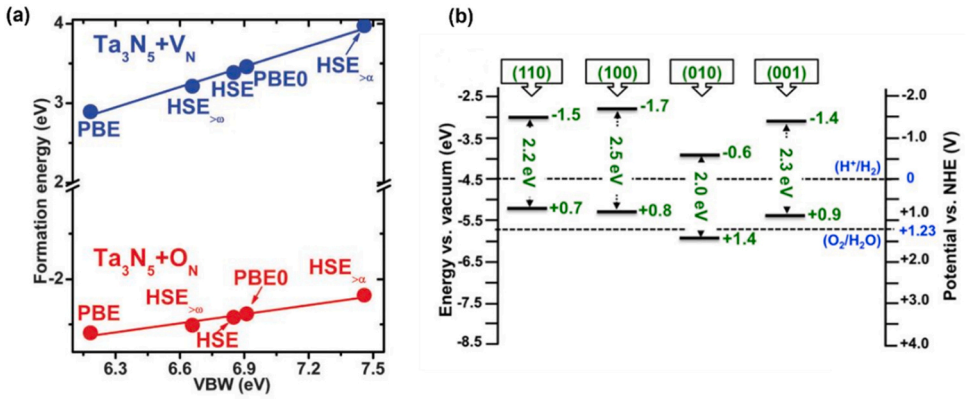

Fig. 20. (a) Lowered formation energy of Ta_3N_5 when incorporated with oxygen vacancies [43], *Reprinted with permission from RSC*; (b) Different facets of Ta_3N_5 and their band-edge positions for water splitting; (110) & (001) surfaces are suitable for HER whereas (010) is ideal for OER [212], *Reprinted (adapted) with permission from American Chemical Society Copyright {2024}*.

adsorption and desorption free energy was also nearly equal to zero on such surfaces, that were in close agreement with various synthesis methodologies exhibiting (110) orientation [212]. Also, in another study, the combinatorial influence of both hydrogen and oxygen impurities by virtue of high temperature pyrolysis in NH_3 environment on the water splitting activity was reported [251]. It was observed that the presence of hydrogen-oxygen as hydroxyl bonds could act as further recombination centers, leading to higher onset potentials and poor stability of Ta_3N_5 (Fig. 21(a)). Various strategies to mitigate the oxygen impurity effects have also been reported. For example, to compensate increased conduction band gap shift due to the electron donating ability of O_N impurities, other electron-accepting constituents such as Ti, Zr, Hf were doped (Fig. 21(b)). These dopants in principle will not allow any increase in electron density of Ta atoms, thus maintaining the charge carrier mobility in Ta_3N_5 [252].

6. Summary and future outlook

In conclusion, this review sheds light on the untapped potential of tantalum nitrides (Ta-N) and tantalum oxynitrides (TaO_xN_y) as electrocatalysts, emphasizing their suitability for diverse applications in renewable energy technologies. Through a comprehensive analysis of recent advancements, we have highlighted the remarkable electrocatalytic performance of these phases in key reactions such as the Hydrogen Evolution Reaction (HER), Oxygen Evolution Reaction (OER), and Oxygen Reduction Reaction (ORR). The bulk of reports focus on Ta_3N_5, which has a propensity to oxidize under electrochemical conditions, diminishing its potential for water splitting applications. Therefore, there is a critical need to explore alternatives to Ta_3N_5. Limited attention has been given to phases such as Ta_5N_6 (exhibiting metallic properties) and Ta_4N_5, which could potentially offer enhanced performance in hydrogen/oxygen evolution reactions. Despite their promising attributes, challenges such as surface oxidation and photocorrosion persist, necessitating the use of co-catalysts and dopants to augment the water splitting kinetics. Use of co-catalysts will only bring additional processing steps and costs in the manufacturing of these photoelectrode sand can also induce parasitic light absorption in these materials, making them a less attractive solution. Moreover, our exploration into correlative spectroscopy techniques has provided valuable insights into understanding the extent of surface oxidation and the effectiveness of various mitigation strategies. A clear dearth of in-situ characterization methods in Ta-N and Ta-O-N system was observed. Given the dynamic nature of the semiconductor-electrolyte interface and the possibility of artefacts that can arise during post-mortem/ex-situ analysis, there is a need to revisit the kinetics of electrocatalytic activity and surface oxidation via operando characterization methodologies. Also, 3D distribution of oxygen (both in bulk and surface) should be further understood using correlative spectroscopy. Spatial distribution of oxygen in different phases with respect to any bulk or surface segregation and its role on electrocatalytic properties can be better understood using such techniques. Furthermore, the review underscores the critical importance of a thorough phase stability analysis for the Ta-N and Ta-O-N systems, stressing the need for continued research to enhance our understanding of phase stability and performance. CALPHAD assisted approaches in this context presents a significant advantage (Fig. 22). The field of water-splitting is yet to reap the

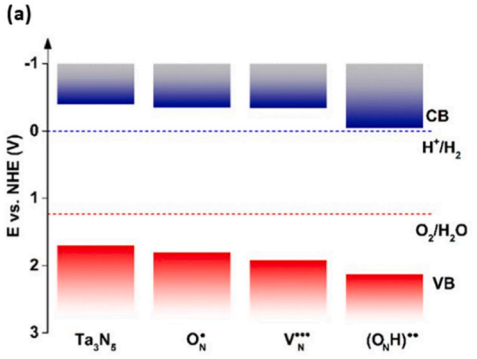

(b)

Dopant	Improvement in onset potential	Improvement in photocurrent density
Ba	-0.05	125 %
Sc	-0.1	132 %
Mg	-0.1	300 %
Zr	-0.125	150 %

Fig. 21.
(a) (a) The presence of hydrogen impurities causes shift in both conduction band minimum and valence band maximum leading to poor stability of Ta_3N_5 [251], *Reprinted (adapted) with permission from American Chemical Society Copyright {2024};* (b) Improvement in photocurrent density and onset potential when doped with Ba, Sc, Mg & Zr [252], *Reprinted (adapted) with permission from Elsevier*.

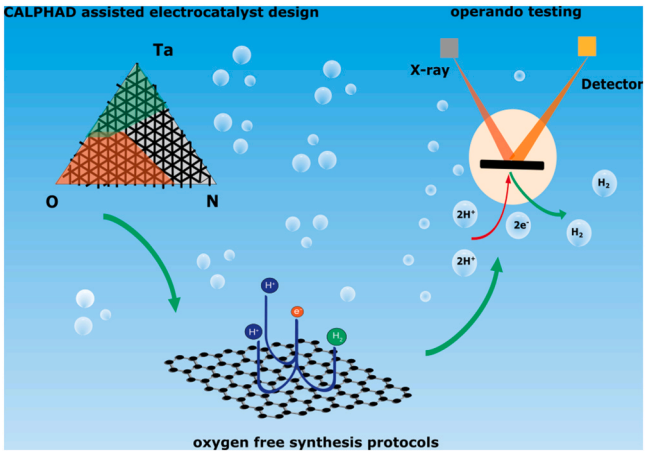

Fig. 22. The right way ahead for Ta-O-N system: A combinatorial approach based on inputs from constitutional studies, DFT concomitant with operando studies to identify the best performing and stable phase for water splitting.

full potential of CALPHAD and especially in the context of Ta-O-N/TaN system, its presence can lead to design of stable electrocatalysts. At a manageable computational cost, CALPHAD offers a robust framework for accurately modeling the thermodynamic properties and phase stability of Ta-O-N system, thus predicting and understanding surface oxidation phenomena. Despite Ta_3N_5 being extensively studied and found on the convex hull, it is notably absent from the current Ta-N phase diagram. This discrepancy underscores the necessity of revisiting and potentially revising the phase diagram to accurately account for the stability and presence of Ta_3N_5 and other relevant phases, such as Ta_5N_6, as indicated by recent quantum mechanical investigations. Identifying the most stable phase in an oxidizing atmosphere based on CALPHAD calculations coupled with DFT studies to identify the most stable surface could accelerate discovery of new catalysts. As an extension, computational studies to understand the role of ideal alloying elements in different phases in Ta-N system and their role in enhancing water reduction/oxidation kinetics is missing. This is extremely important for the less explored phases such as Ta_4N_5, Ta_5N_6 or even TaN. An adequately created database considering the experimental parametric space will also aid material chemists to design single source precursors. Thus, unique synthesis methodologies that do not incorporate oxygen containing tantalum precursors or use highly dangerous NH_3 atmosphere processing, schematically represented in Fig. 22, must be pursued. Also, unique moieties based on metal organic framework derived porous tantalum nitrides are still unexplored for catalytic water splitting. Such processing routes can help in reducing residual oxygen content that plays a detrimental role in surface catalytic reactions. Finally, the chemical design of electrocatalysts both in terms of surface chemistry and phase composition represents the holy grail of chemically engineered electrocatalysts for small molecule (e.g., H_2O, N_2, CO_2) activation and their conversion into fuels and energy carriers [253–255].

CRediT authorship contribution statement

Niraja Mohrana: Data curation, Formal analysis, Writing – original draft. **Bhupendra Singh:** Data curation, Writing – review & editing. **Sehun Kwon:** Writing – review & editing. **Kwang Ho Kim:** Writing – review & editing. **Ravi Kumar:** Conceptualization, Writing – review & editing. **Sanjay Mathur:** Conceptualization, Supervision, Writing – review & editing. **Raghunath Sharma Mukkavilli:** Data curation, Writing – original draft. **Florian Vollnhals:** Data curation, Writing – original draft. **Arun Ichangi:** Data curation, Writing – original draft. **K. C. Hari Kumar:** Conceptualization, Writing – review & editing. **Silke Christiansen:** Writing – review & editing. **Thomas Fischer:** Data curation, Visualization, Writing – review & editing.

Declaration of Competing Interest

The authors declare that they have no known competing financial interests or personal relationships that could have appeared to influence the work reported in this paper.

Data Availability

Data will be made available on request.

Acknowledgements

Authors are thankful to the Indian Institute of Technology and the University of Cologne for providing the infrastructural and financial support. The support obtained by the Department of Science and Technology (DST), India within the framework of SPARC initiative is gratefully acknowledged. SM gratefully acknowledges the support provided by IIT Madras under the Institute of Eminence (IoE) scheme during which this review manuscript was finalized.

References

[1] The Future of Hydrogen: Seizing today's opportunities, Organisation for Economic Co-operation and Development, Paris, 2019. https://www.oecd-ilibrary.org/energy/the-future-of-hydrogen_1e0514c4-en (accessed May 1, 2024).
[2] D. Tonelli, L. Rosa, P. Gabrielli, K. Caldeira, A. Parente, F. Contino, Global land and water limits to electrolytic hydrogen production using wind and solar resources, 14:1 14, Nat. Commun. 2023 (2023) 1–14, https://doi.org/10.1038/s41467-023-41107-x.
[3] J. Jia, L.C. Seitz, J.D. Benck, Y. Huo, Y. Chen, J.W.D. Ng, T. Bilir, J.S. Harris, T. F. Jaramillo, Solar water splitting by photovoltaic-electrolysis with a solar-to-hydrogen efficiency over 30%, Nat. Commun. 2016 7:1 7 (2016) 1–6, https://doi.org/10.1038/ncomms13237.
[4] Y. Gong, J. Yao, P. Wang, Z. Li, H. Zhou, C. Xu, Perspective of hydrogen energy and recent progress in electrocatalytic water splitting, Chin. J. Chem. Eng. 43 (2022) 282–296, https://doi.org/10.1016/J.CJCHE.2022.02.010.
[5] C. Wei, R.R. Rao, J. Peng, B. Huang, I.E.L. Stephens, M. Risch, Z.J. Xu, Y. Shao-Horn, Recommended Practices and Benchmark Activity for Hydrogen and Oxygen Electrocatalysis in Water Splitting and Fuel Cells, Adv. Mater. 31 (2019) 1806296, https://doi.org/10.1002/ADMA.201806296.
[6] H. Wu, Q. Huang, Y. Shi, J. Chang, S. Lu, Electrocatalytic water splitting: Mechanism and electrocatalyst design, Nano Res. 16 (2023) 9142–9157, https://doi.org/10.1007/S12274-023-5502-8/METRICS.
[7] P. Chatterjee, M.S.K. Ambati, A.K. Chakraborty, S. Chakrabortty, S. Biring, S. Ramakrishna, T.K.S. Wong, A. Kumar, R. Lawaniya, G.K. Dalapati, Photovoltaic/photo-electrocatalysis integration for green hydrogen: A review, Energy Convers. Manag. 261 (2022) 115648, https://doi.org/10.1016/J.ENCONMAN.2022.115648.
[8] T. Grube, J. Reul, M. Reuß, S. Calnan, N. Monnerie, R. Schlatmann, C. Sattler, M. Robinius, D. Stolten, A techno-economic perspective on solar-to-hydrogen concepts through 2025, Sustain. Energy Fuels 4 (2020) 5818–5834, https://doi.org/10.1039/d0se00896f.
[9] A. Grimm, W.A. de Jong, G.J. Kramer, Renewable hydrogen production: A techno-economic comparison of photoelectrochemical cells and photovoltaic-electrolysis, Int. J. Hydrog. Energy 45 (2020) 22545–22555, https://doi.org/10.1016/j.ijhydene.2020.06.092.
[10] R.J. Ouimet, J.R. Glenn, D. De Porcellinis, A.R. Motz, M. Carmo, K.E. Ayers, The Role of Electrocatalysts in the Development of Gigawatt-Scale PEM Electrolyzers, ACS Catal. (2022) 6159–6171, https://doi.org/10.1021/ACSCATAL.2C00570/ASSET/IMAGES/LARGE/CS2C00570_0019.JPEG.
[11] S. Shiva Kumar, V. Himabindu, Hydrogen production by PEM water electrolysis – A review, Mater. Sci. Energy Technol. 2 (2019) 442–454, https://doi.org/10.1016/j.mset.2019.03.002.
[12] S. Krishnan, V. Koning, M. Theodorus de Groot, A. de Groot, P.G. Mendoza, M. Junginger, G.J. Kramer, Present and future cost of alkaline and PEM electrolyser stacks, Int. J. Hydrog. Energy 48 (2023) 32313–32330, https://doi.org/10.1016/j.ijhydene.2023.05.031.
[13] F. Yu, L. Yu, I.K. Mishra, Y. Yu, Z.F. Ren, H.Q. Zhou, Recent developments in earth-abundant and non-noble electrocatalysts for water electrolysis, Mater. Today Phys. 7 (2018) 121–138, https://doi.org/10.1016/J.MTPHYS.2018.11.007.
[14] P. Yu, F. Wang, T.A. Shifa, X. Zhan, X. Lou, F. Xia, J. He, Earth abundant materials beyond transition metal dichalcogenides: A focus on electrocatalyzing hydrogen evolution reaction, Nano Energy 58 (2019) 244–276, https://doi.org/10.1016/J.NANOEN.2019.01.017.

[15] Y. Zhang, Y. Zhang, B. Tian, H. Li, Z. Zeng, D. Ho, D-band center optimization of iron carbide via Cr substitution for enhanced alkaline hydrogen evolution, Mater. Today Energy 29 (2022) 101133, https://doi.org/10.1016/J.MTENER.2022.101133.

[16] L. Wang, Z. Li, K. Wang, Q. Dai, C. Lei, B. Yang, Q. Zhang, L. Lei, M.K.H. Leung, Y. Hou, Tuning d-band center of tungsten carbide via Mo doping for efficient hydrogen evolution and Zn–H2O cell over a wide pH range, Nano Energy 74 (2020) 104850, https://doi.org/10.1016/J.NANOEN.2020.104850.

[17] C. Miao, Y. Zang, H. Wang, X. Zhuang, N. Han, Y. Yin, Y. Ma, M. Chen, Y. Dai, S. P. Yip, J.C. Ho, Z. xing Yang, Tunable d-Band Centers of Ni5P4 Ultra-Thin Nanosheets for Highly-Efficient Hydrogen Evolution Reaction, Adv. Mater. Interfaces 9 (2022) 2200739, https://doi.org/10.1002/ADMI.202200739.

[18] H. Sun, Z. Yan, F. Liu, W. Xu, F. Cheng, J. Chen, Self-Supported Transition-Metal-Based Electrocatalysts for Hydrogen and Oxygen Evolution, Adv. Mater. 32 (2020) 1–18, https://doi.org/10.1002/adma.201806326.

[19] Y. Abghoui, E. Skúlason, Hydrogen evolution reaction catalyzed by transition-metal nitrides, J. Phys. Chem. C. 121 (2017) 24036–24045, https://doi.org/10.1021/acs.jpcc.7b06811.

[20] E. Nurlaela, A. Ziani, K. Takanabe, Tantalum nitride for photocatalytic water splitting: concept and applications, Mater. Renew. Sustain. Energy 5 (2016) 1–21, https://doi.org/10.1007/s40243-016-0083-z.

[21] C. Zhen, R. Chen, L. Wang, G. Liu, H.-M. Cheng, Tantalum (oxy)nitride based photoanodes for solar-driven water oxidation, J. Mater. Chem. A 4 (2016) 2783–2800, https://doi.org/10.1039/C5TA07057K.

[22] M. Xiao, S. Wang, S. Thaweesak, B. Luo, L. Wang, Tantalum (Oxy)Nitride: Narrow Bandgap Photocatalysts for Solar Hydrogen Generation, Engineering 3 (2017) 365–378, https://doi.org/10.1016/J.ENG.2017.03.019.

[23] V. Khanal, R. Irani, S. Fiechter, F.F. Abdi, V. (Ravi) Subramanian, The Photoelectrochemical and Photocatalytic Properties of Tantalum Oxide and Tantalum Nitride, J. Electrochem. Soc. 166 (2019) H3294, https://doi.org/10.1149/2.0391905jes.

[24] A. Jolly, Bull Soc, Chim. Fr. 2 (1876) 506.

[25] Nils Schönberg, An X-Ray Study of the Tantalum-Nitrogen System, Acta Chem. Scand. 8 (1954) 199–203.

[26] A.E. van Arkel, An x-ray examination of titanium nitride. I, Phys. (Amst.) 4 (1924) 286–301.

[27] G. Brauer, K.H. Zapp, Die Kristallstruktur des Tantalnitrids TaN, 604–604, Naturwissenschaften 40 (1953), https://doi.org/10.1007/BF00820422.

[28] G. Brauer, K.H. Zapp, Die Nitride des Tantals, ZAAC - J. Inorg. Gen. Chem. 277 (1954) 129–139, https://doi.org/10.1002/zaac.19542770304.

[29] A.N. Christensen, B. Lebech, A Reinvestigation of the Structure of e-Tantalum Nitride, Acta Crystallogr. Sect. B: Struct. Crystallogr. Cryst. Chem. 34 (1978) 261–263, https://doi.org/10.1016/S0040-4039(00)94917-7.

[30] J. Gatterer, G. Dufek, P.E.R. Kieffer, Das kubisehe Tantalmononitrid (B 1-Typ) und seine Mischbar- keit mit den isotypen Ubergangsmetallnitriden und -carbiden, Mon. Fur Chem. 106 (1975) 1137–1147.

[31] A. Zerr, G. Miehe, J. Li, D.A. Dzivenko, V.K. Bulatov, H. Hofer, N. Bolfan-Casanova, M. Fialin, G. Brey, T. Watanabe, M. Yoshimura, High-Pressure Synthesis of Tantalum Nitride Having Orthorhombic U2S3 Structure, Adv. Funct. Mater. 05 (2009) 2282–2288, https://doi.org/10.1002/adfm.200801923.

[32] N. Moharana, C. Ghosh, A. Dasgupta, R. Maezono, R. Kumar, K.C.H. Kumar, Thermal decomposition of oxygen-containing Ta3N5{\rm Ta_3\rm N_5\, J. Am. Ceram. Soc. 107 (2024) 6342–6352, https://doi.org/10.1111/jace.19869.

[33] C.R. Weinberger, X. Yu, H. Yu, G.B. Thompson, Ab initio investigations of the phase stability in group IVB and VB transition metal nitrides, Comput. Mater. Sci. 138 (2017) 333–345, https://doi.org/10.1016/j.commatsci.2017.07.005.

[34] L.E. Conroy, A.N. Christensen, Preparation and crystal structure of β-Ta2N, J. Solid State Chem. 20 (1977) 205–207, https://doi.org/10.1016/0022-4596(77)90069-X.

[35] A.Y. Ganin, L. Kienle, V.G. Vajenine, Plasma-enhanced CVD synthesis and structural characterization of Ta2N3, Eur. J. Inorg. Chem. (2004) 3233–3239, https://doi.org/10.1002/ejic.200400227.

[36] N. Schönberg, An X-Ray Study of the Tantalum-Nitrogen System, Acta Chem. Scand. 8 (1954) 199–203, https://doi.org/10.3891/acta.chem.scand.08-0199.

[37] V.J. Strähle, Die Kristallstruktur des Tantal(V)-nitrids Ta3N5, ZAAC - J. Inorg. Gen. Chem. 402 (1973) 47–57, https://doi.org/10.1002/zaac.19734020107.

[38] N. Terao, Structure of Tantalum Nitrides, Jpn. J. Appl. Phys. 10 (1971) 248–259.

[39] S.J. Henderson, A.L. Hector, Structural and compositional variations in Ta3N5 produced by high-temperature ammonolysis of tantalum oxide, J. Solid State Chem. 179 (2006) 3518–3524, https://doi.org/10.1016/j.jssc.2006.07.021.

[40] M. Grumski, P.P. Dholabhai, J.B. Adams, Ab initio study of the stable phases of 1:1 tantalum nitride, Acta Mater. 61 (2013) 3799–3807, https://doi.org/10.1016/j.actamat.2013.03.018.

[41] P. Violet, E. Blanquet, L.O. Bacq, Density functional study of the stability and electronic properties of TaxNy compounds used as copper diffusion barriers 83 (2006) 2077–2081, https://doi.org/10.1016/j.mee.2006.09.011.

[42] C. Stampfl, A.J. Freeman, Metallic to insulating nature of (formula presented) Role of Ta and N vacancies, Phys. Rev. B 67 (2003) 1–7, https://doi.org/10.1103/PhysRevB.67.064108.

[43] J. Wang, J. Feng, L. Zhang, Z. Li, Z. Zou, Role of oxygen impurity on the mechanical stability and atomic cohesion of Ta3N5 semiconductor photocatalyst, Phys. Chem. Chem. Phys. 16 (2014) 15375–15380, https://doi.org/10.1039/c4cp00120f.

[44] J. Wang, T. Fang, L. Zhang, J. Feng, Z. Li, Z. Zou, Eff. Oxyg. doping Opt. Band. gap Band. edge Positions Ta3N5 Photocatal.: A GGA+*U* Calc. 309 (2014) 291–299.

[45] X.P. Du, Y.X. Wang, V.C. Lo, Vacancy and Oxygen Substitution for Nitrogen-Induced Structural Stability of Ta2N3, J. Phys. Chem. C. 115 (2011) 3129–3135, https://doi.org/10.1021/jp110919w.

[46] R. Chen, C. Zhen, Y. Yang, X. Sun, J.T.S. Irvine, L. Wang, G. Liu, H.-M. Cheng, Boosting photoelectrochemical water splitting performance of Ta3N5 nanorod array photoanodes by forming a dual co-catalyst shell, Nano Energy 59 (2019) 683–688, https://doi.org/10.1016/j.nanoen.2019.03.009.

[47] J. Liu, W. Luo, K. Zhu, X. Wen, F. Xiu, J. Yuan, Z. Zou, W. Huang, Cathodic shift of a photo-potential on a Ta3N5 photoanode by post-heating a TiO2 passivation layer, RSC Adv. 7 (2017) 30650–30656, https://doi.org/10.1039/C7RA04647B.

[48] A. Abdel Haleem, N. Perumandla, Y. Naruta, Preparation of Nanostructured Ta3N5 Electrodes by Alkaline Hydrothermal Treatment Followed by NH3 Annealing and Their Improved Water Oxidation Performance, ACS Omega 4 (2019) 7815–7821, https://doi.org/10.1021/acsomega.9b00382.

[49] Y. Horiuchi, S. Mine, M. Moriyasu, M. Anpo, T.-H. Kim, M. Matsuoka, Preparation of tantalum oxynitride thin film photocatalysts by reactive magnetron sputtering deposition under high substrate temperature, Res Chem. Inter. 43 (2017) 5123–5136, https://doi.org/10.1007/s11164-017-3040-2.

[50] Y. Pihosh, T. Minegishi, V. Nandal, T. Higashi, M. Katayama, T. Yamada, Y. Sasaki, K. Seki, Y. Suzuki, M. Nakabayashi, M. Sugiyama, K. Domen, Ta 3 N 5 -Nanorods enabling highly efficient water oxidation via advantageous light harvesting and charge collection, Energy Environ. Sci. 13 (2020) 1519–1530, https://doi.org/10.1039/D0EE00220H.

[51] D. Dastan, K. Shan, A. Jafari, F. Gity, X.-T. Yin, Z. Shi, N.D. Alharbi, B.A. Reshi, W. Fu, Ş. Ţălu, L. Aljerf, H. Garmestani, L. Ansari, Influence of nitrogen concentration on electrical, mechanical, and structural properties of tantalum nitride thin films prepared via DC magnetron sputtering, Appl. Phys. A 128 (2022) 400, https://doi.org/10.1007/s00339-022-05501-4.

[52] S.A. Shostachenko, R.V. Zakharchenko, R.V. Ryzhuk, S.V. Leshchev, Thermal stability of tantalum nitride based thin film resistors, IOP Conf. Ser.: Mater. Sci. Eng. 498 (2019) 012014, https://doi.org/10.1088/1757-899X/498/1/012014.

[53] D. Cristea, C. Croitoru, A. Marin, M. Dobromir, E.L. Ursu, I.L. Velicu, V. Tiron, V. Crăciun, L. Cunha, On the chemistry, photocatalytical, and corrosion behavior of co-sputtered tantalum and titanium oxynitride thin films, Appl. Surf. Sci. 592 (2022) 153260, https://doi.org/10.1016/j.apsusc.2022.153260.

[54] C.L. Yeh, E.W. Liu, Y.C. Chang, Effect of preheating on synthesis of tantalum nitride by self-propagating combustion, J. Eur. Ceram. Soc. 24 (2004) 3807–3815, https://doi.org/10.1016/j.jeurceramsoc.2003.12.032.

[55] C.-L. Yeh, Combustion Synthesis of Nitrides of Vanadium, Niobium, and Tantalum. in: Nitride Ceramics, John Wiley & Sons, Ltd, 2014, pp. 165–184, https://doi.org/10.1002/9783527684533.ch6.

[56] T. Mashimo, S. Tashiro, T. Toya, M. Nishida, H. Yamazaki, S. Yamaya, K. Oh-Ishi, Y. Syono, Synthesis of the B1-type tantalum nitride by shock compression, J. Mater. Sci. 28 (1993) 3439–3443, https://doi.org/10.1007/BF01159819.

[57] X. Chen, G.G. Peterson, C. Goldberg, G. Nuesca, H.L. Frisch, A.E. Kaloyeros, B. Arkles, J. Sullivan, Low-temperature chemical vapor deposition of tantalum nitride from tantalum pentabromide for integrated circuitry copper metallization applications, J. Mater. Res. 14 (1999) 2043–2052, https://doi.org/10.1557/JMR.1999.0276.

[58] T. Chen, C. Xu, T.H. Baum, G.T. Stauf, J.F. Roeder, A.G. DiPasquale, A. L. Rheingold, New Tantalum Amido Complexes with Chelate Ligands as Metalorganic (MO) Precursors for Chemical Vapor Deposition (CVD) of Tantalum Nitride Thin Films, Chem. Mater. 22 (2010) 27–35, https://doi.org/10.1021/cm9009767.

[59] H. Hajibabaei, D.J. Little, A. Pandey, D. Wang, Z. Mi, T.W. Hamann, Direct Deposition of Crystalline Ta3N5 Thin Films on FTO for PEC Water Splitting, ACS Appl. Mater. Interfaces 11 (2019) 15457–15466, https://doi.org/10.1021/acsami.8b21194.

[60] H. Hajibabaei, O. Zandi, T.W. Hamann, Tantalum nitride films integrated with transparent conductive oxide substrates via atomic layer deposition for photoelectrochemical water splitting, Chem. Sci. 7 (2016) 6760–6767, https://doi.org/10.1039/C6SC02116F.

[61] Z. Fang, H.C. Aspinall, R. Odedra, R.J. Potter, Atomic layer deposition of TaN and Ta3N5 using pentakis(dimethylamino)tantalum and either ammonia or monomethylhydrazine, J. Cryst. Growth 331 (2011) 33–39, https://doi.org/10.1016/j.jcrysgro.2011.07.012.

[62] J.-D. Kwon, J. Yun, S.-W. Kang, Comparison of Tantalum Nitride Films for Different NH3/H2/Ar Reactant States in Two-Step Atomic Layer Deposition, Jpn. J. Appl. Phys. 48 (2009) 025504, https://doi.org/10.1143/JJAP.48.025504.

[63] S.-H. Kim, S.-J. Im, K.-B. Kim, The effect of ion beam bombardment on the properties of Ta(C)N films deposited from pentakis-diethylamido-tantalum, Thin Solid Films 415 (2002) 177–186, https://doi.org/10.1016/S0040-6090(02)00505-9.

[64] N. Arshi, J. Lu, C.G. Lee, B.H. Koo, F. Ahmed, Effects of Nitrogen Content on the Phase and Resistivity of TaN Thin Films Deposited by Electron Beam Evaporation, JOM 66 (2014) 1893–1899, https://doi.org/10.1007/s11837-014-1028-6.

[65] H. Lee, Y. Zhou, S. Jung, H. Li, Z. Cheng, J. He, J. Chen, P. Sokalski, A. Dolocan, R. Gearba-Dolocan, K.C. Matthews, F. Giustino, J. Zhou, L. Shi, High-Pressure Synthesis and Thermal Conductivity of Semimetallic θ-Tantalum Nitride, Adv. Funct. Mater. 33 (2023) 2212957, https://doi.org/10.1002/adfm.202212957.

[66] M. Bykov, E. Bykova, A.V. Ponomareva, I.A. Abrikosov, S. Chariton, V. B. Prakapenka, M.F. Mahmood, L. Dubrovinsky, A.F. Goncharov, Stabilization of Polynitrogen Anions in Tantalum–Nitrogen Compounds at High Pressure, Angew. Chem. Int. Ed. 60 (2021) 9003–9008, https://doi.org/10.1002/anie.202100283.

[67] Z. Su, L. Wang, S. Grigorescu, K. Lee, P. Schmuki, Hydrothermal growth of highly oriented single crystalline Ta2O5 nanorod arrays and their conversion to Ta3N5

for efficient solar driven water splitting, Chem. Commun. 50 (2014) 15561–15564, https://doi.org/10.1039/C4CC05673F.
[68] B. Mazumder, A.L. Hector, Use of low temperature solvothermal reactions in the synthesis of nanocrystalline tantalum nitrides including nanorods, J. Mater. Chem. 18 (2008) 1392–1398, https://doi.org/10.1039/B717723B.
[69] Tao Fang, Huiting Huang, Jianyong Feng, Yingfei Hu, Yongsheng Guo, Shiying Zhang, Zhaosheng Li, Zhigang Zou, Exploring facile strategies for high-oxidation-state metal nitride synthesis: carbonate-assisted one-step synthesis of Ta3N5 films for solar water splitting, Science Bulletin 63 (n.d.) 1404–1410. https://doi.org/10.1016/j.scib.2018.10.005.
[70] Y. Xiang, B. Zhang, J. Liu, S. Chen, T. Hisatomi, K. Domen, G. Ma, A one-step synthesis of a Ta3N5 nanorod photoanode from Ta plates and NH4Cl powder for photoelectrochemical water oxidation, Chem. Commun. 56 (2020) 11843–11846, https://doi.org/10.1039/D0CC05044J.
[71] T. Takata, D. Lu, K. Domen, Synthesis of Structurally Defined Ta3N5 Particles by Flux-Assisted Nitridation, Cryst. Growth Des. 11 (2011) 33–38, https://doi.org/10.1021/cg901025e.
[72] Y.W. Kim, S. Cha, I. Kwak, I.S. Kwon, K. Park, C.S. Jung, E.H. Cha, J. Park, Surface-Modified Ta3N5 Nanocrystals with Boron for Enhanced Visible-Light-Driven Photoelectrochemical Water Splitting, ACS Appl. Mater. Interfaces 9 (2017) 36715–36722, https://doi.org/10.1021/acsami.7b09040.
[73] C.-T. Ho, K.-B. Low, R.F. Klie, K. Maeda, K. Domen, R.J. Meyer, P.T. Snee, Synthesis and Characterization of Semiconductor Tantalum Nitride Nanoparticles, J. Phys. Chem. C. 115 (2011) 647–652, https://doi.org/10.1021/jp110105u.
[74] Q. Gao, C. Giordano, M. Antonietti, Controlled Synthesis of Tantalum Oxynitride and Nitride Nanoparticles, Small 7 (2011) 3334–3340, https://doi.org/10.1002/smll.201101207.
[75] P.K. Das, M. Arunachalam, R.P. Sivasankaran, K.-S. Ahn, J.-S. Ha, S.H. Kang, Bulk and interfacial engineering of Ta3N5 nanotube arrays by Sn(IV) doping, proper passivation and co-catalysts for efficient solar water oxidation, Catal. Sci. Technol. 12 (2022) 6444–6457, https://doi.org/10.1039/D2CY01232D.
[76] Zixue Su, Sabina Grigorescu, Lei Wang, Kiyoung Lee, Patrik Schmuki, Fast fabrication of Ta2O5 nanotube arrays and their conversion to Ta3N5 for efficient solar driven water splitting, Electrochem. Commun. 50 (2014) 15–19.
[77] L. Wang, N.T. Nguyen, X. Zhou, I. Hwang, M.S. Killian, P. Schmuki, Enhanced Charge Transport in Tantalum Nitride Nanotube Photoanodes for Solar Water Splitting, ChemSusChem 8 (2015) 2615–2620, https://doi.org/10.1002/cssc.201500632.
[78] Z. Wang, Y. Inoue, T. Hisatomi, R. Ishikawa, Q. Wang, T. Takata, S. Chen, N. Shibata, Y. Ikuhara, K. Domen, Overall water splitting by Ta3N5 nanorod single crystals grown on the edges of KTaO3 particles, Nat. Catal. 1 (2018) 756–763, https://doi.org/10.1038/s41929-018-0134-1.
[79] Y. Li, L. Zhang, A. Torres-Pardo, J.M. González-Calbet, Y. Ma, P. Oleynikov, O. Terasaki, S. Asahina, M. Shima, D. Cha, L. Zhao, K. Takanabe, J. Kubota, K. Domen, Cobalt phosphate-modified barium-doped tantalum nitride nanorod photoanode with 1.5% solar energy conversion efficiency, Nat. Commun. 4 (2013) 2566, https://doi.org/10.1038/ncomms3566.
[80] T. Higashi, H. Nishiyama, Y. Suzuki, Y. Sasaki, T. Hisatomi, M. Katayama, T. Minegishi, K. Seki, T. Yamada, K. Domen, Transparent Ta3N5 Photoanodes for Efficient Oxygen Evolution toward the Development of Tandem Cells, Angew. Chem. Int. Ed. 58 (2019) 2300–2304, https://doi.org/10.1002/anie.201812081.
[81] T. Higashi, H. Nishiyama, V. Nandal, Y. Pihosh, Y. Kawase, R. Shoji, M. Nakabayashi, Y. Sasaki, N. Shibata, H. Matsuzaki, K. Seki, K. Takanabe, K. Domen, Design of semitransparent tantalum nitride photoanode for efficient and durable solar water splitting, Energy Environ. Sci. 15 (2022) 4761–4775, https://doi.org/10.1039/D2EE02090D.
[82] M. de Respinis, M. Fravventura, F.F. Abdi, H. Schreuders, T.J. Savenije, W. A. Smith, B. Dam, R. van de Krol, Oxynitrogenography: Controlled Synthesis of Single-Phase Tantalum Oxynitride Photoabsorbers, Chem. Mater. 27 (2015) 7091–7099, https://doi.org/10.1021/acs.chemmater.5b02938.
[83] M. Harb, P. Sautet, E. Nurlaela, P. Raybaud, L. Cavallo, K. Domen, J.M. Basset, K. Takanabe, Tuning the properties of visible-light-responsive tantalum (oxy) nitride photocatalysts by non-stoichiometric compositions: A first-principles viewpoint, Phys. Chem. Chem. Phys. 16 (2014) 20548–20560, https://doi.org/10.1039/c4cp03594a.
[84] M. Wassner, M. Eckardt, C. Gebauer, G.R. Bourret, N. Hüsing, R.J. Behm, Synthesis and electrocatalytic performance of spherical core-shell tantalum (oxy) nitride@nitrided carbon composites in the oxygen reduction reaction, Electrochim. Acta 227 (2017) 367–381, https://doi.org/10.1016/j.electacta.2016.12.145.
[85] A. Seifitokaldani, M. Perrier, O. Savadogo, Oxygen reduction reaction (ORR) on a mixed titanium and tantalum oxy-nitride catalyst prepared by the urea-based sol-gel method, J. N. Mater. Electrochem. Syst. 17 (2014) 55–65, https://doi.org/10.14447/jnmes.v17i2.424.
[86] A. Higuchi, N.C. Rosero-Navarro, A. Miura, Y. Masubuchi, K. Tadanaga, Preparation of TaON thin films by nitridation of solution process-derived precursor films with urea, J. Sol. -Gel Sci. Technol. (2024), https://doi.org/10.1007/s10971-024-06457-y.
[87] S.D. Cosham, V. Celorrio, A.N. Kulak, G. Hyett, Observation of visible light activated photocatalytic degradation of stearic acid on thin films of tantalum oxynitride synthesized by aerosol assisted chemical vapour deposition, Dalton Trans. 48 (2019) 10619–10627, https://doi.org/10.1039/C8DT04638G.
[88] P. Zhang, T. Wang, J. Zhang, X. Chang, J. Gong, Bridging the transport pathway of charge carriers in a Ta3N5 nanotube array photoanode for solar water splitting, Nanoscale 7 (2015) 13153–13158, https://doi.org/10.1039/C5NR03013G.
[89] L. Wang, F. Dionigi, N.T. Nguyen, R. Kirchgeorg, M. Gliech, S. Grigorescu, P. Strasser, P. Schmuki, Tantalum Nitride Nanorod Arrays: Introducing Ni–Fe Layered Double Hydroxides as a Cocatalyst Strongly Stabilizing Photoanodes in Water Splitting, Chem. Mater. 27 (2015) 2360–2366, https://doi.org/10.1021/cm503887t.
[90] C. Shao, J. Han, G. Liu, Z. Wang, Y. Zhao, X. Zong, C. Li, Fabrication of a Robust Tantalum Nitride Photoanode from a Flame-Heating-Derived Compact Oxide Film, ChemPhotoChem 2 (2018) 249–256, https://doi.org/10.1002/cptc.201700178.
[91] C.M. Jiang, L.I. Wagner, M.K. Horton, J. Eichhorn, T. Rieth, V.F. Kunzelmann, M. Kraut, Y. Li, K.A. Persson, I.D. Sharp, Metastable Ta2N3 with highly tunable electrical conductivity: Via oxygen incorporation, Mater. Horiz. 8 (2021) 1744–1755, https://doi.org/10.1039/d1mh00017a.
[92] Y.-J. Peng, S.-Y. Lee, K.-S. Chang, Facile Fabrication of a Photocatalyst of Ta4N5 Nanocolumn Arrays by Using Reactive Sputtering, J. Electrochem. Soc. 162 (2015) H371, https://doi.org/10.1149/2.0771506jes.
[93] G.B. Thiyagarajan, R.S. Mukkavilli, D. Graf, T. Fischer, M. Wilhelm, S. Christiansen, S. Mathur, R. Kumar, Self-supported amorphous TaNx(Oy)/nickel foam thin film as an advanced electrocatalyst for hydrogen evolution reaction, Chem. Commun. 58 (2022) 3310–3313, https://doi.org/10.1039/D2CC00151A.
[94] I. Narkeviciute, T.F. Jaramillo, Effects of Ta3N5 Morphology and Composition on the Performance of Si-Ta3N-5 Photoanodes, Sol. RRL 1 (2017) 1–9, https://doi.org/10.1002/solr.201700121.
[95] N.S. Alhajri, H. Yoshida, D.H. Anjum, A.T. Garcia-Esparza, J. Kubota, K. Domen, K. Takanabe, Synthesis of tantalum carbide and nitride nanoparticles using a reactive mesoporous template for electrochemical hydrogen evolution, J. Mater. Chem. A 1 (2013) 12606–12616, https://doi.org/10.1039/c3ta12984e.
[96] R.S. Mukkavilli, A. Ichangi, G.B. Thiyagarajan, F. Vollnhals, M. Wilhelm, A. Bhardwaj, S. Christiansen, L. Neelakantan, S. Mathur, R. Kumar, Electrospun 1D Ta3N5-(O) nanofibers as advanced electrocatalysts for hydrogen evolution reaction in proton exchange membrane water electrolyser, Open Ceram. 10 (2022) 100267, https://doi.org/10.1016/j.oceram.2022.100267.
[97] S.-I. Baik, Y.-W. Kim, Microstructural evolution of tantalum nitride thin films synthesized by inductively coupled plasma sputtering, Appl. Microsc. 50 (2020) 7, https://doi.org/10.1186/s42649-020-00026-7.
[98] N.A. Gaida, T. Sasaki, Z. Liu, K. Niwa, M. Hirozawa, T. Ohsuna, M. Hasegawa, Nanowire crystals of tantalum nitride grown in ammonium halide fluxes at high pressures, Appl. Phys. Lett. 116 (2020) 123102, https://doi.org/10.1063/1.5140856.
[99] J. Lin, W. Zhao, F. Huang, Facile and economical synthesis of nitrogen-rich tantalum nitrides via an ammonia looping process under confined space, N. J. Chem. 44 (2020) 9158–9162, https://doi.org/10.1039/D0NJ01390K.
[100] S.G. Han, S.Y. Chae, S.Y. Lee, B.K. Min, Y.J. Hwang, Charge separation properties of Ta3N5 photoanodes synthesized via a simple metal–organic-precursor decomposition process, Phys. Chem. Chem. Phys. 20 (2018) 2865–2871, https://doi.org/10.1039/C7CP05406H.
[101] S. Suzuki, R. Ando, Y. Matsui, K. Isechi, K. Yubuta, K. Teshima, Prismatic Ta3N5-composed spheres produced by self-sacrificial template-like conversion of Ta particles via Na2CO3 flux, CrystEngComm 22 (2020) 5122–5129, https://doi.org/10.1039/D0CE00589D.
[102] T. Garcia-Mendoza, A. Martinez-Garcia, I.G. Becerril-Juarez, E. Lopez-Vazquez, M. Avalos-Borja, M. Valera-Zaragoza, E.A. Juarez-Arellano, Mechanosynthesis of metastable cubic δ-Ta1−xN, Ceram. Int. 46 (2020) 23049–23058, https://doi.org/10.1016/j.ceramint.2020.06.082.
[103] V.M. Orlov, R.N. Osaulenko, V.Ya Kuznetsov, D.V. Lobov, Synthesis of Niobium and Tantalum Nitrides via Nitridation of Powders during Calcium Reduction of Their Oxide Compounds, Inorg. Mater. 58 (2022) 706–714, https://doi.org/10.1134/S0020168522060073.
[104] K. Zhang, L. Wu, C. Zhang, Q. Yang, W. Qian, G. Hu, W. Hu, Y. Kong, L. Wang, G. Li, Low temperature synthesis of nanocrystalline tantalum nitride, J. Ceram. Soc. Jpn. 131 (2023) 178–180, https://doi.org/10.2109/jcersj2.23001.
[105] C. Stampfl, A.J. Freeman, Stable and metastable structures of the multiphase tantalum nitride system, Phys. Rev. B Hedin 71 (2005) 4–8, https://doi.org/10.1103/PhysRevB.71.024111.
[106] D. Kim, H. Lee, D. Kim, Y. Keun Kim, Electrical and mechanical properties of tantalum nitride thin films deposited by reactive sputtering, J. Cryst. Growth 283 (2005) 404–408, https://doi.org/10.1016/j.jcrysgro.2005.06.017.
[107] Y. Hu, M. Rasadujjaman, Y. Wang, J. Zhang, J. Yan, M.R. Baklanov, Study on the Electrical, Structural, Chemical and Optical Properties of PVD Ta(N) Films Deposited with Different N2 Flow Rates, Coatings 11 (2021) 937, https://doi.org/10.3390/coatings11080937.
[108] S. Consiglio, S. Dey, K. Yu, K. Tapily, R.D. Clark, T. Hasegawa, C.S. Wajda, G. J. Leusink, A.C. Diebold, In Situ Ramp Anneal X-ray Diffraction Study of Atomic Layer Deposited Ultrathin TaN and Ta1-xAlxNy Films for Cu Diffusion Barrier Applications, ECS J. Solid State Sci. Technol. 5 (2016) P509, https://doi.org/10.1149/2.0201609jss.
[109] M. Alishahi, F. Mahboubi, S.M.M. Khoie, M. Aparicio, E. Lopez-Elvira, J. Méndez, R. Gago, Structural properties and corrosion resistance of tantalum nitride coatings produced by reactive DC magnetron sputtering, RSC Adv. 6 (2016) 89061–89072, https://doi.org/10.1039/C6RA17869C.
[110] A.H. Ramezani, M.R. Hantehezadeh, M. Ghoranneviss, E. Darabi, Corrosion resistance behavior of nitrogen ion-implanted in tantalum, Appl. Phys. A 122 (2016) 179, https://doi.org/10.1007/s00339-016-9712-8.
[111] A. Ishihara, S. Doi, S. Mitsushima, K. Ota, Tantalum (oxy) nitrides prepared using reactive sputtering for new nonplatinum cathodes of polymer electrolyte fuel cell 53 (2008) 5442–5450, https://doi.org/10.1016/j.electacta.2008.02.092.

[112] F. Zhang, S. Xi, G. Lin, X. Hu, X.W. (David) Lou, K. Xie, Metallic Porous Iron Nitride and Tantalum Nitride Single Crystals with Enhanced Electrocatalysis Performance, Adv. Mater. 31 (2019), https://doi.org/10.1002/adma.201806552.
[113] Q. Liu, F. Lan, J. Chen, C. Zeng, J. Wang, A review of proton exchange membrane fuel cell water management: Membrane electrode assembly, J. Power Sources 517 (2022) 230723, https://doi.org/10.1016/j.jpowsour.2021.230723.
[114] Z. Hua, Z. Zheng, E. Pahon, M.C. Péra, F. Gao, A review on lifetime prediction of proton exchange membrane fuel cells system, J. Power Sources 529 (2022) 231256, https://doi.org/10.1016/j.jpowsour.2022.231256.
[115] L. Zhao, J. Zhu, Y. Zheng, M. Xiao, R. Gao, Z. Zhang, G. Wen, H. Dou, Y. Deng, A. Yu, Z. Wang, Z. Chen, Materials Engineering toward Durable Electrocatalysts for Proton Exchange Membrane Fuel Cells, Adv. Energy Mater. 12 (2022) 2102665, https://doi.org/10.1002/aenm.202102665.
[116] E. Zhu, M. Wu, H. Xu, B. Peng, Z. Liu, Y. Huang, Y. Li, Stability of Platinum-Group-Metal-Based Electrocatalysts in Proton Exchange Membrane Fuel Cells, Adv. Funct. Mater. 32 (2022) 2203883, https://doi.org/10.1002/adfm.202203883.
[117] F. Xiao, Y. Wang, Z. Wu, G. Chen, F. Yang, S. Zhu, K. Siddharth, Z. Kong, A. Lu, J. Li, C. Zhong, Z. Zhou, M. Shao, Recent Advances in Electrocatalysts for Proton Exchange Membrane Fuel Cells and Alkaline Membrane Fuel Cells, Adv. Mater. 33 (2021) 2006292, https://doi.org/10.1002/adma.202006292.
[118] R. Zeng, Y. Yang, X. Feng, H. Li, L.M. Gibbs, F.J. DiSalvo, H.D. Abruña, Nonprecious transition metal nitrides as efficient oxygen reduction electrocatalysts for alkaline fuel cells, Sci. Adv. 8 (2022), https://doi.org/10.1126/sciadv.abj1584.
[119] L. Lin, S. Piao, Y. Choi, L. Lyu, H. Hong, D. Kim, J. Lee, W. Zhang, Y. Piao, Nanostructured Transition Metal Nitrides as Emerging Electrocatalysts for Water Electrolysis: Status and Challenges, EnergyChem 4 (2022) 100072, https://doi.org/10.1016/j.enchem.2022.100072.
[120] H. Koivuluoto, J. Näkki, P. Vuoristo, Corrosion properties of cold-sprayed tantalum coatings, J. Therm. Spray. Technol. 18 (2009) 75–82, https://doi.org/10.1007/s11666-008-9281-2.
[121] D.B. Wei, X.H. Chen, P.Z. Zhang, F. Ding, F.K. Li, Z.J. Yao, Plasma surface tantalum alloying on titanium and its corrosion behavior in sulfuric acid and hydrochloric acid, Appl. Surf. Sci. 441 (2018) 448–457, https://doi.org/10.1016/j.apsusc.2018.02.058.
[122] N. Elsayed, M.M. El-Rabiei, M. Negem, F.E.T. Heakal, The potential of tantalum as an efficient electrocatalyst for green hydrogen production, Electrochim. Acta 404 (2022) 139783, https://doi.org/10.1016/j.electacta.2021.139783.
[123] A. Ishihara, K. Lee, S. Doi, S. Mitsushima, N. Kamiya, M. Hara, K. Domen, K. Fukuda, K. Ota, Tantalum Oxynitride for a Novel Cathode of PEFC, Electrochem. Solid-State Lett. 8 (2005) A201, https://doi.org/10.1149/1.1865612.
[124] Y. Shibata, A. Ishihara, S. Mitsushima, N. Kamiya, K.I. Ota, Effect of heat treatment on catalytic activity for oxygen reduction reaction of TaOxNyTi prepared by electrophoretic deposition, Electrochem. Solid-State Lett. 10 (2007) 43–46, https://doi.org/10.1149/1.2402983.
[125] M. Chisaka, A. Ishihara, N. Uehara, M. Matsumoto, H. Imai, K. Ota, Nano-TaOxNy particles synthesized from oxy-tantalum phthalocyanine: how to prepare precursors to enhance the oxygen reduction reaction activity after ammonia pyrolysis? J. Mater. Chem. A 3 (2015) 16414–16418, https://doi.org/10.1039/C5TA03860J.
[126] E. Watanabe, H. Ushiyama, K. Yamashita, Theoretical studies on the stabilities and reactivities of Ta3N5 (100) surfaces, Chem. Phys. Lett. 561–562 (2013) 57–62, https://doi.org/10.1016/j.cplett.2012.12.068.
[127] A.M. Pasqualeti, E. Padgett, D. Kuo, D.A. Muller, F.H.B. Lima, J. Suntivich, Influence of Aliovalent Substitutions on Oxygen Reduction on Tantalum Oxynitrides 164 (2017) 645–650, https://doi.org/10.1149/2.1361706jes.
[128] Y. Ohgi, A. Ishihara, K. Matsuzawa, S. Mitsushima, K. Ota, M. Matsumoto, H. Imai, Oxygen reduction reaction on tantalum oxide-based catalysts prepared from TaC and TaN, Electrochim. Acta 68 (2012) 192–197, https://doi.org/10.1016/j.electacta.2012.02.059.
[129] S. Wirth, F. Harnisch, M. Weinmann, U. Schröder, Comparative study of IVB – VIB transition metal compound electrocatalysts for the hydrogen evolution reaction, Appl. Catal. B, Environ. 126 (2012) 225–230, https://doi.org/10.1016/j.apcatb.2012.07.023.
[130] A. Ishikawa, T. Takata, J.N. Kondo, M. Hara, K. Domen, Electrochemical behavior of thin Ta3N5 semiconductor film, J. Phys. Chem. B 108 (2004) 11049–11053, https://doi.org/10.1021/jp048802u.
[131] Y. Gao, Z. Tong, X. Fan, 3D Ta3N5 thin film confined-growth Co nanoparticles for efficient bifunction electrolyzed water, Electrochim. Acta 390 (2021) 138797, https://doi.org/10.1016/j.electacta.2021.138797.
[132] Y. Yan, Y. Gao, H. Zheng, B. Yuan, Q. Zhang, Y. Gu, G. Zhuang, Z. Wei, Z. Yao, X. Zhong, X. Li, J. Wang, Simultaneous electrochemical ozone production and hydrogen evolution by using tantalum-based nanorods electrocatalysts, Appl. Catal. B: Environ. 266 (2020), https://doi.org/10.1016/j.apcatb.2020.118632.
[133] R.S. Mukkavilli, A. Saxena, S. Ji, G.B. Thiyagarajan, H. Choi, S. Mathur, R. Kumar, Large-scale synthesis of centrifugally spun tantalum oxynitride fiber electrocatalysts for hydrogen evolution reaction, J. Am. Ceram. Soc. (2023) 1–15, https://doi.org/10.1111/jace.19274.
[134] N. Ye, Y. Bai, Z. Jiang, T. Fang, Design the PdCu/TaNC electrocatalyst with core-shell structure having high efficiency for methanol and formic acid oxidation reactions, Electrochim. Acta 383 (2021) 138365, https://doi.org/10.1016/j.electacta.2021.138365.
[135] N. Ye, P. Zhao, X. Qi, W. Sheng, Z. Jiang, T. Fang, Understanding the high performance of PdSn–TaN(tantalum nitride)/C electrocatalysts for the methanol oxidation reaction: coupling nitrides and oxophilic elements, J. Mater. Chem. A 10 (2022) 266–287, https://doi.org/10.1039/D1TA07382F.
[136] N. Ye, P. Zhao, X. Qi, W. Sheng, Z. Jiang, T. Fang, Ethanol electro-oxidation on the PdSn-TaN/C catalyst in alkaline media: Making TaN capable of splitting CC bond, Appl. Catal. B: Environ. 314 (2022) 121473, https://doi.org/10.1016/j.apcatb.2022.121473.
[137] J. Dang, S. Yun, X. Zhou, Y. Zhang, Z. Wu, An integrated approach to construct tantalum derivatives for electrocatalysis beyond the triiodide reduction reaction, Ceram. Int. 47 (2021) 23066–23077, https://doi.org/10.1016/j.ceramint.2021.05.021.
[138] X. Wang, S. Yun, Y. Zhang, L. Zhang, J. Dang, M. Sun, Z. Liu, Y. Wang, Boosting catalytic activity of niobium/tantalum-nitrogen active-sites for triiodide reduction in photovoltaics, J. Colloid Interface Sci. 603 (2021) 651–665, https://doi.org/10.1016/j.jcis.2021.06.128.
[139] S. Yu, Y. Zhang, S. Yang, K. Xiao, D. Cai, H. Nie, Z. Yang, High-density oxygen-doped nano-TaN enables robust polysulfide interconversion in Li−S batteries, Chin. Chem. Lett. 34 (2023) 107911, https://doi.org/10.1016/j.cclet.2022.107911.
[140] Q. Li, G. Qin, L. Wu, Y. Zhao, X. Wang, High catalytic performance of a Pd-loaded TaN-TaC electrocatalyst for ethylene glycol oxidation in an alkaline medium, Appl. Surf. Sci. 537 (2021) 147849, https://doi.org/10.1016/j.apsusc.2020.147849.
[141] T. Yang, C. Zhang, J. Zhang, H. Li, P. Bai, Z. Wang, X. Wang, Z. Chai, Defects induced growth of Pt on the heterojunction of TaON|N-rGO as highly CO-tolerant electrocatalyst for ethylene glycol oxidation, Appl. Surf. Sci. 536 (2021) 147668, https://doi.org/10.1016/j.apsusc.2020.147668.
[142] N. Ye, Z. Jiang, T. Fang, Probing the enhanced methanol electrooxidation mechanism by promoted CO tolerance on the Pd catalyst modified with TaN: A combined experimental and theoretical study, Int. J. Hydrog. Energy 46 (2021) 37321–37332, https://doi.org/10.1016/j.ijhydene.2021.09.056.
[143] Y. Bai, N. Ye, Z. Jiang, R. Zhang, T. Fang, Enhancing the activity and stability by coupling Ni-M bimetals and TaN for methanol oxidation reaction in alkaline media, Fuel 341 (2023) 127758, https://doi.org/10.1016/j.fuel.2023.127758.
[144] N. Ye, P. Zhao, X. Qi, R. Zhang, B. Yan, W. Sheng, Z. Jiang, T. Fang, Probing the activity origin of the enhanced methanol electrooxidation on Ni-induced PdNix(OH)y-TaN/C catalyst with nitrogen vacancies, Appl. Catal. B: Environ. 322 (2023) 122142, https://doi.org/10.1016/j.apcatb.2022.122142.
[145] S. Jiao, X. Fu, H. Huang, Descriptors for the Evaluation of Electrocatalytic Reactions: d-Band Theory and Beyond, Adv. Funct. Mater. 32 (2022) 2107651, https://doi.org/10.1002/adfm.202107651.
[146] S. González-Poggini, Hydrogen evolution descriptors: A review for electrocatalyst development and optimization, Int. J. Hydrog. Energy 59 (2024) 30–42, https://doi.org/10.1016/j.ijhydene.2024.01.362.
[147] Y. Hu, D. Huang, J. Zhang, Y. Huang, M.-S.J.T. Balogun, Y. Tong, Dual Doping Induced Interfacial Engineering of Fe2N/Fe3N Hybrids with Favorable d-Band towards Efficient Overall Water Splitting, ChemCatChem 11 (2019) 6051–6060, https://doi.org/10.1002/cctc.201901224.
[148] N. Yao, P. Li, Z. Zhou, Y. Zhao, G. Cheng, S. Chen, W. Luo, Synergistically Tuning Water and Hydrogen Binding Abilities Over Co4N by Cr Doping for Exceptional Alkaline Hydrogen Evolution Electrocatalysis, Adv. Energy Mater. 9 (2019) 1902449, https://doi.org/10.1002/aenm.201902449.
[149] Z. Chen, Y. Song, J. Cai, X. Zheng, D. Han, Y. Wu, Y. Zang, S. Niu, Y. Liu, J. Zhu, X. Liu, G. Wang, Tailoring the d-Band Centers Enables Co4N Nanosheets To Be Highly Active for Hydrogen Evolution Catalysis, Angew. Chem. Int. Ed. 57 (2018) 5076–5080, https://doi.org/10.1002/anie.201801834.
[150] Z. Liu, X. Zhang, H. Song, Y. Yang, Y. Zheng, B. Gao, J. Fu, P.K. Chu, K. Huo, Electronic Modulation between Tungsten Nitride and Cobalt Dopants for Enhanced Hydrogen Evolution Reaction at a Wide Range of pH, ChemCatChem 12 (2020) 2962–2966, https://doi.org/10.1002/cctc.202000391.
[151] H. Yang, Y. Hu, D. Huang, T. Xiong, M. Li, M.-S. Balogun, Y. Tong, Efficient hydrogen and oxygen evolution electrocatalysis by cobalt and phosphorus dual-doped vanadium nitride nanowires, Mater. Today Chem. 11 (2019) 1–7, https://doi.org/10.1016/j.mtchem.2018.10.004.
[152] H.S. Gujral, G. Singh, J.H. Yang, C.I. Sathish, J. Yi, A. Karakoti, M. Fawaz, K. Ramadass, A.H. Al-Muhtaseb, X. Yu, M.B.H. Breese, A. Vinu, Mesoporous titanium carbonitride derived from mesoporous C3N5 for highly efficient hydrogen evolution reaction, Carbon 195 (2022) 9–18, https://doi.org/10.1016/j.carbon.2022.03.060.
[153] W. Wang, C. Liu, D. Zhou, L. Yang, J. Zhou, D. Yang, *In-situ* synthesis of coupled molybdenum carbide and molybdenum nitride as electrocatalyst for hydrogen evolution reaction, J. Alloy. Compd. 792 (2019) 230–239, https://doi.org/10.1016/j.jallcom.2019.03.397.
[154] R. Kumar, Z. Ahmed, R. Rai, A. Gaur, S. Kumari, T. Maruyama, V. Bagchi, Uniformly Decorated Molybdenum Carbide/Nitride Nanostructures on Biomass Templates for Hydrogen Evolution Reaction Applications, ACS Omega 4 (2019) 14155–14161, https://doi.org/10.1021/acsomega.9b02321.
[155] J. Sun, B. Liang, Y. Huang, X. Wang, Synthesis of nanostructured tungsten carbonitride (WN*x*C*y*) by carbothermal ammonia reduction on activated carbon and its application in hydrazine decomposition, Catal. Today 274 (2016) 123–128, https://doi.org/10.1016/j.cattod.2016.01.031.
[156] R. Sharma Mukkavilli, B.R. Arunkumar, S. Mathur, R. Kumar, One-step synthesis and electrocatalytic hydrogen evolution in self-supported tantalum carbonitrides, Mater. Lett. 372 (2024) 137025, https://doi.org/10.1016/j.matlet.2024.137025.
[157] S. Adimi, W. Qi, T. Thomas, R. Gebauer, M. Yang, S. Ruan, Surface oxidation for enhancing the hydrogen evolution reaction of metal nitrides: a theoretical study

on vanadium nitride, Mater. Adv. 2 (2021) 3394–3404, https://doi.org/10.1039/D1MA00231G.
[158] Y. Yuan, S. Adimi, X. Guo, T. Thomas, Y. Zhu, H. Guo, G.S. Priyanga, P. Yoo, J. Wang, J. Chen, P. Liao, J.P. Attfield, M. Yang, A Surface-Oxide-Rich Activation Layer (SOAL) on Ni2Mo3N for a Rapid and Durable Oxygen Evolution Reaction, Angew. Chem. Int. Ed. 59 (2020) 18036–18041, https://doi.org/10.1002/ANIE.202008116.
[159] J. Fu, Z. Fan, M. Nakabayashi, H. Ju, N. Pastukhova, Y. Xiao, C. Feng, N. Shibata, K. Domen, Y. Li, Interface engineering of Ta3N5 thin film photoanode for highly efficient photoelectrochemical water splitting, Nat. Commun. 13 (2022) 1–9, https://doi.org/10.1038/s41467-022-28415-4.
[160] V. Nandal, Y. Pihosh, T. Higashi, T. Minegishi, T. Yamada, K. Seki, M. Sugiyama, K. Domen, Probing fundamental losses in nanostructured Ta3N5 photoanodes: Design principles for efficient water oxidation, Energy Environ. Sci. 14 (2021) 4038–4047, https://doi.org/10.1039/d1ee01004b.
[161] A. Ishihara, M. Chisaka, Y. Ohgi, K. Matsuzawa, S. Mitsushima, K. Ota, Synthesis of nano-TaOx oxygen reduction reaction catalysts on multi-walled carbon nanotubes connected via a decomposition of oxy-tantalum phthalocyanine, Phys. Chem. Chem. Phys. 17 (2015) 7643–7647, https://doi.org/10.1039/c5cp00317b.
[162] W. Yang, R.R. Prabhakar, J. Tan, S.D. Tilley, J. Moon, Strategies for enhancing the photocurrent, photovoltage, and stability of photoelectrodes for photoelectrochemical water splitting, Chem. Soc. Rev. 48 (2019) 4979–5015, https://doi.org/10.1039/c8cs00997j.
[163] Y. He, R. Chen, W. Fa, B. Zhang, D. Wang, Surface chemistry and photoelectrochemistry - Case study on tantalum nitride, J. Chem. Phys. 151 (2019), https://doi.org/10.1063/1.5122996.
[164] S. Chen, L.W. Wang, Thermodynamic oxidation and reduction potentials of photocatalytic semiconductors in aqueous solution, Chem. Mater. 24 (2012) 3659–3666, https://doi.org/10.1021/cm302533s.
[165] X. Feng, T.J. LaTempa, J.I. Basham, G.K. Mor, O.K. Varghese, C.A. Grimes, Ta3N5 Nanotube Arrays for Visible Light Water Photoelectrolysis, Nano Lett. 10 (2010) 948–952, https://doi.org/10.1021/nl903886e.
[166] Y. Li, T. Takata, D. Cha, K. Takanabe, T. Minegishi, J. Kubota, K. Domen, Vertically Aligned Ta3N5 Nanorod Arrays for Solar-Driven Photoelectrochemical Water Splitting, Adv. Mater. 25 (2013) 125–131, https://doi.org/10.1002/adma.201202582.
[167] L. Pei, B. Lv, S. Wang, Z. Yu, S. Yan, R. Abe, Z. Zou, Oriented Growth of Sc-Doped Ta3N5 Nanorod Photoanode Achieving Low-Onset-Potential for Photoelectrochemical Water Oxidation, ACS Appl. Energy Mater. 1 (2018) 4150–4157, https://doi.org/10.1021/acsaem.8b00809.
[168] Q. Wang, L. Zhang, B. Li, H. Zhu, J. Shi, 3D interconnected nanoporous Ta3N5 films for photoelectrochemical water splitting: thickness-controlled synthesis and insights into stability, Sci. China Mater. 64 (2021) 1876–1888, https://doi.org/10.1007/s40843-020-1584-6.
[169] Y. Chen, H. Xia, X. Feng, Y. Liu, W. Zheng, L. Ma, R. Li, Synergy of porous structure and cation doping in Ta3N5 photoanode towards improved photoelectrochemical water oxidation, J. Energy Chem. 52 (2021) 343–350, https://doi.org/10.1016/j.jechem.2020.04.034.
[170] L. Pei, Z. Xu, Z. Shi, H. Zhu, S. Yan, Z. Zou, Mg-doped Ta3N5 nanorods coated with a conformal CoOOH layer for water oxidation: bulk and surface dual modification of photoanodes, J. Mater. Chem. A 5 (2017) 20439–20447, https://doi.org/10.1039/C7TA06227C.
[171] P.K. Das, M. Arunachalam, K.Rohini Subhash, Y.Jun Seo, K.-S. Ahn, J.-S. Ha, S. Hyung Kang, Nanoporous Ta3N5 via electrochemical anodization followed by nitridation for solar water oxidation, Dalton Trans. 49 (2020) 15023–15033, https://doi.org/10.1039/D0DT03056B.
[172] Yanqing Cong, Hyun S. Park, Shijun Wang, Hoang X. Dang, Fu-Ren F. Fan, C. Buddie Mullins, Allen J. Bard, Synthesis of Ta3N5 Nanotube Arrays Modified with Electrocatalysts for Photoelectrochemical Water Oxidation, J. Phys. Chem. C. 116 (2012) 14541–14550.
[173] Jungang Hou, Zheng Wang, Chao Yang, Huijie Cheng, Shuqiang Jiao, Hongmin Zhu, Cobalt-bilayer catalyst decorated Ta3N5 nanorod arrays as integrated electrodes for photoelectrochemical water oxidation, Energy Environ. Sci. 6 (2013) 3322–3330.
[174] G. Liu, J. Shi, F. Zhang, Z. Chen, J. Han, C. Ding, S. Chen, Z. Wang, H. Han, C. Li, A Tantalum Nitride Photoanode Modified with a Hole-Storage Layer for Highly Stable Solar Water Splitting, Angew. Chem. Int. Ed. 53 (2014) 7295–7299, https://doi.org/10.1002/anie.201404697.
[175] Y. Kado, C.-Y. Lee, K. Lee, J. Müller, M. Moll, E. Spiecker, P. Schmuki, Enhanced water splitting activity of M-doped Ta3N5 (M = Na, K, Rb, Cs), Chem. Commun. 48 (2012) 8685–8687, https://doi.org/10.1039/C2CC33822J.
[176] J. Feng, D. Cao, Z. Wang, W. Luo, J. Wang, Z. Li, Z. Zou, Ge-Mediated Modification in Ta3N5 Photoelectrodes with Enhanced Charge Transport for Solar Water Splitting, Chem. – A Eur. J. 20 (2014) 16384–16390, https://doi.org/10.1002/chem.201402760.
[177] S.S.K. Ma, T. Hisatomi, K. Maeda, Y. Moriya, K. Domen, Enhanced Water Oxidation on Ta3N5 Photocatalysts by Modification with Alkaline Metal Salts, J. Am. Chem. Soc. 134 (2012) 19993–19996, https://doi.org/10.1021/ja3095747.
[178] X. Wang, H. Zhang, C. Feng, Y. Wang, Engineering band structuring via dual atom modification for an efficient photoanode, Chem. Sci. 15 (2024) 896–905, https://doi.org/10.1039/D3SC05420A.
[179] J. Cui, Y. Luo, B. Dong, Y. Qi, M. Jia, F. Zhang, C. Li, Investigation on the Influence of Sc Ions Doping on the Structure and Performance of Ta3N5 Photocatalyst for Water Oxidation under Visible Light Irradiation, Sol. RRL 4 (2020) 1900445, https://doi.org/10.1002/solr.201900445.
[180] P. Zhang, T. Wang, J. Gong, Passivation of surface states by ALD-grown TiO2 overlayers on Ta3N5 anodes for photoelectrochemical water oxidation, Chem. Commun. 52 (2016) 8806–8809, https://doi.org/10.1039/C6CC03411J.
[181] M. Zhong, T. Hisatomi, Y. Sasaki, S. Suzuki, K. Teshima, M. Nakabayashi, N. Shibata, H. Nishiyama, M. Katayama, T. Yamada, K. Domen, Highly Active GaN-Stabilized Ta3N5 Thin-Film Photoanode for Solar Water Oxidation, Angew. Chem. - Int. Ed. 56 (2017) 4739–4743, https://doi.org/10.1002/anie.201700117.
[182] F. Li, J. Jian, Y. Xu, W. Liu, Q. Ye, F. Feng, C. Li, L. Jia, H. Wang, Surface defect passivation of Ta3N5 photoanode via pyridine grafting for enhanced photoelectrochemical performance, J. Chem. Phys. 153 (2020) 024705, https://doi.org/10.1063/5.0012873.
[183] N.T. Thanh Truc, N. Thi Hanh, D.T. Nguyen, H.T. Trang, V.N. Nguyen, M.N. Ha, T.D.C. Nguyen, T.D. Pham, Novel overall photocatalytic water splitting of tantalum nitride sensitized/protected by conducting polymers, J. Solid State Chem. 269 (2019) 361–366, https://doi.org/10.1016/j.jssc.2018.10.005.
[184] N.T. Thanh Truc, D.T. Tran, N.T. Hanh, T.D. Pham, Novel visible light-driven Nb-doped Ta3N5 sensitized/protected by PPy for efficient overall water splitting, Int. J. Hydrog. Energy 43 (2018) 15898–15906, https://doi.org/10.1016/j.ijhydene.2018.06.128.
[185] Y. Zhao, H. Xie, W. Shi, H. Wang, C. Shao, C. Li, Unravelling the essential difference between TiOx and AlOx interface layers on Ta3N5 photoanode for photoelectrochemical water oxidation, J. Energy Chem. 64 (2022) 33–37, https://doi.org/10.1016/j.jechem.2021.04.042.
[186] Y. Pihosh, V. Nandal, T. Higashi, R. Shoji, R. Bekarevich, H. Nishiyama, T. Yamada, V. Nicolosi, T. Hisatomi, H. Matsuzaki, K. Seki, K. Domen, Tantalum Nitride-Enabled Solar Water Splitting with Efficiency Above 10%, Adv. Energy Mater. 13 (2023) 2301327 https://doi.org/10.1002/aenm.202301327.
[187] G. Liu, S. Ye, P. Yan, F. Xiong, P. Fu, Z. Wang, Z. Chen, J. Shi, C. Li, Enabling an integrated tantalum nitride photoanode to approach the theoretical photocurrent limit for solar water splitting, Energy Environ. Sci. 9 (2016) 1327–1334, https://doi.org/10.1039/C5EE03802B.
[188] K. Xu, A. Chatzitakis, I.J.T. Jensen, M. Grandcolas, T. Norby, Ta3N5/Co(OH)x composites as photocatalysts for photoelectrochemical water splitting, Photochem. Photobiol. Sci. 18 (2019) 837–844, https://doi.org/10.1039/c8pp00312b.
[189] E. Nurlaela, Y. Sasaki, M. Nakabayashi, N. Shibata, T. Yamada, K. Domen, Towards zero bias photoelectrochemical water splitting: onset potential improvement on a Mg:GaN modified-Ta3N5 photoanode, J. Mater. Chem. A 6 (2018) 15265–15273, https://doi.org/10.1039/C8TA05300F.
[190] Y. Zhao, G. Liu, H. Wang, Y. Gao, T. Yao, W. Shi, C. Li, Interface engineering with an AlOx dielectric layer enabling an ultrastable Ta3N5 photoanode for photoelectrochemical water oxidation, J. Mater. Chem. A 9 (2021) 11285–11290, https://doi.org/10.1039/d1ta00206f.
[191] P.K. Das, R. Poonchi Sivasankaran, M. Arunachalam, K.R. Subhash, J.-S. Ha, K.-S. Ahn, S.H. Kang, Highly efficient and stable *g*-C3N4 decorated Ta3N5 nanotube on *n*-Si substrate for solar water oxidation, Appl. Surf. Sci. 565 (2021) 150456, https://doi.org/10.1016/j.apsusc.2021.150456.
[192] S. Youn Chae, E. Duck Park, Enhanced photoelectrochemical stability of Ta3N5 in the acidic electrolyte conditions, Appl. Surf. Sci. 583 (2022) 152566, https://doi.org/10.1016/j.apsusc.2022.152566.
[193] K. Li, B. Miao, W. Fa, R. Chen, J. Jin, K.H. Bevan, D. Wang, Evolution of Surface Oxidation on Ta3N5 as Probed by a Photoelectrochemical Method, ACS Appl. Mater. Interfaces 13 (2021) 17420–17428, https://doi.org/10.1021/acsami.0c21780.
[194] Y. He, J.E. Thorne, C.H. Wu, P. Ma, C. Du, Q. Dong, J. Guo, D. Wang, What Limits the Performance of Ta3N5 for Solar Water Splitting? Chem 1 (2016) 640–655, https://doi.org/10.1016/j.chempr.2016.09.006.
[195] M. Liao, J. Feng, W. Luo, Z. Wang, J. Zhang, Z. Li, T. Yu, Z. Zou, Co3O4 Nanoparticles as Robust Water Oxidation Catalysts Towards Remarkably Enhanced Photostability of a Ta3N5 Photoanode, Adv. Funct. Mater. 22 (2012) 3066–3074, https://doi.org/10.1002/adfm.201102966.
[196] P. Krisna, R. Poonchi, M. Arunachalam, Appl. Surf. Sci. Highly Effic. stable G. -C3N4 Decor. Ta3N5 Nanotub. N. -Si Substr. Sol. Water Oxid. 565 (2021) 14–19.
[197] P. Wang, P. Fu, J. Ma, Y. Gao, Z. Li, H. Wang, F. Fan, J. Shi, C. Li, Ultrathin Cobalt Oxide Interlayer Facilitated Hole Storage for Sustained Water Oxidation over Composited Tantalum Nitride Photoanodes, ACS Catal. 11 (2021) 12736–12744, https://doi.org/10.1021/acscatal.1c03298.
[198] G. Liu, P. Fu, L. Zhou, P. Yan, C. Ding, J. Shi, C. Li, Efficient Hole Extraction from a Hole-Storage-Layer-Stabilized Tantalum Nitride Photoanode for Solar Water Splitting, Chem. – A Eur. J. 21 (2015) 9624–9628, https://doi.org/10.1002/chem.201500745.
[199] M. Sindhu, A. Sharma, K.S. Maan, V. Patel, P.P. Singh, V.-H. Nguyen, Fabrication and characterization of novel V, S co-doped Ta3N5 protected with PANI composite materials for hydrogen generation from light-driven water splitting, J. Taiwan Inst. Chem. Eng. (2023) 105024, https://doi.org/10.1016/j.jtice.2023.105024.
[200] B. Niu, Z. Xu, A stable Ta3N5@PANI core-shell photocatalyst: Shell thickness effect, high-efficient photocatalytic performance and enhanced mechanism, J. Catal. 371 (2019) 175–184, https://doi.org/10.1016/j.jcat.2019.01.025.
[201] M. Sindhu, A. Sharma, V. Patel, A. Gahlawat, P.P. Singh, K.S. Maan, D. Kumar, V.-H. Nguyen, Characteristic studies of Ta3N5/BSC@PANI nanocomposites for hydrogen production via water-splitting under visible light irradiation, Chem. Eng. Res. Des. 197 (2023) 572–580, https://doi.org/10.1016/j.cherd.2023.07.050.
[202] L. Tao, J. Wang, Z. Luo, J. Ren, D. Yin, Fabrication of an S-Scheme Heterojunction Photocatalyst MoS2/PANI with Greatly Enhanced Photocatalytic Performance,

Langmuir 39 (2023) 11426–11438, https://doi.org/10.1021/acs.langmuir.3c01295.
[203] C. Yang, W. Dong, G. Cui, Y. Zhao, X. Shi, X. Xia, B. Tang, W. Wang, Enhanced photocatalytic activity of PANI/TiO2 due to their photosensitization-synergetic effect, Electrochim. Acta 247 (2017) 486–495, https://doi.org/10.1016/j.electacta.2017.07.037.
[204] Y. Xiao, C. Feng, J. Fu, F. Wang, C. Li, V.F. Kunzelmann, C.-M. Jiang, M. Nakabayashi, N. Shibata, I.D. Sharp, K. Domen, Y. Li, Band structure engineering and defect control of Ta3N5 for efficient photoelectrochemical water oxidation, Nat. Catal. 3 (2020) 932–940, https://doi.org/10.1038/s41929-020-00522-9.
[205] L.I. Wagner, E. Sirotti, O. Brune, G. Grötzner, J. Eichhorn, S. Santra, F. Munnik, L. Olivi, S. Pollastri, V. Streibel, I.D. Sharp, Defect Engineering of Ta3N5 Photoanodes: Enhancing Charge Transport and Photoconversion Efficiencies via Ti Doping, Adv. Funct. Mater. 34 (2024) 2306539, https://doi.org/10.1002/adfm.202306539.
[206] Y. Wang, D. Zhu, X. Xu, Zr-Doped Mesoporous Ta3N5 Microspheres for Efficient Photocatalytic Water Oxidation, ACS Appl. Mater. Interfaces 8 (2016) 35407–35418, https://doi.org/10.1021/acsami.6b14230.
[207] Y. Xiao, Z. Fan, M. Nakabayashi, Q. Li, L. Zhou, Q. Wang, C. Li, N. Shibata, K. Domen, Y. Li, Decoupling light absorption and carrier transport via heterogeneous doping in Ta3N5 thin film photoanode, Nat. Commun. 13 (2022) 7769, https://doi.org/10.1038/s41467-022-35538-1.
[208] J. Wang, A. Ma, Z. Li, J. Jiang, J. Chen, Z. Zou, Effects of Mg–Zr codoping on the photoelectrochemical properties of a Ta3N5 semiconductor: a theoretical insight, J. Mater. Chem. A 5 (2017) 6966–6973, https://doi.org/10.1039/C6TA10294H.
[209] J. Seo, T. Takata, M. Nakabayashi, T. Hisatomi, N. Shibata, T. Minegishi, K. Domen, Mg–Zr Cosubstituted Ta3N5 Photoanode for Lower-Onset-Potential Solar-Driven Photoelectrochemical Water Splitting, J. Am. Chem. Soc. 137 (2015) 12780–12783, https://doi.org/10.1021/jacs.5b08329.
[210] M. Li, W. Luo, D. Cao, X. Zhao, Z. Li, T. Yu, Z. Zou, A Co-catalyst-Loaded Ta3N5 Photoanode with a High Solar Photocurrent for Water Splitting upon Facile Removal of the Surface Layer, Angew. Chem. Int. Ed. 52 (2013) 11016–11020, https://doi.org/10.1002/anie.201305350.
[211] E. Nurlaela, S. Ould-Chikh, M. Harb, S. del Gobbo, M. Aouine, E. Puzenat, P. Sautet, K. Domen, J.-M. Basset, K. Takanabe, Critical Role of the Semiconductor–Electrolyte Interface in Photocatalytic Performance for Water-Splitting Reactions Using Ta3N5 Particles, Chem. Mater. 26 (2014) 4812–4825, https://doi.org/10.1021/cm502015q.
[212] M. Harb, J.M. Basset, Predicting the Most Suitable Surface Candidates of Ta3N5 Photocatalysts for Water-Splitting Reactions Using Screened Coulomb Hybrid DFT Computations, J. Phys. Chem. C. 124 (2020) 2472–2480, https://doi.org/10.1021/acs.jpcc.9b09707.
[213] J. Wang, Y. Jiang, A. Ma, J. Jiang, J. Chen, B. Li, J. Feng, Z. Li, Z. Zou, Effects of oxygen impurity concentration on the interfacial properties of Ta3N5/Ta5N6 composite photoelectrode: A DFT calculation, Appl. Catal. B: Environ. 278 (2020) 119296, https://doi.org/10.1016/j.apcatb.2020.119296.
[214] G. Chen, Y. Si, M. Li, Z. Zhou, T. Yu, Y. Liu, M. Liu, Regulate chemical environment to control the formation of defects on Ta3N5 (110) surface: From theoretical perspectives, Chem. Phys. Lett. 782 (2021) 139026, https://doi.org/10.1016/j.cplett.2021.139026.
[215] S. Khan, M.J.M. Zapata, D.L. Baptista, V.R. Gonçalves, J.A. Fernandes, J. Dupont, M.J.L. Santos, S.R. Teixeira, Effect of Oxygen Content on the Photoelectrochemical Activity of Crystallographically Preferred Oriented Porous Ta3N5 Nanotubes, J. Phys. Chem. C. 119 (2015) 19906–19914, https://doi.org/10.1021/acs.jpcc.5b05475.
[216] M. Rudolph, I. Vickridge, E. Foy, J. Alvarez, J.-P. Kleider, D. Stanescu, H. Magnan, N. Herlin-Boime, B. Bouchet-Fabre, T. Minea, M.-C. Hugon, Oxygen incorporated during deposition determines the crystallinity of magnetron-sputtered Ta3N5 films, Thin Solid Films 685 (2019) 204–209, https://doi.org/10.1016/j.tsf.2019.06.031.
[217] M. Rudolph, D. Stanescu, J. Alvarez, E. Foy, J.-P. Kleider, H. Magnan, T. Minea, N. Herlin-Boime, B. Bouchet-Fabre, M.-C. Hugon, The role of oxygen in magnetron-sputtered Ta3N5 thin films for the photoelectrolysis of water, Surf. Coat. Technol. 324 (2017) 620–625, https://doi.org/10.1016/j.surfcoat.2016.09.007.
[218] C.-W. Hsu, K. Awaya, M. Tsushida, T. Sato, M. Koinuma, S. Ida, Preparation of Ta3N5 Nanosheet by Nitridation of Monolayer Tantalum Oxide Nanosheet, ChemistrySelect 5 (2020) 13761–13765, https://doi.org/10.1002/slct.202004129.
[219] V.K.V.L. Narayanachari, D.B. Buchholz, E.A. Goldfine, J.K. Wenderott, S.M. Haile, M.J. Bedzyk, Combinatorial Approach for Single-Crystalline TaON Growth: Epitaxial β-TaON (100)/α-Al2O3 (012), ACS Appl. Electron. Mater. 2 (2020) 3571–3576, https://doi.org/10.1021/acsaelm.0c00622.
[220] J. Čapek, Š. Batková, M. Matas, Š. Kos, T. Kozák, S. Haviar, J. Houška, J. Schusser, J. Minár, F. Dvořák, P. Zeman, Bixbyite-Ta2N2O film prepared by HiPIMS and postdeposition annealing: Structure and properties, J. Vac. Sci. \ Technol. A 38 (2020) 33409, https://doi.org/10.1116/6.0000066.
[221] J. Eichhorn, S.P. Lechner, C.M. Jiang, G. Folchi Heunecke, F. Munnik, I.D. Sharp, Indirect bandgap, optoelectronic properties, and photoelectrochemical characteristics of high-purity Ta3N5photoelectrodes, J. Mater. Chem. A 9 (2021) 20653–20663, https://doi.org/10.1039/d1ta05282a.
[222] S. Munusamy, K. Sivaranjan, P. Sabhapathy, P.S. Ramesh, V. Narayanan, F. Mohammad, S. Sagadevan, Electrochemical and photocatalytic studies of Ta3N5-TaON-PEDOT-PANI nanohybrids, Chem. Phys. Lett. 780 (2021) 138947, https://doi.org/10.1016/j.cplett.2021.138947.
[223] T. Higashi, H. Nishiyama, Y. Otsuka, Y. Kawase, Y. Sasaki, M. Nakabayashi, M. Katayama, T. Minegishi, N. Shibata, K. Takanabe, T. Yamada, K. Domen, Efficient Water Oxidation Using Ta3N5 Thin Film Photoelectrodes Prepared on Insulating Transparent Substrates, ChemSusChem 13 (2020) 1974–1978, https://doi.org/10.1002/cssc.202000397.
[224] J. Čapek, Š. Batková, S. Haviar, J. Houška, R. Čerstvý, P. Zeman, Effect of annealing on structure and properties of Ta–O–N films prepared by high power impulse magnetron sputtering, Ceram. Int. 45 (2019) 9454–9461, https://doi.org/10.1016/j.ceramint.2018.09.019.
[225] R. Simpson, R.G. White, J.F. Watts, M.A. Baker, XPS investigation of monatomic and cluster argon ion sputtering of tantalum pentoxide, Appl. Surf. Sci. 405 (2017) 79–87, https://doi.org/10.1016/j.apsusc.2017.02.006.
[226] D. Cristea, L. Cunha, C. Gabor, I. Ghiuta, C. Croitoru, A. Marin, L. Velicu, A. Besleaga, B. Vasile, Tantalum Oxynitride Thin Films: Assessment of the Photocatalytic Efficiency and Antimicrobial Capacity, Nanomaterials 9 (2019) 476, https://doi.org/10.3390/nano9030476.
[227] A. Jablonski, C.J. Powell, Information depth and the mean escape depth in Auger electron spectroscopy and x-ray photoelectron spectroscopy, J. Vac. Sci. Technol. A 21 (2002) 274–283, https://doi.org/10.1116/1.1538370.
[228] C. Joseph, P. Bourson, M.D. Fontana, Amorphous to crystalline transformation in Ta2O5 studied by Raman spectroscopy, J. Raman Spectrosc. 43 (2012) 1146–1150, https://doi.org/10.1002/jrs.3142.
[229] E. Nurlaela, M. Harb, S. del Gobbo, M. Vashishta, K. Takanabe, Combined experimental and theoretical assessments of the lattice dynamics and optoelectronics of TaON and Ta3N5, J. Solid State Chem. 229 (2015) 219–227, https://doi.org/10.1016/j.jssc.2015.06.029.
[230] J.-C. Chang, F. Eriksson, M.A. Sortica, G. Greczynski, B. Bakhit, Z. Hu, D. Primetzhofer, L. Hultman, J. Birch, C.-L. Hsiao, Orthorhombic Ta3-xN5-yOy thin films grown by unbalanced magnetron sputtering: The role of oxygen on structure, composition, and optical properties, Surf. Coat. Technol. 406 (2021) 126665, https://doi.org/10.1016/j.surfcoat.2020.126665.
[231] L.J. Guo, J.W. Luo, T. He, S.H. Wei, S.S. Li, Photocorrosion-Limited Maximum Efficiency of Solar Photoelectrochemical Water Splitting, Phys. Rev. Appl. 10 (2018) 064059 https://doi.org/10.1103/PHYSREVAPPLIED.10.064059/FIGURES/5/MEDIUM.
[232] S. Chen, D. Huang, P. Xu, W. Xue, L. Lei, M. Cheng, R. Wang, X. Liu, R. Deng, Semiconductor-based photocatalysts for photocatalytic and photoelectrochemical water splitting: will we stop with photocorrosion? J. Mater. Chem. A 8 (2020) 2286–2322, https://doi.org/10.1039/C9TA12799B.
[233] S. Pishgar, S. Gulati, J.M. Strain, Y. Liang, M.C. Mulvehill, J.M. Spurgeon, In Situ Analytical Techniques for the Investigation of Material Stability and Interface Dynamics in Electrocatalytic and Photoelectrochemical Applications, Small Methods 5 (2021) 2100322, https://doi.org/10.1002/SMTD.202100322.
[234] D.I. Patel, T. Roychowdhury, V. Jain, D. Shah, T.G. Avval, S. Chatterjee, S. Bahr, P. Dietrich, M. Meyer, A. Thißen, M.R. Linford, Introduction to near-ambient pressure x-ray photoelectron spectroscopy characterization of various materials, Surf. Sci. Spectra 26 (2019) 016801, https://doi.org/10.1116/1.5109118.
[235] J. Timoshenko, B. Roldan Cuenya, In Situ/ Operando Electrocatalyst Characterization by X-ray Absorption Spectroscopy, Chem. Rev. 121 (2021) 882–961, https://doi.org/10.1021/acs.chemrev.0c00396.
[236] G.F. Samu, C. Janáky, Photocorrosion at Irradiated Perovskite/Electrolyte Interfaces, J. Am. Chem. Soc. 142 (2020) 21595–21614, https://doi.org/10.1021/jacs.0c10348.
[237] Ø. Dahl, M.F. Sunding, V. Killi, I.-H. Svenum, M. Grandcolas, M. Andreassen, O. Nilsen, A. Thøgersen, I.J.T. Jensen, A. Chatzitakis, Interrogation of the Interfacial Energetics at a Tantalum Nitride/Electrolyte Heterojunction during Photoelectrochemical Water Splitting by Operando Ambient Pressure X-ray Photoelectron Spectroscopy, ACS Catal. 13 (2023) 11762–11770, https://doi.org/10.1021/acscatal.3c02423.
[238] A. Venugopal, R. Kas, K. Hau, W.A. Smith, Operando Infrared Spectroscopy Reveals the Dynamic Nature of Semiconductor-Electrolyte Interface in Multinary Metal Oxide Photoelectrodes, J. Am. Chem. Soc. 143 (2021) 18581–18591, https://doi.org/10.1021/jacs.1c08245.
[239] K. Frisk, Anal. phase Diagr. Thermochem. Ta–N. Ta–C. –N. Syst. 278 (2000) 216–226.
[240] P. Hohenberg, W. Kohn, Inhomogeneous electron gas, Phys. Rev. 136 (1964) B864, https://doi.org/10.1007/BF01198136.
[241] W. Kohn, L.J. Sham, Self-Consistent Equations Including Exchange and Correlation Effects, Phys. Rev. 140 (1965) A1133.
[242] E. Zhao, B.O. Hong, J. Meng, Z. Wu, First Principles Investigation on the Ultra-Incompressible and Hard TaN, J. Comput. Chem. 30 (2009) 2358–2363, https://doi.org/10.1002/jcc.
[243] D. Li, F. Tian, D. Duan, K. Bao, B. Chu, X. Sha, B. Liu, T. Cui, Mechanical and metallic properties of tantalum nitrides from first-principles calculations, RSC Adv. 4 (2014) 10133–10139, https://doi.org/10.1039/c3ra46734a.
[244] A.R. Oganov, C.W. Glass, Crystal structure prediction using ab initio evolutionary techniques: Principles and applications, J. Chem. Phys. 124 (2006), https://doi.org/10.1063/1.2210932.
[245] A.O. Lyakhov, A.R. Oganov, H.T. Stokes, Q. Zhu, New developments in evolutionary structure prediction algorithm USPEX, Comput. Phys. Commun. 184 (2013) 1172–1182, https://doi.org/10.1016/j.cpc.2012.12.009.
[246] C. Jiang, Z. Lin, Y. Zhao, Thermodynamic and Mechanical Stabilities of Tantalum Nitride, Phys. Rev. Lett. 103 (2009) 30–33, https://doi.org/10.1103/PhysRevLett.103.185501.

[247] J.D. Houmes, H.C. Zur Loye, Iron-promoted synthesis of tantalum and niobium oxynitrides, J. Solid State Chem. 127 (1996) 267–275, https://doi.org/10.1006/jssc.1996.0383.
[248] J. Wang, J. Jiang, J. Chen, Y. Li, A. Ma, Theoretical study of the oxygen impurity doped Ta5N6, Comput. Mater. Sci. 143 (2018) 368–373, https://doi.org/10.1016/j.commatsci.2017.11.037.
[249] J. Fu, F. Wang, Y. Xiao, Y. Yao, C. Feng, L. Chang, C.-M. Jiang, V.F. Kunzelmann, Z.M. Wang, A.O. Govorov, I.D. Sharp, Y. Li, Identifying Performance-Limiting Deep Traps in Ta3N5 for Solar Water Splitting, ACS Catal. 10 (2020) 10316–10324, https://doi.org/10.1021/acscatal.0c02648.
[250] J. Wang, A. Ma, Z. Li, J. Jiang, Effects of oxygen impurities and nitrogen vacancies on the surface properties of the Ta3N5 photocatalyst: a DFT study, Phys. Chem. Chem. Phys. 17 (2015) 23265–23272, https://doi.org/10.1039/C5CP03290C.
[251] X. Wang, H. Huang, G. Fan, Z. Li, Z. Zou, Theoretical Insight into Charge-Recombination Center in Ta3N5 Photocatalyst: Interstitial Hydrogen, J. Phys. Chem. C. 122 (2018) 489–494, https://doi.org/10.1021/acs.jpcc.7b09738.
[252] J. Wang, Y. Jiang, A. Ma, J. Jiang, J. Chen, M. Li, J. Feng, Z. Li, Z. Zou, Charge compensation doping to improve the photocatalytic and photoelectrochemical activities of Ta3N5: A theoretical study, Appl. Catal. B: Environ. 244 (2019) 502–510, https://doi.org/10.1016/j.apcatb.2018.11.076.
[253] A. Mettenbörger, T. Singh, A.P. Singh, T.T. Järvi, M. Moseler, M. Valldor, S. Mathur, Plasma-chemical reduction of iron oxide photoanodes for efficient solar hydrogen production, Int. J. Hydrog. Energy 39 (2014) 4828–4835, https://doi.org/10.1016/j.ijhydene.2014.01.080.
[254] I. Giebelhaus, E. Varechkina, T. Fischer, M. Rumyantseva, V. Ivanov, A. Gaskov, J. R. Morante, J. Arbiol, W. Tyrra, S. Mathur, One-dimensional CuO–SnO2 p–n heterojunctions for enhanced detection of H2S, J. Mater. Chem. A 1 (2013) 11261–11268, https://doi.org/10.1039/C3TA11867C.
[255] D. Barreca, G. Carraro, A. Gasparotto, C. Maccato, C. Sada, A.P. Singh, S. Mathur, A. Mettenbörger, E. Bontempi, L.E. Depero, Columnar Fe2O3 arrays *via* plasma-enhanced growth: Interplay of fluorine substitution and photoelectrochemical properties, Int. J. Hydrog. Energy 38 (2013) 14189–14199, https://doi.org/10.1016/j.ijhydene.2013.08.119.

Raghunath Sharma is a postdoctoral researcher at the Laboratory for High-Performance Ceramics, Department of Metallurgical and Materials Engineering, IIT Madras, India. His doctoral work on novel synthesis methodologies for 1D fibres and thin films based on tantalum carbonitrides and oxynitrides for electrocatalytic hydrogen evolution reaction is conferred with the Institute Research Award for the best thesis. As a PhD student, he co-founded a startup focusing on advanced ceramics. Additionally, he worked as a SPARC Visiting Fellow in the Group of Prof. Mathur at the University of Cologne. His research interests encompass electrocatalysis, green hydrogen, and sustainable materials development.

Niraja Moharana is a doctoral student working with Prof. K. C. Hari Kumar and Prof. Ravi Kumar N V in the Department of Metallurgical and Materials Engineering at the IIT Madras, India. Her research interests focus on the thermodynamic modelling of transition metal nitrides using the Calphad approach coupled with *ab initio* calculations and calculations.

Bhupendra Singh is a Postdoctoral Researcher in research group of Prof. Mathur at the Chair of Inorganic and Materials Chemistry at the University of Cologne in Germany. His research interests are focussed on the synthesis and characterization of materials for low/intermediate temperature fuel calls and electrolysers.

Thomas Fischer is a Senior Research Scientist associated with the Chair of Inorganic and Materials Chemistry at the University of Cologne in Germany. His research interests are focused on thin film growth of functional materials by atomic layer deposition and chemical vapor deposition. He is currently engaged in metal oxide-based gas sensing devices.

Florian Vollnhals is a Senior Research Scientist at the Institute for Nanotechnology and Correlative Microscopy (INAM) in Forchheim, Germany. He received his PhD in physical chemistry from the Friedrich-Alexander University Erlangen-Nürnberg, Germany, in 2014 on the topic of electron beam induced chemistry and worked as a Postdoc at the Luxembourg Institute of Science and Technology (LIST), working on helium ion microscopy and secondary ion mass spectrometry. His research interest focusses on the surface characterization and correlative microscopy in multidisciplinary research environments.

Arun Ichangi is a post-doctoral researcher at the High-Performance Ceramics Laboratory at Empa since 2022 and has been working on the processing and sintering of electroceramics. He acquired a PhD on the synthesis and characterization of 1D ferroelectric inorganic materials for energy harvesting applications from the University of Cologne in 2021, as a Marie Skłodowska-Curie doctoral fellow. His current research interests include cold-sintering and shaping of electroceramics.

Silke Christiansen is a Full Professor of Physics at Free University, Berlin since 2013, and also serves as Site Manager and Department Head for Correlative Microscopy and Materials Data at Fraunhofer IKTS in Forchheim, Germany. A recipient of the MRS Student Award, Bayerische Forschungsstiftung for Columbia University-NY City and Feodor Lynen Fellowship (Alexander von Humboldt Foundation), she worked at IBM T. J. Watson Research Centre, Columbia University, Max Planck Institutes (MPI) for Microstructure Physics, MPI Science of Light, Helmholtz Zentrum Berlin for Materials & Energy, Leibnitz Institute for Photonic Technology, Friedrich-Alexander University Erlangen-Nürnberg, and Chungbuk University Korea (Honorary Professor, 2015–2021). She specializes in materials synthesis, context microscopy and spectroscopy for energy, biomedical sensing, biotechnology, and opto- & large-area electronics. Her contributions include >400 peer-reviewed publications, 12 patents/applications.

K.C. Hari Kumar is Professor at Department of Metallurgical and Materials Engineering, Indian Institute of Technology, Madras. He has received PhD degree in Computation of Phase Diagrams of Iron-base Alloys from the Indian Institute of Technology Delhi in 1992. His research interests include Gibbs energy modelling of materials employing Calphad, modelling of diffusion-controlled transformations in ferrous and non-ferrous alloys, applications of density functional theory in materials science, and alloy design using physical metallurgy & computational thermodynamics. He has published >100 research articles and book chapters.

Ravi Kumar is a Professor of Ceramics in the Dept. of Metallurgical and Materials Engineering at IIT Madras, India since 2018 and the Head of the Central XRD Laboratory. He has been a visiting Professor at the Christian University of Kiel (Germany), Shanghai Institute of Ceramics (China), European Membrane Institute (University of Montpellier, France), University of Stuttgart (Germany), University of Bergamo (Italy), and St. Petersburg University (Russia). He is currently executing bilateral projects with St. Petersburg University & Ioffe Institute, Japan Advanced Institute of Science and Technology, and University of Cologne. He has authored >100 peer reviewed articles and serves on the editorial board of Surface Innovations, Advances in Materials Science and Engineering, and Frontiers in Materials: Ceramics and Glass. His research interests include development of novel non-metallic and inorganic materials for thermal management, catalysis and energy.

Sanjay Mathur is Director and Chair of the Institute of Inorganic Chemistry at University of Cologne, Germany and an adjunct faculty at the Indian Institute of Technology, Madras under the SPARC scheme of the Government of India. He is an Academician of the World Academy of Ceramics and served as the President of the American Ceramic Society (ACerS, 2022–23). A Fellow of the American Ceramics Society, ASM International, Materials Research Society, Royal Society of Chemistry, European Academy of Science, and National Academy of Science, India, Mathur earned his D Phil degree (1992) at the Chemical Laboratories, University of Rajasthan, Jaipur India and Habilitation degree (2004) at the Saarland University, Germany. His research interests include chemical processing of functional inorganic materials by solution and vapor phase methods for applications in batteries, sensors, and hydrogen production. He also has made significant contributions in the development of bioconjugated nanoparticles for drug delivery applications and for tracking intracellular processes. He has published >550 articles and edited/written several books/book chapters, and holds 11 patents.